In situ studies of spin electronics properties of magnetic nanocontacts fabricated using a Lab-on-chip approach

Thèse présentée par

Petru LUNCA POPA

Pour obtenir le titre de Docteur de l'Université de Strasbourg

27 Septembre 2010

Commission d'examen:

Prof. Bernard DOUDIN	Directeur de thèse
Prof. Michel VIRET	Rapporteur externe
Prof. Peter DOWBEN	Rapporteur externe
Prof. Wolfgang WEBER	Examinateur interne

Institut de Physique et Chimie des Matériaux de Strasbourg

IPCMS

CNIS
dépasser les frontières

UNIVERSITÉ DE STRASBOURG

In memoriam **Prof. Dr. Nicolae Sulitanu**

Dept of Physics, "Al. I. CUZA" University of Iasi, ROMANIA

I hope you have some time to read this thesis

Acknowledgements

I would like to thank all the friends and colleagues who helped me to finish this thesis.

I am the most grateful to my supervisor, Prof. Bernard Doudin. Sharing same office with you in last years was a real blessing for me. Sorry to bother you sometimes with my philosophical questions about Physics but I always found in you all support, all patience and all answers that I needed. (Even I will never understand why we need a super double lock-in able to measure simultaneously at eight different frequencies). If I will ever have my own research group I am sure I would try to copy your model.

A special thanks to Neil Kemp, my friend, the first post doc of our group. We built together the actual lab from almost zero. Thank you for teaching me how to prepare carefully experiments. It was a pleasure to be "your young padawan" and I will never forget that "if you have time to lean, you have time to clean". I wish you good luck in building your own lab and team.

Also thanks a lot Hicham for all your help. I always find at you a useful advice and I liked a lot our discussion about science and in particularly about life. You taught me a lot. Now at the end of this thesis I really understand what you told me: "better is the enemy of good" and "slowly but surely".

Vina and Guillaume, you were like sister and brother for me, here in Strasbourg in last four years. I always found a friendly support at you guys. I will never forget the times when we were gossiping in the office or we were playing like young kids. Those moments were the only moments of relaxations after some harsh time in the laboratory. I wish you good luck. Guillaume I am quite sure you will succeed in your plans. Please don't forget me when you will become CEO or even president.

Thank you JB for making me samples when I really needed. Good look in finding BAMR and please don't destroy completely the wire-bonding machine. Congratulations for your kid. This is more important than any BAMR finding. Nabil, I listened tens of times your presentation about MgO and I hope I will never hear it again. Only best wishes in finding what you really want.

A special thanks for the "Romanian group" from IPCS. Cristian, Sorin, Silviu, Ovidiu, Mircea, again Ovidiu, again Mircea, Gabriela, Cristi, Lucian, Ileana, Simona. You helped me a lot and made my life here, in Strasbourg, much nicer.

This thesis is dedicated to investigating spin-dependent electrical properties of magnetic contacts of size as small as a few atoms. New properties are expected when reducing the size of magnetic contacts down to values corresponding to the wavelength of the charge carriers. In this work, we developed an original and sophisticated setup for fabricating and measuring electrical transport through such ultimate nano-sized materials. Samples were obtained by a combination of top down technologies related to patterning two electrodes separated by typically 50 nm distance, with bottom-up construction, involving electrochemistry techniques to close-up the distance and size down to atomic size values. We used a lab on chip approach, taking advantage of microfluidics to control the flow and presence of the electrolytic solution. This whole setup was positioned at the apex of a cryostat, inserted into an electromagnet. This allowed fast setting of magnetic field amplitude and orientation, under possible variable temperature environment. Atomic-size junctions were successfully obtained for several materials: Ag, Au, Ni Co, Pt, and magnetoresistance properties of Ni contacts were systematically investigated. Measurements revealed anisotropic magnetoresistance properties, of magnitudes much larger than bulk intrinsic values. One third of the samples exhibited huge change of resistance under applied magnetic field orientation. By investigating this effect under continuous change of the wet chemistry environment, we unambiguously indentified the paramagnetic metal ions as the origin of this huge effect. This provides novel insight into a debate in the community, which had excluded this observation under the assumption that it is affected by mechanical artifacts. Investigations on Pt contacts and on samples combining mechanical break junctions and electrochemistry junctions confirmed the peculiar role played by the electrochemical environment.

Cette thèse est consacrée à l'étude des propriétés électriques dépendent du spin de contacts magnétiques ayant une taille de quelques atomes seulement. De nouvelles propriétés sont attendues lorsque des contacts magnétiques ont une taille atteignant la longueur d'onde des porteurs de charge. Dans ce travail, nous avons développé un montage original et sophistiqué permettant de fabriquer et mesurer le transport électrique au travers de ces matériaux nanométriques de tailles ultimes. Les échantillons ont été obtenus par une combinaison de techniques de fabrication 'top-down' permettant de définir deux électrodes séparées par une distance de typiquement 50nm, avec une construction de type 'bottom-up' utilisant des techniques d'électrochimie pour ramener la distance et la taille a des dimensions atteignant quelques atomes. Une approche de type 'lab-on-chip', utilisant les méthodes de micro-fluidique, permet de contrôler le flux et la présence de la solution électrolytique. Cet ensemble est placé sur une canne cryogénique, et inséré dans l'entrefer d'un électro-aimant, permettant l'application rapide d'un champ magnétique d'amplitude et d'orientation variables, dans des conditions cryogéniques si désiré. Des contacts de tailles atomique ont été obtenus pour différents matériaux ; Ag, Au, Ni Co, Pt, et les propriétés de magnétorésistance ont été systématiquement étudiées pour le Ni. Les mesures ont montré des propriétés d'anisotropie de la magnétorésistance, d'amplitude largement supérieure aux propriétés du Ni massif. Le tiers des échantillons a montré un changement énorme de la résistance en fonctions de l'orientation du champ magnétique. En étudiant cet effet sous changement de l'environnement chimique de l'échantillon, nous avons pu irrévocablement identifier l'origine de cet effet comme étant la présence des ions métalliques paramagnétiques en solution. Ceci éclaire d'un jour nouveau un débat dans la communauté,, ayant exclu ce type d'observation en argumentant d'effet mécaniques affectant les mesures. Des mesures complémentaires sur les contacts de Pt et sur des échantillons combinant des jonctions a brisure mécanique avec l'électrochimie, confirment le rôle particulier joué par l'environnement chimique.

In situ studies of spin electronic
properties of magnetic nanocontacts fabricated using
a Lab-on-chip approach

"If you really want to find the truth, your mind you should clear"

Yoda, Star Wars

Chapter 1
Introduction

Almost two thousand years ago Leucip and Democrit claimed that atoms are the bricks of matter and cannot be divided further in smaller parts. In the last 50 years the atomic size limit of matter draws again the attention of scientists interested in electrical properties of ferromagnetic materials. Progress in miniaturization and the perspective of realizing devices of few atoms call attention to the need of understanding properties of matter at the smallest size.

Electrical resistance in materials is governed by Ohm's law, which tells us that the resistance is proportional to the length of a conductor and inversely proportional to its area. This concept does not apply on samples made of a few atoms only. Charges passing through such a small contact exhibit a ballistic behavior, namely passing without being affected by scattering. The concept of resistance must be therefore revisited and the wave nature of conduction charges must be taken into account [1]. Investigations on samples reaching atomic size also require novel tools for fabrication, manipulation and characterization. Understanding and performing experiments at such nanoscale is one of the most active and challenging current research fields. New fundamental understanding as well as the potential, the possibilities of future applications are the two driving forces of interest in such nanoscale electronic studies. At this time of writing this manuscript the smallest size of components in industrial large scale production of integrated circuits is around 30 nm and it is believed that this value, corresponding of 100 atoms disposed in a row is approaching the technological minimum [2]. Realizing prototypes extending this limit by more than order of magnitude allows us to test the absolute miniaturization limit: the atomic scale.

Investigation of magnetic systems and the relationship between electrical transport and magnetic properties is another very active field of research. Electrical devices taking advantage of the spin of carriers hold premises of new possibilities for detectors, memory elements and new reconfigurable elements. This field of spintronics [3], was triggered by the discovery of large changes of magnetoresistive properties - 80%- reported back in 1988 [4] for samples consisting in alternative layers of ferromagnetic – non magnetic layers. This "spin valve" effect corresponds of large changes of resistance when two adjacent magnetic entities change their relative orientation from parallel to antiparallel. This Giant Magneto Resistance (GMR) contrasts to bulk MR properties (normal MR) as it has a larger amplitude and can be tailored through control of local magnetization configuration. More than 20 years of worldwide intensive research activities conveyed to the idea that spin-dependent diffusion in the bulk of ferromagnetic materials and at their interface with non magnetic

materials are the origins of GMR. Similar effects were found when using a thin dielectric as separator between the two ferromagnetic materials. A spin-dependent model was elaborated, were the spin dependent number of tunneling electrons, as well as their tunneling probability was the source of the phenomena. The effect is already exploited commercially by manufacturers of hard disk drives. When reducing the size of samples one can expect that the diffusive model of transport becomes less predominant. The spin valve effect in the ballistic regime of conduction is enhanced. [5].

This thesis is dedicated to the investigation of electrical properties of metallic nanocontacts under applied external magnetic field. The thesis is structured in six chapters. After first introductory chapter, the second chapter is a comprehensive introduction to theoretical concepts, as well as a summary of the status of the current research in the field.

Fabricating nanocontacts exhibiting giant spin valve effect at room temperature attracted considerable attention in view of potential possibility of using them in information storage technologies or as highly sensitive magnetic sensors [6]. Experimental results reported for magnetoresistive effects in nanocontacts are covering a wide range. Nickel nanocontacts with a GMR of 100 or 300% at room temperature were obtained several years ago by electrodeposition between two Ni wires. More recently values up to 4000 % and even GMR going to infinity [7] were observed. However results on junctions obtained by mechanically breaking a small contact (or mechanical break junctions MBJ) indicates much lower values and reports indicating the complete absence [8] of MR properties can be found. For nickel junctions obtained by electromigration technique MR values up to 70% were obtained [9], in agreement with MBJ but still far from electrodeposition. A controversy related to real values of MR is still on. Various artifacts, possibly altering the results, have been invoked [10], mostly questioning the mechanical stability of the samples.

The third and fourth chapters are dedicated to the description of experimental setup and to the process of fabrication of the nanocontacts. A new experimental tool was developed, aimed at fabricating and to measuring transport properties of nanocontacts. Besides high speeds for data acquisition and for magnetic field rates, crucial in the case of fragile samples, the novelty consists in a lab on chip approach in using electrochemistry as tool for fabricating atomic size contacts. A system of microfluidic channels was inserted. This gave us the ability to exchange and to control the electrolyte flowing in the micro-electrochemical cell. This new feature, never

reported before, allowed us in obtaining new and interesting results about the influence of electrolyte on transport properties across the contacts, possibly shinning new light for explaining discrepancies in reported results.

A section is dedicated to a separate set of experiments, where a dual approach for fabricating nanocontacts was tested. We combined our lab on chip electrochemistry method with mechanical break technique taking advantage of the experience of Prof. Michel Viret from CEA, Saclay. The results obtained for such samples confirmed the influence of electrolyte on electrical transport properties of the nanocontact.

Last part of this comprehensive chapter is ending with the discussion of results and the possible future plans. We tried to give an explanation of our results, for which there is no model yet. Several hypotheses were discarded, some were enounced and new clarifying experiments are suggested.

The thesis is ending with a summarizing chapter where several conclusions are drawn and possible improvements are suggested.

Bibliography

[1] R. Landauer, *Phil. Mag.,* **21**, (1970), 863

[2] N. Agrait, A. L. Yeyati, J. M. van Ruitenbeek, *Physics Reports*, **377**,(2003), 81-279

[3] I. Žutić, F. Jaroslav,S. Das Sarma, *Rev Mod Phys,* **76,** (2004), 323

[4] M. N. Baibich, J. M. Broto, A. Fert, F. Nguyen Van Dau, F. Petro ,P. Eitenne, G. Creuzet, A. Friederich, and J. Chazelas, *Phys. Rev. Lett.*, **61**, (1988), 2472

[5] B. Doudin and M. Viret, J.*Phys:Condens.Matter*, **20**, (2008), 083201

[6] A. Sokolov, C. Zhang, E. Y. Tsymbal, J. Redepenning and B. Doudin, *Nature Nanotechnology*, **2**, (2007), 36

[7] S. Z. Hua and H. D. Chopra, Phys. Rev. B, **67**, (2003), 060401

[8] J. Mallett, E. B. Svedberg, H. Ettedgui, T. P. Moffat and W. F. Egelhoff, *Phys. Rev. B*, **70**, (2004) ,172406

[9] Z. K. Keane, L. H. Yu, D. Natelson, *Appl. Phys. Lett.,* **88** (2006), 062514-3

[10] W.F. Egelhoff Jr, L. Gan, H. Ettedgui, Y. Kadmon, C.J. Powell, P.J. Chen, A.J. Shapiro, R.D. McMichael, J.J. Mallett, T.P. Moffat, M.D. Stiles, E.B. Svedberg, *Journal of Magnetism and Magnetic Materials,* **287,** (2005), 496-500

Chapter 2

Fundamentals and current experimental results

2.1. Ballistic regime

2.2. Fabrication of nanogaps

2.3. Electrical transport in nanocontacts

This chapter is an introduction to the basic concepts, as well as a summary of the status of the current research in the field. It starts by the basic models for ballistic transports through nanocontacts. The Maxwell, Sharvin and Landauer models for conductance in small size electrical contacts are described. The differences between diffusive and ballistic conductance are described and the conditions for having a ballistic transport are specified. The concept of ballistic transport in ferromagnetic nanocontacts implies spin dependent transmission properties in a nanocontacts, detailed in one section. The main experimental methods for fabricating nanogap and nanocontacts are presented: mechanical and electrical break junctions, as well as electrochemistry techniques. Each of these is critically reviewed in this chapter, emphasizing their peculiarities and presenting their advantages and disadvantages. The electrochemistry, which is the technique used in the work of this thesis, is presented in more details. This second chapter is also a bibliographical chapter, reviewing the experimental results and related theoretical concepts in the field up to now. The results related to studying the magnetoresistance properties in nanojunctions, obtained by using those three different techniques, are detailed with emphasis on the common experimental outcomes and the remaining discrepancies found in the literature.
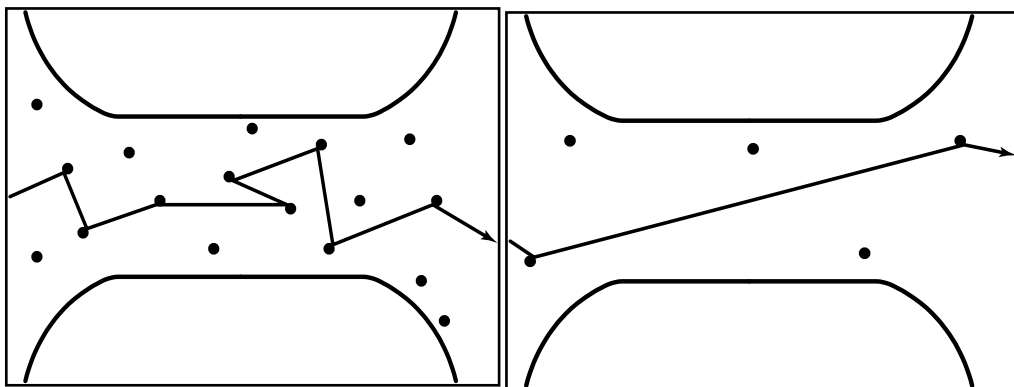
2.1 Ballistic regime

For metals of macroscopic size, the electrical conduction can be described using Ohm's law:

$$\vec{j}(\vec{r}) = \sigma\vec{E}(\vec{r}) \qquad [2.1]$$

where the current density **j** that passes through a conductor is proportional to the electric field through, **σ**, the conductivity of the conductor, that is an intrinsic property of the material. When considering the shape of a piece of conductor one can express its resistance as:

$$R = \frac{1}{G} = \rho\frac{l}{A} = \frac{1}{\sigma}\frac{l}{A} \qquad [2.2]$$

where ρ is the resistivity, G is the conductance and R is the resistance of a conductor of length l and cross section area A. The conduction in such a macroscopic conductor can be explained using the Drude model of conduction, where the electrons gain momentum from the applied electrical field and lose their momentum due to the scatterings **[1]**. The mean distance separating two consecutive scatterings events is electron mean free path **λ$_e$**. Below this length, one expects that the average properties of carriers can be modified, in the so-called *ballistic regime* of conduction.

Fig. 2.1 Schematic illustration of – (left) - a diffusive conductor – (right) – a ballistic conductor

In the diffusive regime, the resistance of the sample is related to the number of scatterings, and is proportional to the length of the conductor, whereas in the ballistic regime, due to the absence of scattering processes, the resistance should ideally falls down to zero. Many experiments however show non-zero values for the resistance of ballistic conductors. Therefore, it has been shown that in this case the resistance results from boundaries between the ballistic channel and the leads.

The simplest extension of a diffuse conductor of reduced size is an aperture of diameter **a** separating two electrodes (fig 2.2.)
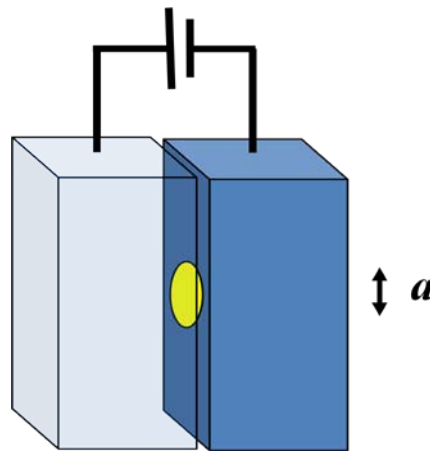
Fig. 2.2 Point contact consisting in an aperture between two electrodes

Using this model for a point contact, Maxwell calculated the conductance in diffusive regime in the asymptotic case of a hyperboloid shape **[2]**

$$G_M = 2a\sigma = \frac{2a}{\rho} \qquad\qquad [2.3]$$

With the resistivity given by:

$$\rho = \frac{mv_F}{ne^2l} \qquad\qquad [2.4]$$

where *m* is the electron mass, v_F the Fermi velocity, *n* the electron density and *e* is the electron charge. This value for conductance, obtained in the diffusive regime, is showing the resistance dependence only on **a**, the aperture radius. .

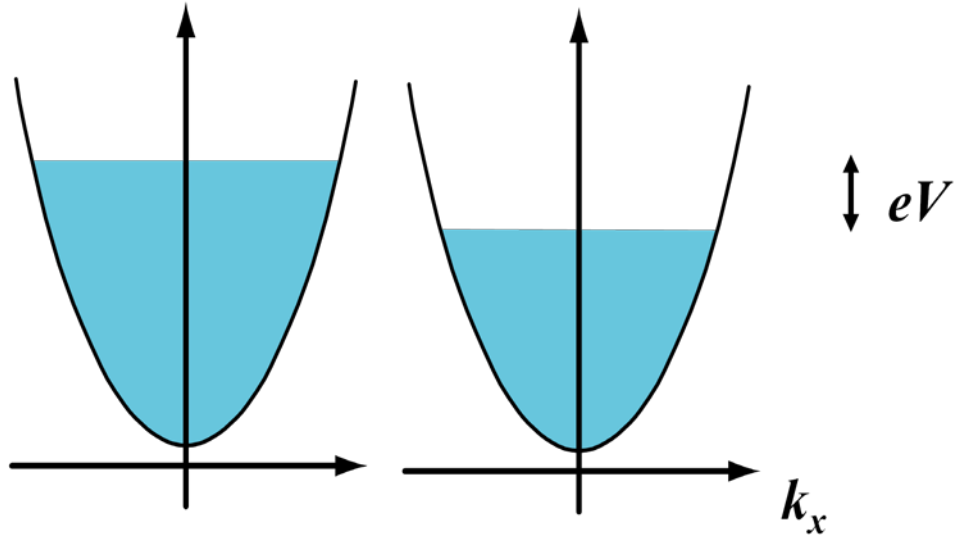A semi classical approach for calculating the conductance of a point contact (fig.2.3) was considered by Sharvin **[3]**

Fig.2.3 The model used in calculating the Sharvin conductance **[3]**

He made the analogy with the problem of a dilute gas passing through a small hole. The current density is the product of electron charge, average velocity and the density of states at the Fermi level.

$$j(x) = e\langle v_x \rangle \rho(\varepsilon_F) \frac{eV}{2}$$

[2.5]

If the average velocity and the density of states are expressed as a function of the Fermi wave vector k_F for independent free particles:

$$\langle v_x \rangle = \frac{hk_F}{2m} \qquad \rho(\varepsilon_F) = \frac{mk_F}{\pi^2 h^2}$$

the conductance is expressed in the form

$$G_S = \frac{2e^2}{h} \left(\frac{\pi a}{\lambda_F}\right)^2$$

[2.6]

for a disk of radius **a**.

This Sharvin conductance is independent on wavelength of electrons, λ_e, and depends linearly only on the cross section of the contact. Torres **[4]** made a correction to Sharvin conductance but the differences related are relatively small especially for

nanometers size contacts. At the limit between Maxwell conductance, depending on the free mean path of electrons, and the Sharvin conductance, independent on λ_e, Wexler **[5]** gave the expression

$$G_W = G_S \left[1 + \frac{3\pi}{8} \Gamma \left(\frac{\lambda_e}{a} \right) \frac{a}{\lambda e} \right]^{-1} \qquad [2.7]$$

that expresses Sharvin-type in series with a Maxwell-type resistance, following the idea that a realistic constriction has a diameter continuously evolving between the two regimes of conduction.

      The main hypothesis of Sharvin's model is that there are no correlated collisions during electronic transport and that electron can be treated as corpuscular. This hypothesis is not holding anymore when the diameter of aperture, **a,** is comparable or smaller than λ_F, the wavelength of the conduction electrons. In this case, the wave aspect of electron transport should be considered and a quantum mechanics formalism should be applied.

      For calculating the conductance in this limit, Landauer **[6]** introduced the idea that the conductance can be expressed in the terms of scattering matrix. He considered the contact as a waveguide in which the wave functions of the electrons are confined. This is analogous to the electromagnetic waves propagating through an electromagnetic waveguide. In analogy to the discrete modes of electromagnetic waves propagating in a waveguide, discrete modes of electrons traveling through a metallic contact are expected. The model is shown in fig.2.4 and it consists in two perfect leads connecting a very narrow channel. The electrodes act as ideal electron reservoirs, at quasi-equilibrium defining chemical potentials μ_1 and μ_2.

      Good simplified examples are given in fig.2.4., where a one-dimensional wire separate the two reservoirs. Due to the lateral confinement, the transverse momentum of electron is quantized, which defines independent longitudinal channels along which electrons propagate as plane waves.

      The band structure of the point contact can be obtained solving Schrodinger equation, writing the Hamiltonian in a single particle approximation

$$H = \frac{p^2}{2m^*} + eV_y \qquad [2.8]$$

where the last term is the confinement potential. If we consider as parabolic confinement potential, the eigenvalues for energy are of the form

$$E\left(k_x, n_y\right) = \frac{\hbar^2 k_x^2}{2m^*} + \left[n_y + \frac{1}{2}\right]\hbar\omega_0 \qquad [2.9]$$
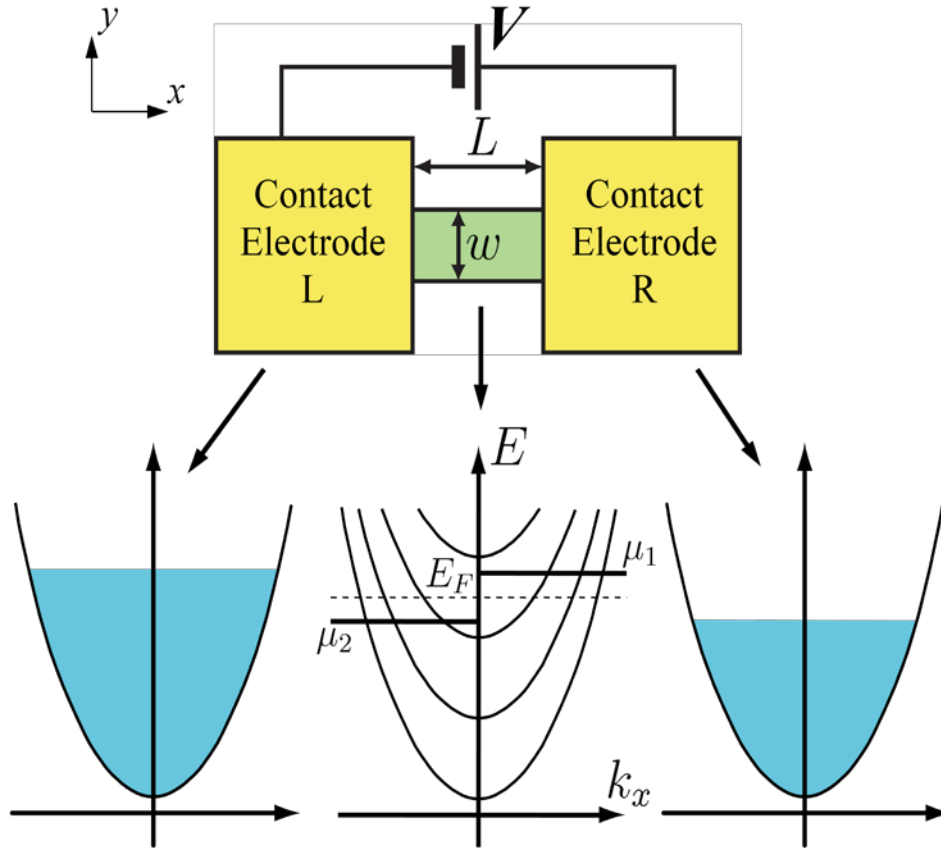
Fig. 2.4 The principle schematic diagram of a two terminal one-dimensional ballistic conductor of length L and wire w, separating two infinite reservoirs, defined by their chemical potentials. The energy diagram for free particles is schematized in the bottom, with transverse confinement resulting in 1-D sub-band for the conductor

The voltage applied V = (μ_1- μ_2)/e causes the appearance of a current I due to uncompensated electron states between μ_1 and μ_2

$$I = \frac{2e}{h}\int\left(f_L(\varepsilon) - f_R(\varepsilon)\right)d\varepsilon \qquad [2.10]$$

The total current flow is obtained by integrating over all states between μ_1 and μ_2. Hence:

$$I = e \frac{1}{2} \sum_{n=1}^{N} \int_{\mu_1}^{\mu_2} \frac{dN_n}{dE} v_n(E) T_n(E) dE \qquad [2.11]$$

where T_n is the probability of transmission for the nth channel, dN_n/dE is the density of states and v_n the velocity of the electron in channel n. For small voltages applied, therefore small deviation around Fermi level, the expression for conductance of the nanocontact becomes:

$$G = \frac{I}{V} = \frac{Ie}{(\mu_1 - \mu_2)} = \frac{2e^2}{h} \sum_{n=1}^{n} T_n \qquad [2.12]$$

This equation is called Landauer formula and if processes of backscattering are neglected, or perfect transmission case fulfilled ($T_n = 1$, a very rare and special case)

$$G = \frac{2e^2}{h} N \qquad [2.13]$$

In the simplest case of a single one-dimensional channel eq. 2.13 simplifies to

$$G_0 = \frac{2e^2}{h} \qquad [2.14]$$

where G_0 is called the quantum of conductance.

In summary, the confinement of electron due to the leads and finite width w is the source of apparition of sub-bands in the narrow conductor (channels of conductions). Each channel **j** has a conduction of $T_j G_0$, with a transmission factor T_j between zero and one; therefore, the whole conduction is the sum of all individual conductions for each channel. Transmission factors T_j depends on the scattering processes and they are very sensitive on the contact's geometry and on the orbitals considered. Realistic geometries for contacts considering full overlap of orbitals and

bonding have in results considerable deviations from a perfect one-dimensional system.

For itinerant ferromagnetic materials, the conducting channels can be considered spin dependent, and the spin degeneracy indicated by the factor 2 in the expression of G_0 should be lifted. More specifically eq. 2.13 can be straightforwardly generalized if we limit the consideration to parallel and antiparallel magnetic configurations of the two reservoirs.

For a parallel alignment

$$\mathbf{G_{\uparrow\uparrow} = \frac{e^2}{h} N_{\uparrow\uparrow} T_{\uparrow\uparrow}} \qquad [2.15]$$

while for antiparallel one

$$\mathbf{G_{\uparrow\downarrow} = \frac{e^2}{h} N_{\uparrow\downarrow} T_{\uparrow\downarrow}} \qquad [2.16]$$

so assuming - $N_{\uparrow\uparrow} = N_{\downarrow\uparrow} = 1$ (only one channel conduction);

- $T_{\uparrow\uparrow} = 1$ but $T_{\downarrow\uparrow} = 0$ (perfect transmission in one sense and no

transmission in the opposite)

one can get a very abrupt change in the resistance of the contact from a finite value to an infinite one.

As explained above, to observe quantization of conductance the cross section of the nanocontacts should be comparable with the Fermi wavelength. Van Wees *et al* **[7, 8]** realized the most convincing demonstration of conductance quantization. They took advantage of relatively high Fermi wavelength (around 50 nm) of a two dimensional gas formed at the GaAs/AlGaAs interface. Adequate electrostatic gate pinched the width of the conductive path separating the two halves of the 2DEG, with adequate dimensionality of the path. They were able to adjust continuously the width of constriction by adjusting the gate voltage and they observed a step like decrease of conductance as width was decreasing. The step size was exactly $1G_0$ (fig.2.5) corresponding to a calculated ballistic mode of transport.

Studying the same phenomena on metals is more challenging due to their Fermi wavelength that is only few Angstroms. Another condition to observe the quantization of conductance in constriction geometries is the adiabaticity, which
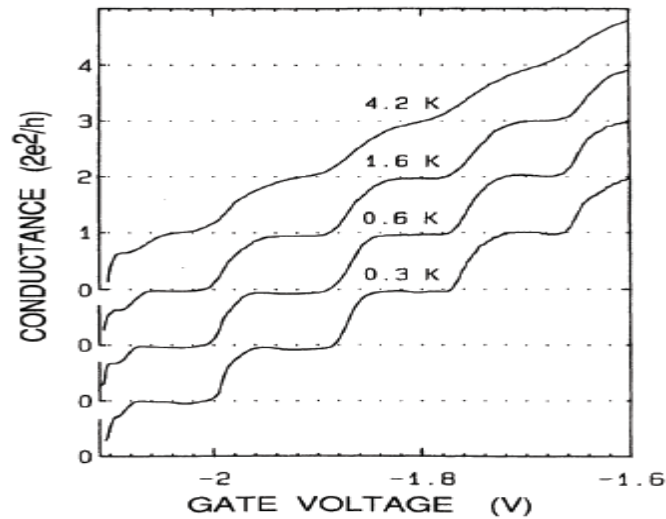
Fig. 2. 5 The breaking of quantized conductance in GaAs/AlGaAs structures; with the increase of temperature the steps are fading due thermal interference **[8]**

requires that the cross section of the constriction vary slowly, compared to the scale of λ_F **[9]**. In addition, the jumps in the conductance may be not due to the closure or opening of conducting channels but correspond to rearrangements in the atomic contacts **[10]**.

Convincing experiments on studying quantization of conductance in metals were done in gold by Brandbyge **[11]** and Ohnishi **[12].** These experiments were shown clear steps in conductance, which was attributed to the formation of short atomic chains (fig.2. 6)
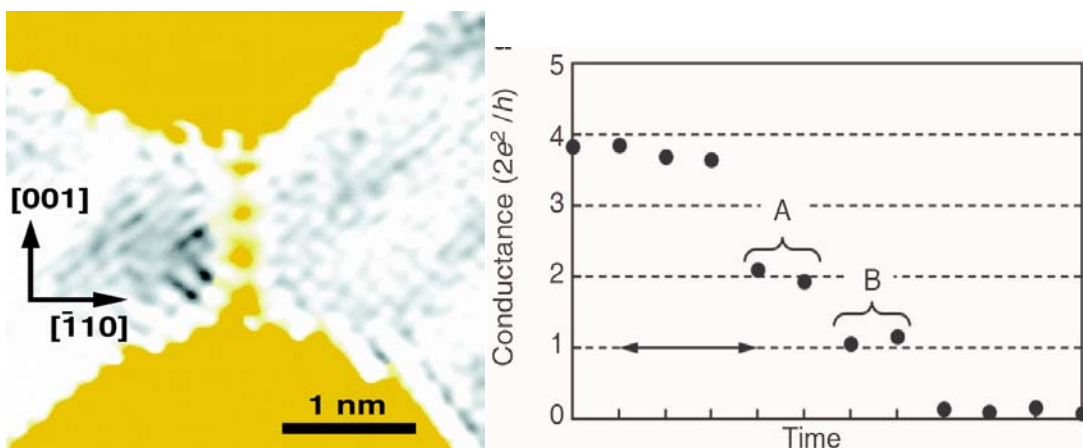
Fig. 2.6 Quantized conductance in gold nanocontacts; **Left** – electronic microscope image of a gold nanocontacts; **Right** – the conductance during breaking of the gold junction **[12]**

Krans **[13]** was introduced the use the conductance histograms in the study of conductance quantization. The method consists in the breaking, reforming of contacts many times (up to tens of thousands of times); all values for conductance are accounted. Clear and strong peaks around integer values of G_0 indicate a clear and reproducible quantization (fig.2.7). Not all metals shows pronounced histogram peaks corresponding to integers conductance values. Ruitenbeek and Yanson **[14]** studied the potassium nanocontacts and obtained conductance peaks around 1, 3, 5 and 6 G_0
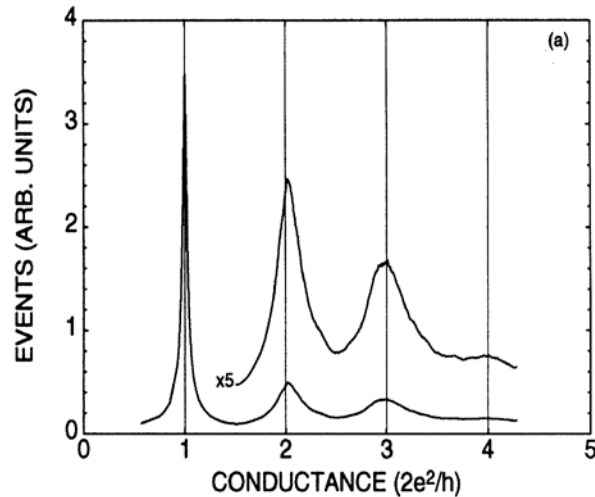

Fig. 2.7 Conductance histogram for an Au break junction. **[11]**

which is in agreement with a model of free electrons in a near perfect cylindrical symmetry (fig.2.8). In this model, described by Bessel function the first steps in conductance should be 1, 2, 2 G_0, therefore the first peaks should be around 1, 3, 5 G_0 as exactly obtained by experiment.
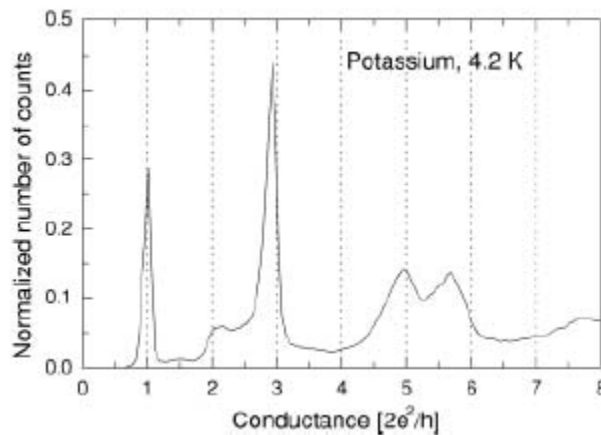

Fig. 2.8 Histogram of conductance values measured for Potassium at 4.2 K using an MBJ device. **[14]**

Krans studied the conductance in one-atom point contacts for Copper, Aluminum and Platinum (fig.2.9). He used MBJ devices, breaking them using a piezoelectric element. The experiment was focused on the study of last plateau of conductance, exactly before breaking of the contact, this state being assumed a one-atom point contact. For Copper and Aluminum the conductance value for one atom contact are very close to 1 G_0, while for Platinum the peak is higher implying that the electronic structure of atoms is relevant for one atom conduction processes **[15]**.
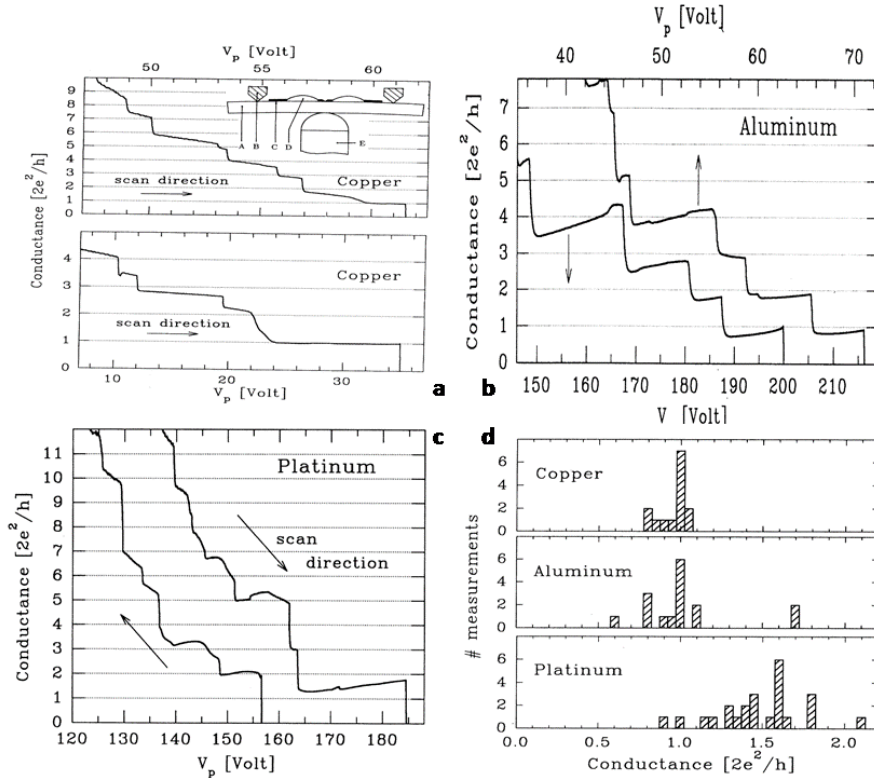

Fig. 2. 9 G (V) Conductance curves for a – Copper; b – Aluminum; c – Platinum. d – Corresponding histograms to conductance curves. **[15]**

With this frequent occurrence of the relation between transport properties and electronic structure of atoms, Scheer *et al.* developed a experimental setup able to study the transmission probability for each propagation mode (i.e. each channel) **[16]** using superconducting point contacts. Assuming that the IV curves in the contact regime cannot be described by a single channel theory they decomposed the total current as follows:

$$\mathbf{I(V)} = \sum_{n=1}^{N} \mathbf{i(T_n, V)} \qquad [2.17]$$

where $i(T_n, V)$ is the current of channel n.

Their experiment was focusing on study the transport in point contacts from Pb ($6s^2, 6p^2$), Al ($3s^2, 3p^1$), Au ($6s^1$) and Nb ($5s^1$) taking in account only channels with a transmission probability larger than 1%. Their conclusion was that the number of available valence orbitals determines the number of channels (fig. 2.10) of a one-atom contact and the transmission for each channel is depending on the numbers of neighbors and the bond distance. For monovalent metals (s – type like Au or Na), the transport
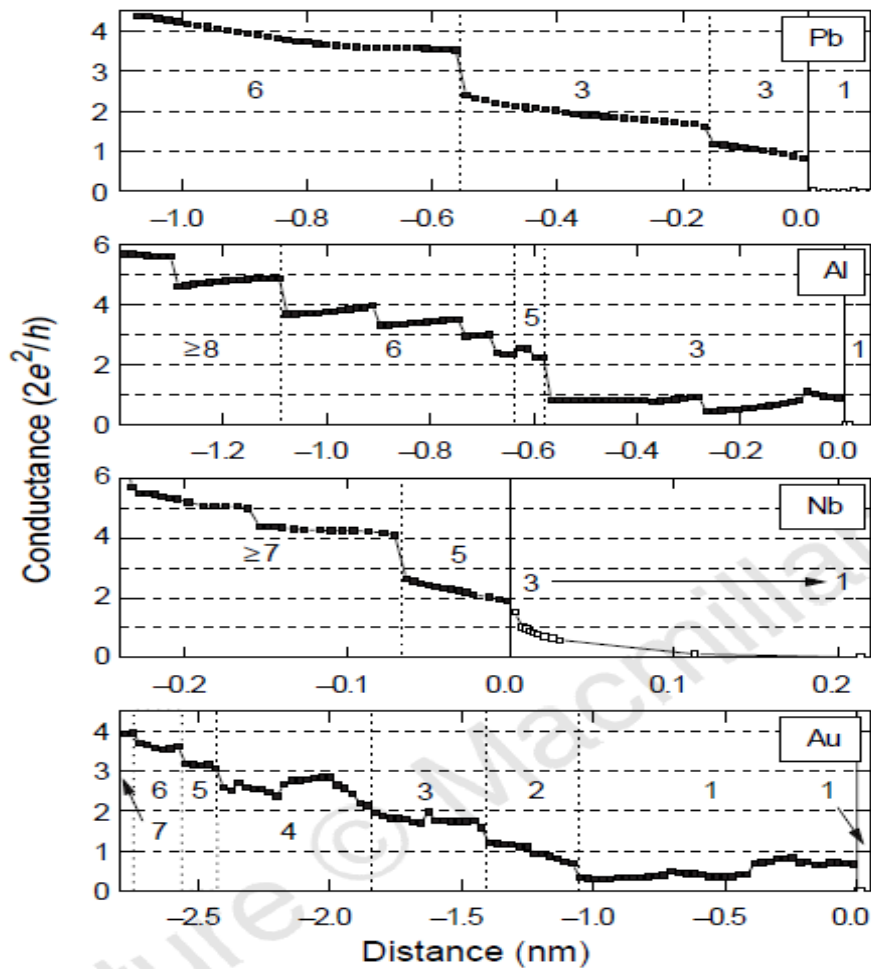
Fig.2.10 Typical conductance *G* as a function of distance, recorded during a continuous opening of the samples, for four different metals. The numbers N of the channels found at different plateau of conductance are indicated. **[16]**

through a single atom contact will be due to only one channel with a transmission close to unity while for other metals the total transmission will be a combinations of channels with different transmission probability**.**

These results were in very good agreement with theoretical calculation using the analysis of subgap structure done by Agrait **[17]**. One-atom sp metallic contacts

like Al or Pb, are characterized by a maximum of four channels of transmission, while for metals where d electrons play a dominant role the conduction is due to five channels.

2.2 Fabrication of nanogaps

As Moore's law indicates, the size of electronic elements is rapidly reducing and huge amount of efforts are being invested for developing electrical elements smaller. Understanding and mastering electronic properties of devices reaching molecular or atomic size are among the top challenges for realizing new ultra-miniaturized devices that go beyond the limits of current systems. During the last decade, many tools were elaborated for studying mechanical and transport properties of smallest possible sizes contacts.

There many issues which have to be solved, depending on the techniques used and on the type of planned measurements. One key parameter is the temperature at which the experiment is performed. At low temperatures, atomic sized contacts can be kept stable for longer time, allowing detailed investigations. However, some techniques are not suitable for low temperature measurements (like electrochemistry that are using liquids electrolytes) so fast scanning and measurement methods become crucial. Another issue is related to the cleanliness of the contact. Contamination with different impurities affects significantly the transport properties of the nanocontact **[51]**. One way to solve this is to work in Ultra High Vacuum conditions or to find ways to isolate the nanocontact form the environment influence. One crucial issue on the case of studying magnetic properties of nanocontacts relates to the mechanical effects what can intervene and alter significant the electrical properties. Magnetostatic forces, magnetoelastic modifications of the electrodes and strain in substrate can affect the configuration and the environment of the nanocontact. In the next section, I will limit my presentation to the fabrication methods of nanocontacts where data on magnetic systems is reported in literature, putting emphasis on advantages and disadvantages of each approach.

Mechanically Controllable Break Junctions (MCBJ)

This technique is the most used and clearly the most documented method for fabricating atomic sized contact. Originally used by Moreland **[18]** for studying superconductors the name of MBCJ was introduced by Muller **[19]**; Ruitenbeek **[20]** brought further improvements later. The principle of this technique, illustrated in fig.2.11 (top), relies on breaking of a metallic bridge by bending a flexible substrate (which usually is kapton) on which the material was previously deposited and patterned.

The substrate is bent by pushing the piezoelement (or just by a screw) and, by doing this, a strain is applied on the bridge, which can break or bring back in the junction. The resistance of the contact can be monitored during breaking process, which can be stopped or reversed many times thereby allowing a large number of measurements to be performed, providing therefore statistical information. The sensitivity of this method is given by the ratio between the length of the bridge (u) and the squared length of full beam support (L) between the two counter supports. Typically, these distances are 1 cm for the support and 1 micrometer for the orifice thus the sensitivity is in the 10 pm range.
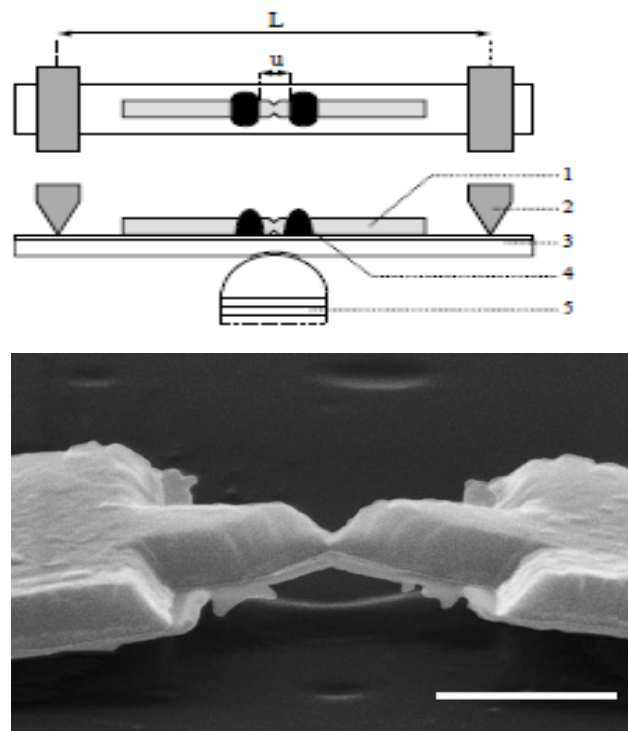
Fig. 2.11 Top: schematic top and side view of one MCBJ mounting; 1 – the metallic wire; 2- two fixed counter supports; 3 – bending flexible support; 4 – adhesive; 5 – piezoelement
Bottom: SEM image for a gold MCBJ. The horizontal scale bar is 1micrometer **[17]**

The junction can be installed in a cryostat where low temperature and high purity measurements can be realized. The only limitation of the use of this method for investigating magnetic nanocontacts is that using mechanical means for creating the contact might interfere with the search for experiments exempt of mechanical artifacts. This limitation can be overcomed by limiting the over-etched area defining the suspended bridge, but at the expenses of control of the breaking position.

In same category of MCBJ techniques, the fabrication of nanocontacts using STM can be included. Briefly, the system consists in a STM tip that can be extended and retracted onto a metallic thin film, grabbing in this way a few number of atoms as illustrated in fig. 2.12.**[17]**


approach   first contact   indentation

elongation   monoatomic contact   rupture
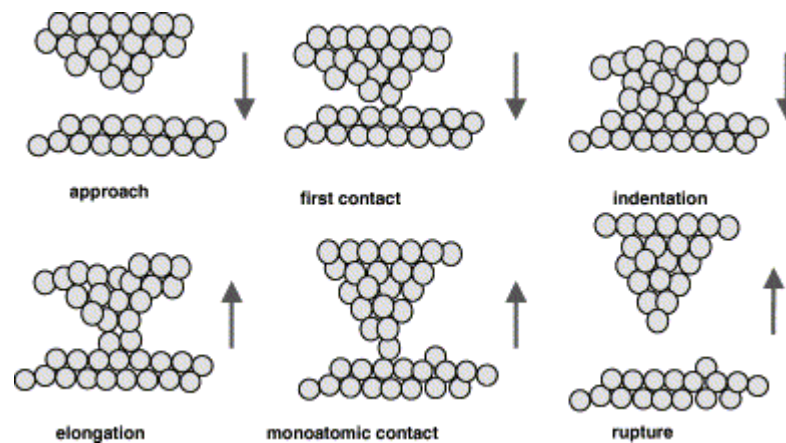
Fig. 2.12 Cartoon representation of nanocontact fabrication using an STM **[17]**

When is inserted inside a electron microscope the system is allowing imaging the nanocontacts during breaking process this one being the main advantage of the method. The problem in this set up is the short lifetime of the nanocontacts, due to the suspended design of the structure. This problem also severely limits its use for experiments under swept external magnetic field.

Electrically break junction

An alternative method to create nanoscale junction is by using the electromigration: the migration of the atoms caused by a high electrical currents density. Park **[21]** pioneered the procedure in 1999. It is starting from a nanometric metallic wire, realized usually by e-beam lithography. For localizing the process a constriction is patterned in the wire ensuring the highest locally current density. The nanocontact or the nanogap is created by controlling the amount of the current passing through the wire. The resistance is monitored during the increasing of the current and typical fast feedback loop allow a pre-set given resistance value to be obtained. Electromigration (fig. 2.13) **[22, 23]** is working by transferring momentum from electrons to atoms. It requires higher atoms mobility, which is increasing with the temperature. The process is irreversible (i.e. the forming back the contact is difficult and non controllable) but this disadvantage can be overcomed by patterning a large amount of samples of same chip, allowing many single attempts. Obtaining nanogap via electromigration is widely used in molecular electronics. The main advantage of these kinds of gaps is the compatibility with gating measurements so electrostatic coupling between molecule and the gate is allowed **[24]**. Using the gate the orbital levels of molecules can be shifted, hence many charge states became accessible for spectroscopic studies.
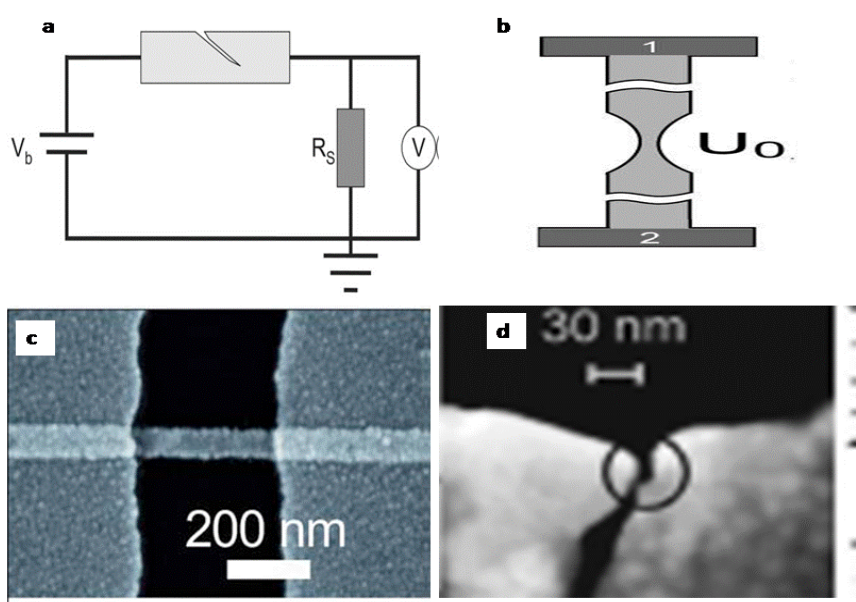
Fig. 2.13 Different stages in fabrication of electro migrated junctions. **a** - the circuit used for electromigration; **b** - schematic of the junction with leads attached; **c** - SEM of a nanowire after e-beam lithography; **d** - SEM of a nanojunction after electromigration **[22, 23]**

The main problem when one use electromigration for obtaining under 2 nm gaps (needed for molecular electronics) is the Joule heating which results in melting and surface tension effects **[25, 26]**.It is therefore crucial that the process to be indeed dominated by electromigration **[27]** to avoid the formation of gold islands. One more inconvenience related to nanogap built via this method is related to the structural quality of electrodes that must trigger the breakage **[28]**.

The electromigration is having the advantage of being suitable for ultra high vacuum and low temperature experiments. Also a very important asset is the absence of freestanding length of the sample, which is very important when MR studies are performed on nanojunctions **[29].**

Electrochemical Junctions

The electrodeposition technique for fabricating nanogaps was originally reported by Morpurgo *et al.* **[30]**, who used it for realizing Au nanocontacts. Electroplating was used to fill an initial 100 nm gap done by e beam lithography. In a very basic definition, the electrodeposition consists in the deposition of a metal on an electrode (called Working Electrode) under an electric potential. A typical electrochemistry cell (fig.2.14) consists in three electrodes, counter (auxiliary), working and reference electrode, immersed in an electrochemical bath, all connected to a controlled current or voltage source. Typical experiments relates to imposing potentiostatic conditions, namely ensuring constant voltage of the working electrode versus reference, using the counter as source or sink of current closing the circuit.
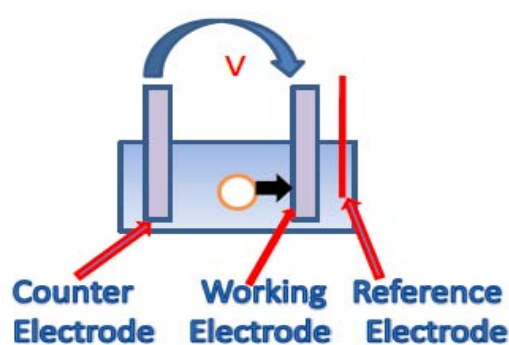
Fig. 2.14 Typical electrochemistry cell containing three electrodes

The main function **[31]** of a potentiostat is to control potential and measure current. It controls the potential of the working electrode with respect to the reference electrode while simultaneously measuring the current flowing between the working electrode and the auxiliary electrode. The potentiostatic mode refers to using a feedback loop ensuring that the requested potential value is kept constant. This also ensures constant Gibbs free energy at working electrode interface, controlling therefore the rates of chemical reactions taking place at the working electrode surface. The galvanostatic mode refers to keeping the current constant and measuring the potential.

The ***working electrode*** is that one where the reduction or oxidation reaction of interest takes place. Working electrodes are made of metals with a very clean surface that is exposed to the chemical bath. Preferred metals are platinum, gold, mercury because of their chemical inertness in a wide range of potentials but of course, one is

using the working electrode in accord with his experiment. Geometrical parameters f the working electrode are crucial in determining the current that pass the electrode, as chemical reaction will involve current density values. To give estimates in our experiments involving deposition of metals over areas in the squared millimeters range, the current is of the order of milliamps while for microelectrodes (squared microns) the values for the currents are in nano or picoamps range. In our experiments, we used mainly gold working electrodes as initial electrodes. After covering the gold with a typical transition metal (like Nickel for example), the chemical bath is in contact with the new metal, which becomes therefore the new working electrode material.
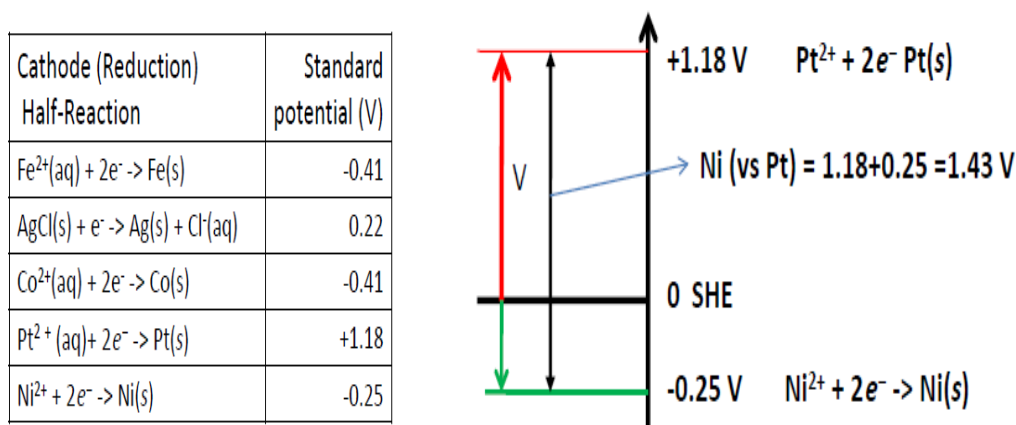
The **reference electrode** is used as a definition of absolute potential value, in order to compare experiments where a difference of potential is applied versus the working electrode. A stable indication is usually obtained by using a redox system (a system in which oxidation and reduction occur) under constant concentrations conditions. The most used and known to be more accurate is the Standard Hydrogen Electrode (SHE), (fig.2.15), which is based on the following redox half-cell:

$$2\mathbf{H^+(aq)} + 2\mathbf{e^-} \rightarrow \mathbf{H_2(g)} \hspace{3cm} [\mathbf{2.18}]$$
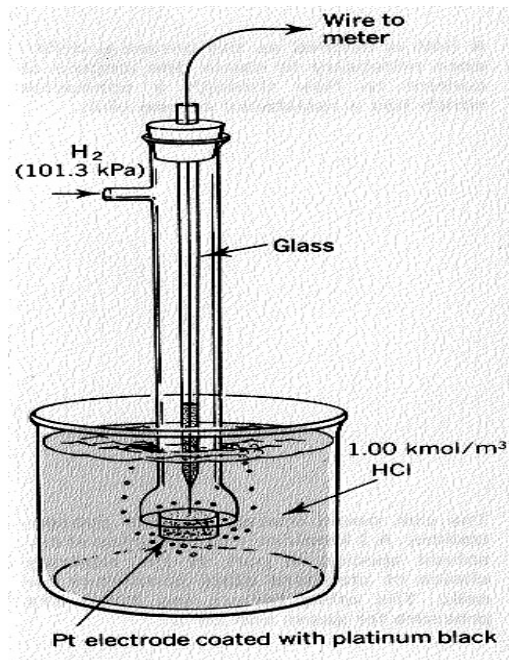
Fig. 2.15 Standard hydrogen electrode is a system in which hydrogen ion and gaseous hydrogen are present in their standard states **[33]**

This one is a redox electrode that forms the basis of the thermodynamic scale of oxidation-reduction potentials. It's absolute electrode potential is estimated to be (4.44 ± 0.02) V at 25 °C, related to the work function of Hg atom. A reference for comparison with all other electrode reactions, hydrogen's standard electrode potential (E^0) is declared zero at all temperatures [32]. Potentials of any other electrodes are compared with that of the standard hydrogen electrode at the same temperature.

SHE is often inconvenient for size, compatibility and price issues. A number of other reference electrodes have therefore been developed. Experimental measurements of potential are made relative to these alternate reference electrodes, and then the potentials are "corrected" by simple addition or subtraction and reported against the SHE [34] (fig. 2.16). In my work, I used a Platinum wire as reference, using the redox couple in the solution as reference. This is evident not a good choice, since it requires the surface of Pt to remain invariant under the variable experiment conditions occurring (non-polarizable). Pt has the advantage of being particularly inert and not modified for our metal deposition-dissolution experimental conditions. We systematically checked that using such electrode shifted the potential by typically 200-250 mV. An example calculating the $Ni^{2+} + 2e^- \rightarrow Ni(s)$ potential with respect a Pt reference is shown in fig.2.16

| Cathode (Reduction) Half-Reaction	Standard potential (V)
$Fe^{2+}(aq) + 2e^- \rightarrow Fe(s)$	-0.41
$AgCl(s) + e^- \rightarrow Ag(s) + Cl^-(aq)$	0.22
$Co^{2+}(aq) + 2e^- \rightarrow Co(s)$	-0.41
$Pt^{2+}(aq) + 2e^- \rightarrow Pt(s)$	+1.18
$Ni^{2+} + 2e^- \rightarrow Ni(s)$	-0.25

Fig. 2.16 left – standard electrode potentials in aqueous solution at 25 C (vs. S.H.E.); right – example for calculating Ni potentials vs Pt reference electrode

The **counter reference** is used to close the circuit with the working electrode, typically under monitoring of the reference electrode. If current flows through the reference electrode, its interface chemical composition may be significantly altered, causing its potential to drift away from the expected standard value. For this, it is desirable to make electrochemical measurements without current flowing through the

reference electrode. The constituent and the geometry of the counter electrode are not so essential but should nevertheless avoid polluting the bath by releasing redox by products and hindering the current in the system by limiting area exposed to the electrolyte. For our deposition-dissolution reactions, a wire made of Pt or the metal to be deposited are adequate choices.

The electrochemical bath is constituted from the analyte solution dissolved in an electrolyte. The supporting electrolyte is present in chemical bath for to increase the conductivity of solution and is normally made of ions not exhibiting redox reactions within the range of working potentials. If conductive enough, the electrolyte causes most of the potential drop to occur within a few nanometers of the electrode surfaces.

For studying the solutions in an electrochemical cell various methods are used but here, I will focus on voltametry. In voltametry the potentials is controlled and the current is measured .The cyclic voltametry consists in sweeping back and forth the potential and measuring the current. A typical IV curve obtained in this way is called a voltammogram and is shown in fig 2.17
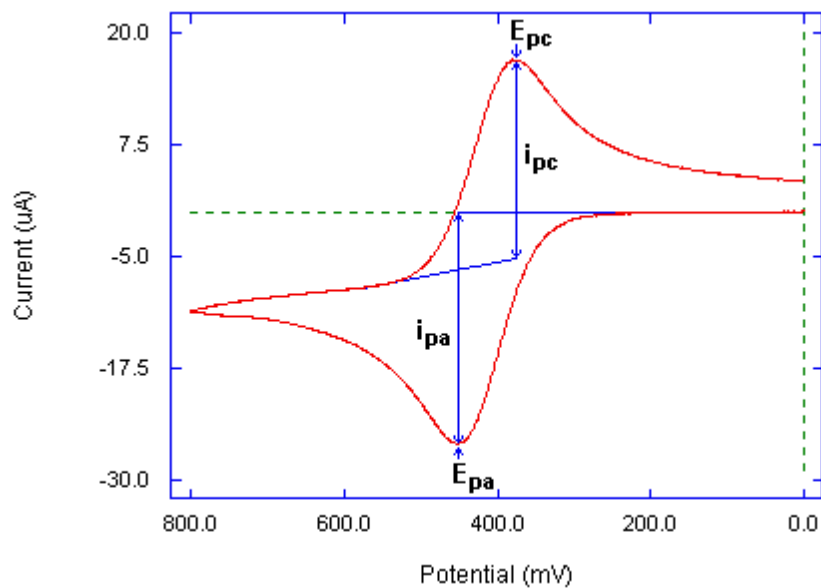
**Fig. 2.17** A typical cyclic voltammogram

The shape of a recorded voltammogram is depending mainly on:
- The rate of the electron transfer reaction(s)
- The chemical reactivity of the electro active species
- The voltage scan rate

The peaks appearing in a voltammogram are similar to those found in a spectrum or chromatography. Each peak corresponds to a particular electro active analyte in the test solution, and the height of a peak is proportional to the concentration of that analyte. For the voltammogram example from fig 2.17, we can distinguish separate regions of the curve. When decreasing the applied voltage from initial 0 V value, a current appears, indicating that electrons are starting to be transferred to electrolyte. In this specific case, ions reduced at the surface of working electrodes relate to metal depositing. The current rises as the voltage is swept further, thus converting more reactant. The peak occurs, since at some point the diffusion layer has grown sufficiently above the electrode so that the flow of reactant to the electrode becomes limited. When switching to positive potentials starts, the process is exactly the opposite, therefore at some point electrons are transferred to electrode and ions are coming back in solution (i.e. the dissolution process occurs). A peak of dissolution appears (called cathodic peak). In conclusion: it is possible to deposit or to remove a metal from an electrode only by choosing right potentials and of course an adequate analyte solution. This is the basis of building nanocontacts or nanogaps via electrochemistry method.

A common experimental setups used for nanocontacts fabrication involves two working electrodes initially separated by a gap. The deposition is taking place on both electrodes until the closure of the gap or until the desired size is reached. A typical setup for doing nanocontacts via electrochemistry is presented in figure 2.18
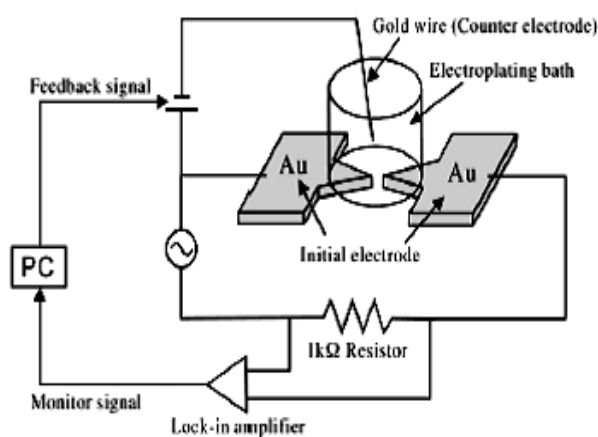
Fig. 2.18 Electroplating system used to fabricate nanogaps **[35]**

The working electrodes are immersed in the plating solution and connected to a potentiostat that is maintaining them at right potential for deposition (or dissolution). In the bath are introduced also the counter electrode and the reference (not depicted in fig.2.18). The gap is carefully monitored by measuring the impedance of the contacts, with several reported feedback parameters to stabilize the contact: high **[36]** (fig 2.19) or low **[37]** (fig.2.20) frequencies impedances, capacitance of electric double layer **[38]** (fig.2.21). The feedback information is used to change the electrochemical settings for closing, opening, or stabilizing the contact between the two working electrodes. In my thesis, I used a low frequencies technique because this one was more suitable for my experiments (considering the impedances of electrochemical baths used, as detailed explained in chapter 4).

A special case of fabricating nanogaps using electrochemistry is the so-called "self termination" method **[39]**, which is using one electrode from the contact as the counter electrode. In this method, an oxidation reaction takes place at one electrode
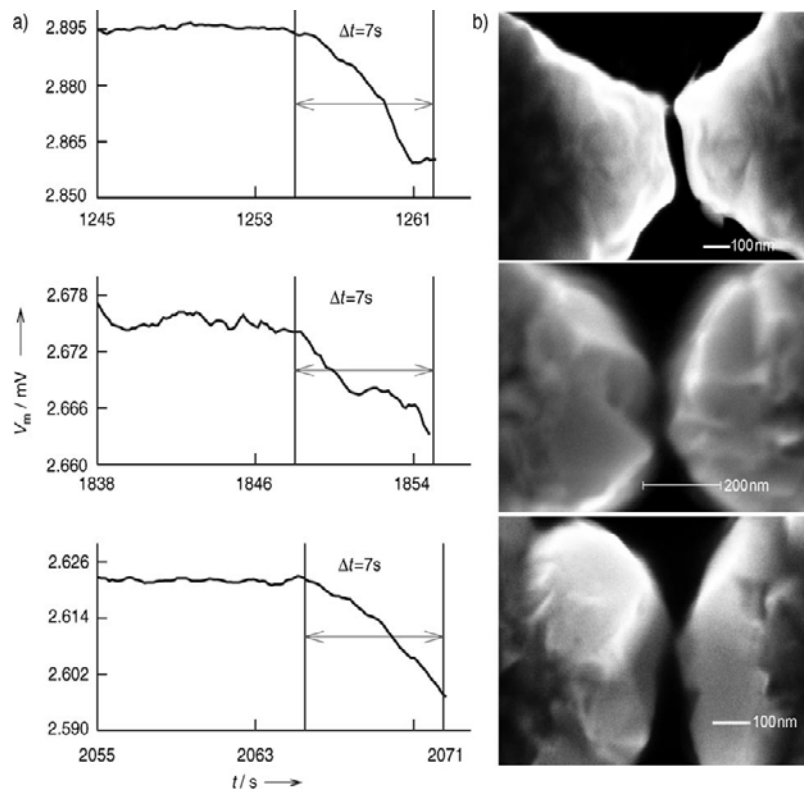

Fig. 2.19 a) The Vm–t curves of three samples prepared at 3 KHz, only the last part is shown. The controlling program stopped the deposition at the last point. Dt is defined as the interval between the inflexion of the curve and the last point. **b)** The SEM images of the resulting gap in the three samples prepared as in (a), with a gap distance of 27, 35, and 25 nm, respectively; from **[36]**

while a reduction process is occurring on other one. The possible chemical contamination of the counter electrode and the unknowns in electrochemistry processes in such confined geometry severely limit the use of such method.

In conclusion, one can say that the nanocontacts built via electrochemistry are completely different from the others due to their room temperature and liquid environment. They are in particular far from pure. As example, when depositing
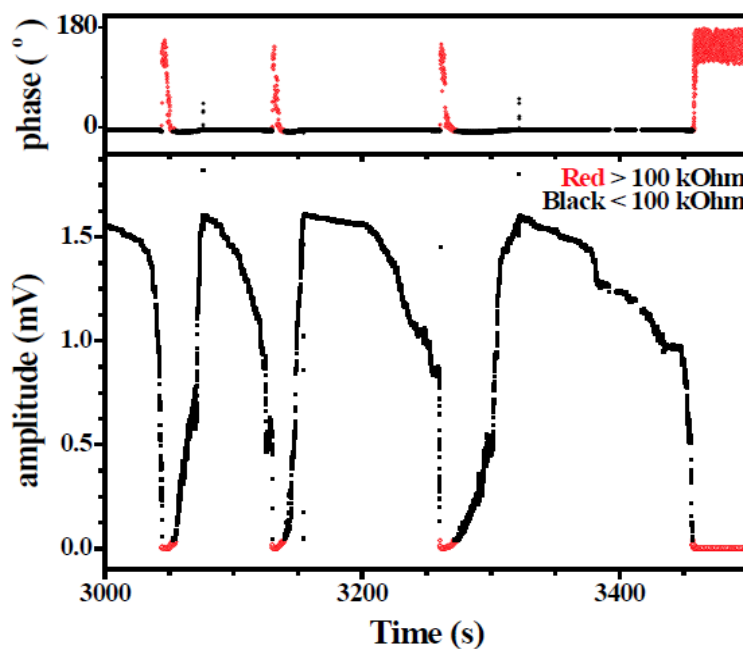
Fig. 2.20 Time trace of lock-in detection showing amplitude and phase data. Red data points correspond to the impedance large than 100 k. Using two values of DC potential, deposition and dissolution was controlled. **[37]**
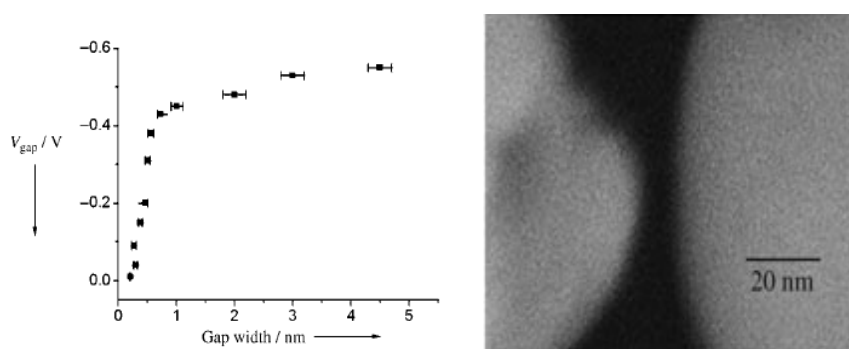
Fig. 2.21 Right - Correlation of the monitored gap width versus Vgap.
Left - An SEM image of the gap at the preset Vgap of 0.6 V. **[38]**

transition metals, the necessary reduction potentials exceed the reduction potential of water, resulting in significant H^+ evolution at the working electrode. This ensures that no oxidation occurs, but can also results in H_2 adsorption on the electrode surface. However, such electrodes are expected to have optimum mechanical and electrical stability, which are making them of interest for MR studies. The absence of surface oxidation is also a decisive advantage for MR studies, as all other fabricated electrodes have oxide on their surface due to their air exposure to air prior cooling. One can see these like an advantage in the perspective of creating applicable devices and stabilizing the surface **[29].**

2.3 Electrical transport in magnetic nanocontacts

Quantized conductance

For ferromagnetic metals (Fe, Co, Ni) the electronics states are split by the exchange interactions in two sets of band related to spin projections, which would possible, give rise to half integer steps on conductance. The large exchange energy (~eV) can make splitting observed at room temperature. The conductance of ferromagnetic metals can be represented as the sum of the contribution of majority and minority spin electrons (relative to a quantization axis)

$$G = \frac{e^2}{h}[T_\uparrow(E_F) + T_\downarrow(E_F)] \qquad [2.19]$$

where $T_\uparrow$ and $T_\downarrow$ are the spin transmission functions. If there is no scattering

$$G = \frac{e^2}{h}N(E_F) \qquad [2.20]$$

where N is the total number of channels.
For these metals, having a 3d structure the models predicts five propagation modes, partially open, resulting in a total conductance in the range of 1,5 – 3G_0. Models involving multi-orbital structures indicate no spin – dependent half integer conductance and no full polarization in ferromagnetic one – contacts **[40]**. Having a significant d electron density at Fermi level where intervene the orbital blocking **[41]**, the ferromagnetic metals are not expected to produce a perfect transmission and thus no (e^2/h) conductance quantization is expected.

Several research groups performed experiments on ferromagnetic nanocontacts and the results reveal big discrepancies. For Ni nanocontacts obtained by different methods spin – dependent conductance quantization was observed.

Ono **[42]**, who studied the conductance in MBJ Ni nanocontacts, observed this kind of behavior, sensitive to an applied magnetic field. By applying a magnetic field, the conductance steps changed from G_0 to ½ G_0 due to lifting of the spin degeneracy (fig. 2. 23).

Elhoussine **[43]** obtained same behavior for electrodeposition of Ni within the pores of track-etched polymer membranes. For Fe nanocontacts obtained by STM

technique at 4,2 K Komory **[44]** also obtained steps in conductance with (e^2/h) height, which were attributed to lifting of the spin degeneracy (fig. 2.23).
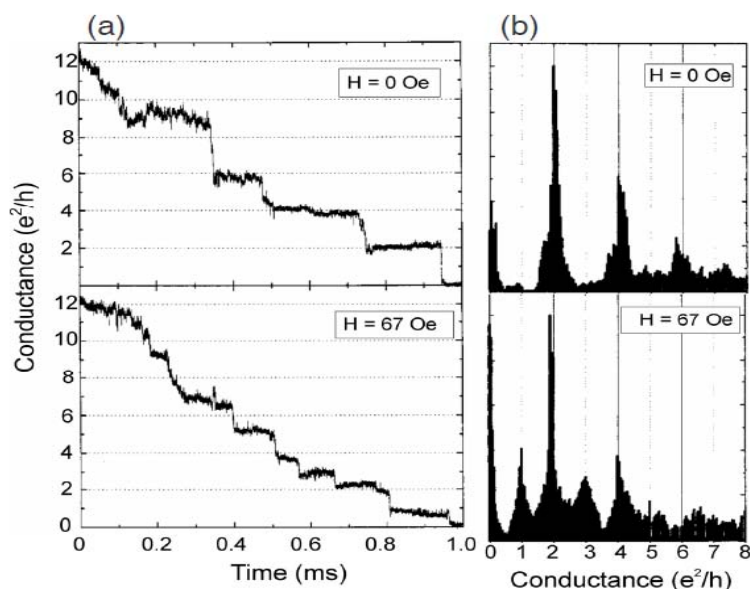

Fig. 2.22 Conductance's changes in time **(a)** and the corresponding histograms **(b)** for MBJ Ni nanocontacts magnetic field. **[42]**. Curves without (**top**) and with (**bottom**) applied magnetic field
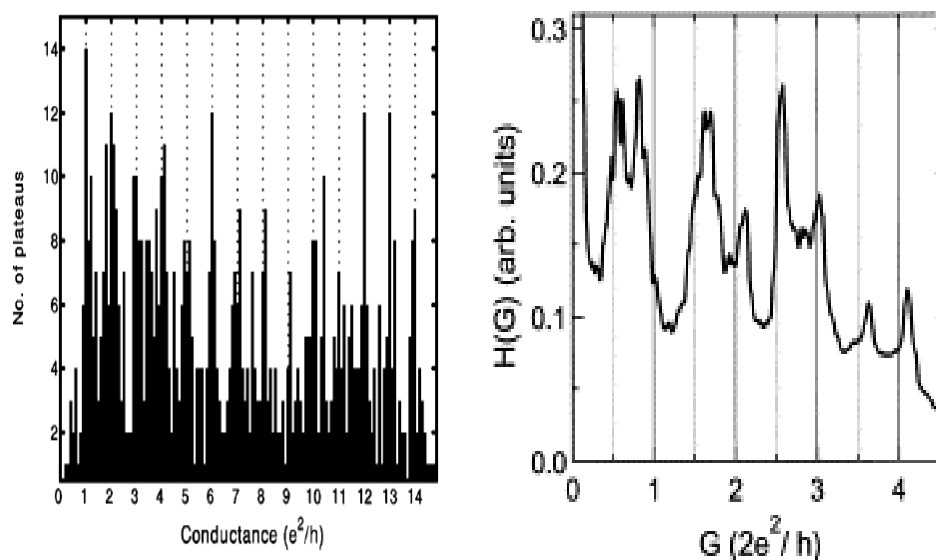
Fig. 2.23 Conductance's curves for Ni –**left [43]** and for iron – **right [44]**. Steps of (1/2 G_0) were attributed to lifting spin degeneracy.

Rodrigues **[45]** performed conductance studies on Co, Pd and Pt nanowires obtained by MBJ method. The studies were done in UHV conditions ($p<10^{-8}$ barr), at room temperature. TEM studies confirmed that structures are short chain of atoms. For all metals studied, he found steps in conductance corresponding of half G_0 (fig.2.24).

His study emphasized the fact that low dimensionality can induce or enhance a magnetic behavior **[46].**
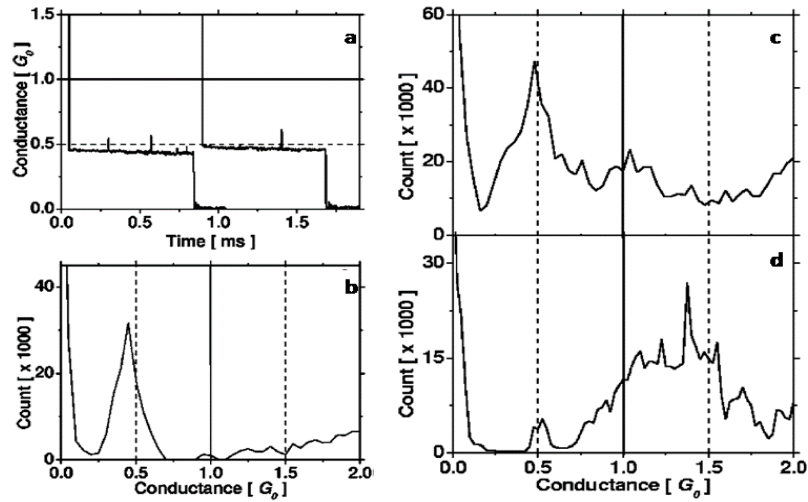
Fig. 2.24 (a) Conductance's plateau for a Cobalt MBJ nanocontact;
Histograms of conductance for Ni **(b)**, Pd **(c)** and Pt **(d)**
obtained at room temperature without magnetic field **[45]**

However, several reports of absence of simple quantization of conductance in transition metals can be found in literature. Calvo **[47]** perform experiments on Ni STM –MBJ which have shown no dependency on the magnetic field (fig. 2. 25)
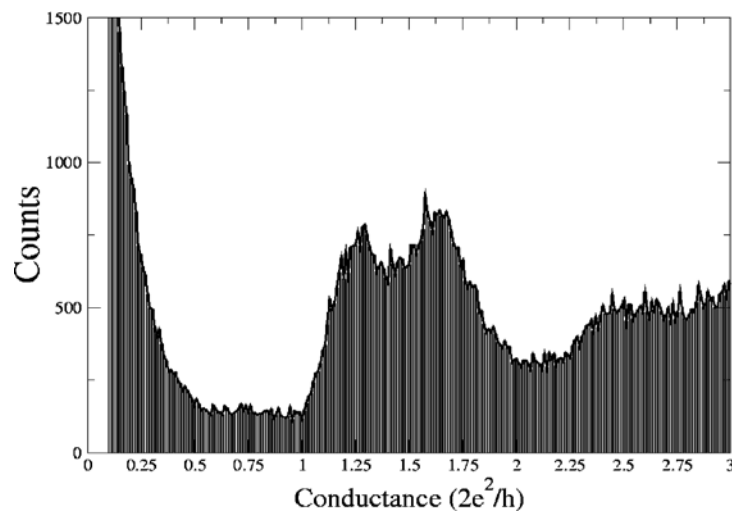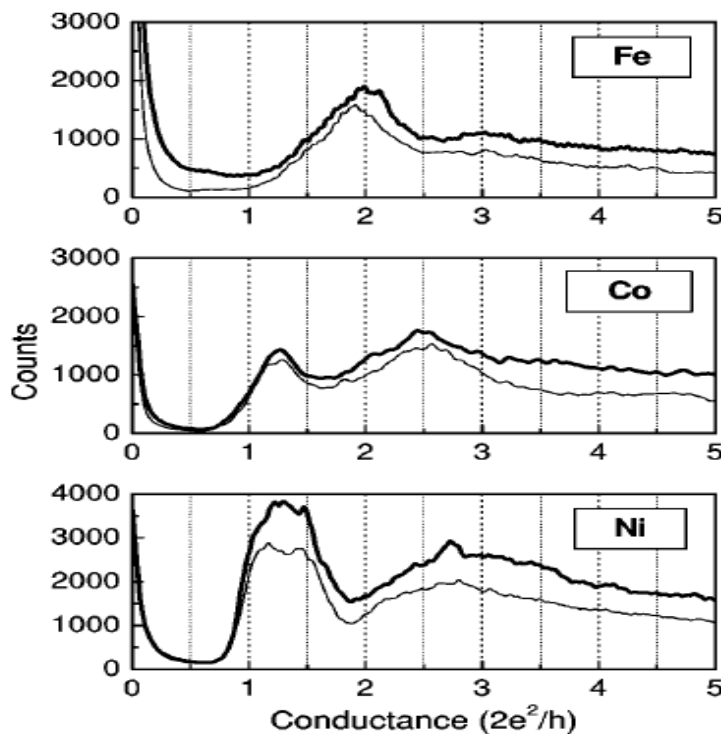

Fig. 2.25 Conductance histograms for Ni nanocontacts done by STM technique in UHV conditions at 4,2K. There are no peaks around integer's values of (e^2/h) **[47].**

Theoretical studies **[48, 49]** involving realistic atomic models involving multiorbital electronic structures of ferromagnetic nanocontacts suggested the absence of spin dependent quantization of conductance.

A very insightful experiment in this controversial field was produced by Untied **[50]**. He studied ferromagnetic nanocontacts obtained by MBJ. The experiment was performed in UHV conditions at 4,2K and he did not observed spin dependent quantum conductance even in high magnetic fields. (fig.2.26). Trying to explain the differences between his experiment and others he looked very carefully at the conditions of the experiments. Knowing that the conductance in Pt is affected by the presence of hydrogen on the nanocontact region, **[51]**, he intentionally contamined his samples with hydrogen. After contamination, new peaks appear statistically around integers values for conductance that were attributed to conduction through the hydrogen. In addition, when experiments on Pt in a CO atmosphere were performed, new peaks appeared in histograms, peaks situated close to $G_0/2$ and G_0. Fractional quantized conductance observed in some experiments can be therefore attributed to presence of some gas molecules and is not a characteristic of the contact (fig.2.27).

Fig. 2.26. Conductance histograms for ferromagnetic nanocontacts built via MBJ in UHV conditions at 4,2K. Thin lines corresponding to no magnetic field applied while thick lines are for a 5T field **[50]**
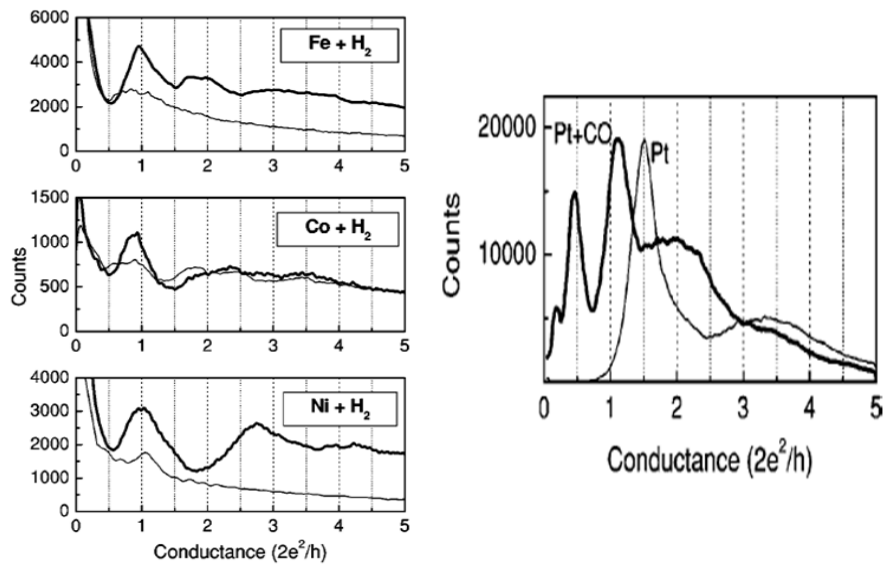
Fig.2.27. Conductance histograms for nanocontacts in an atmosphere
contaminated with H_2 (left) and CO (right) **[50]**

conduction steps in multiples of quantum conductance and for sure the controversy in this field is far to be solved. More experiments are needed where the control of atomic structure must be better controlled. Clearer indications of the statistics more detailed studies on its evolution with the number of recorded events or selection criteria are needed.. From a theoretical perspective, new phenomena (like strong electron – electron correlation) must be taken in account to possibly explain all these discrepancies **[9]**.

Magnetoresistive effects in ferromagnetic nanocontacts.

Experiments of MR properties of ferromagnetic contacts built by MBJ, ECJ and EBJ were performed due to potential very interesting applications. Garcia showed the first report (fig.2.28) of huge MR effects in 1999 **[52]** that triggered high hopes of getting new spectacular GMR-type devices when reducing the size of the conductor and entering in the ballistic regime of conduction.
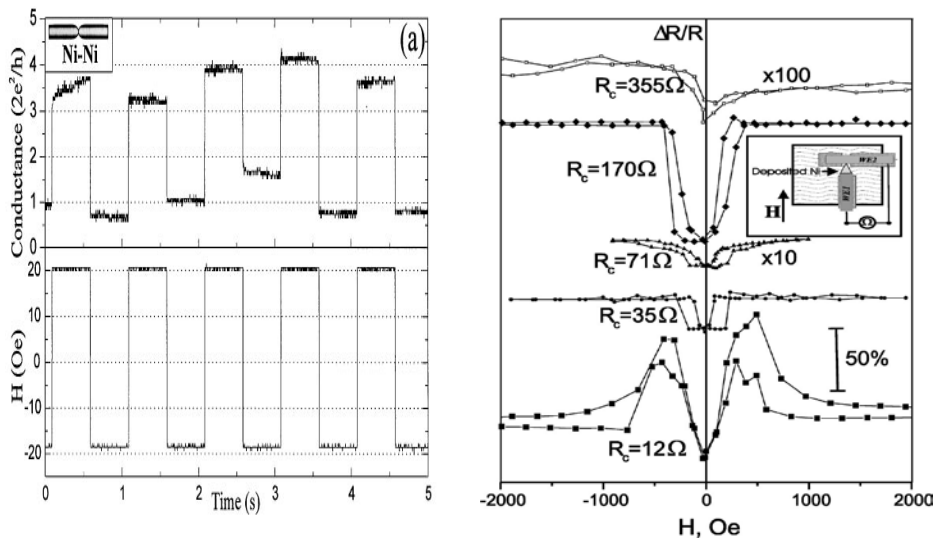
Fig. 2.28 The results of high BMR by Garcia:
left - first report of high MR effect -280%- on Ni break junction **[52]**
right – 50 % effects on Ni electrodeposited between two Ni wires **[53]**

The effect was observed for sample exhibiting low conductance of a few G_0, therefore a ballistic regime was assumed (and the effects was called Ballistic Magnetic Resistance – BMR), attributed to the formation of very thin magnetic domain walls. This first result have been stimulated the research in the field due to potential applications in spintronics devices. Garcia **[53]**, Chung **[54]** and Versluijs **[55]** obtained similar results.

More spectacular results were obtained by Chopra, Hua and Garcia, MR effects about 10,000 percent being reported **[56, 57, 58]**. In fig. 2.29 are presented results of Chopra and Garcia for electrodeposited Ni, nanocontacts showing a BMR of 3150 %, respectively 4100% at room temperature. The results were attributed to spin-dependent electron transport across nanometer sharp domain walls within the nanocontacts **[56]**.They claimed that the electronic transport essentially occurs through spin-polarized oxygen states, mechanism that gives a much higher magneto-conductance than that obtained assuming atomically sharp domain walls alone.

The highest values obtained for BMR effects were obtained also from Chopra **[58]** which used the self – termination electrochemical method described in **[39]**. He used mechanically broken Ni wires between which the deposition took place. The results were spectacular:100,000%. (fig. 2.30)
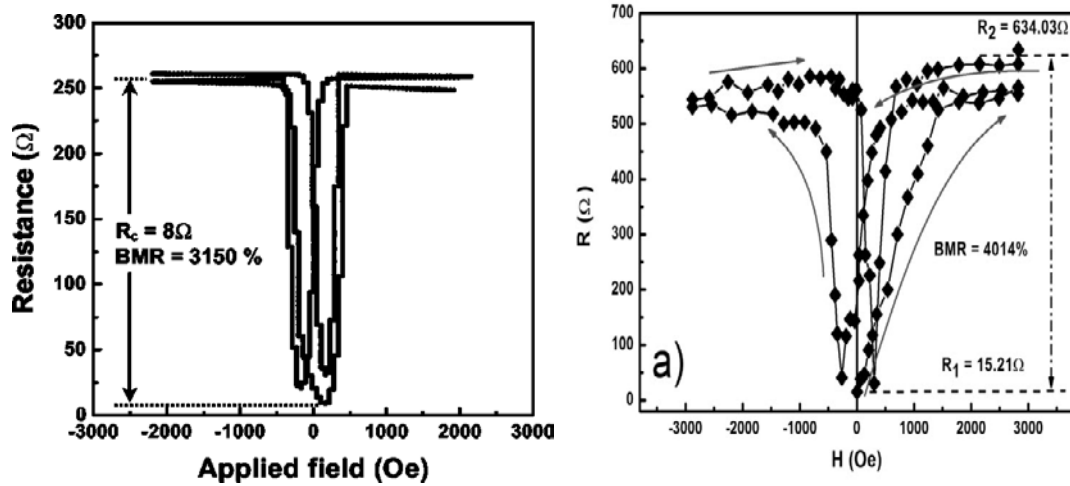

Fig. 2.29. BMR effects obtained in Ni electrodeposited nanocontacts by
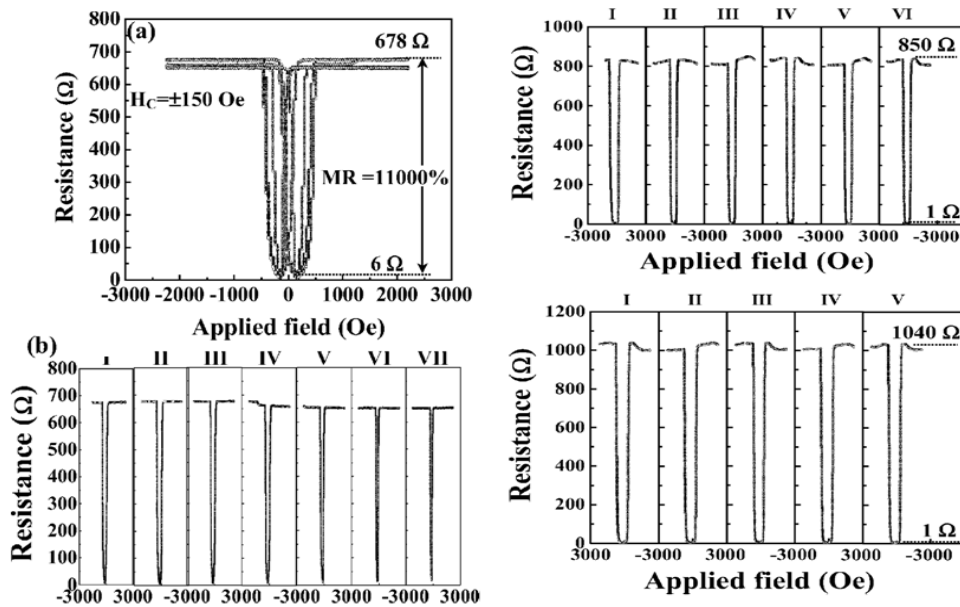**left** Chopra **[56]; right** Garcia **[57]**

Fig. 2.30 MR effects about 11 000 % (**left**) and 100 000 % (**right**) obtained by
self termination Ni electrodeposition **[58]**

The enthusiasm after getting this impressive results , with a potential huge impact on the spintronics, started to fade when researchers who were studying MR effects in ferromagnetic nanocontacts obtained by electromigration or mechanically breaking couldn't reproduce the results (fig.2.31). Viret, who performed MR studies on Ni MBJ at low temperatures obtained a maximum 40 % when the sample had a conductance of a few G_0 [59]. Experiments performed on EBJ by Bolotin [60] and Keane [61] have
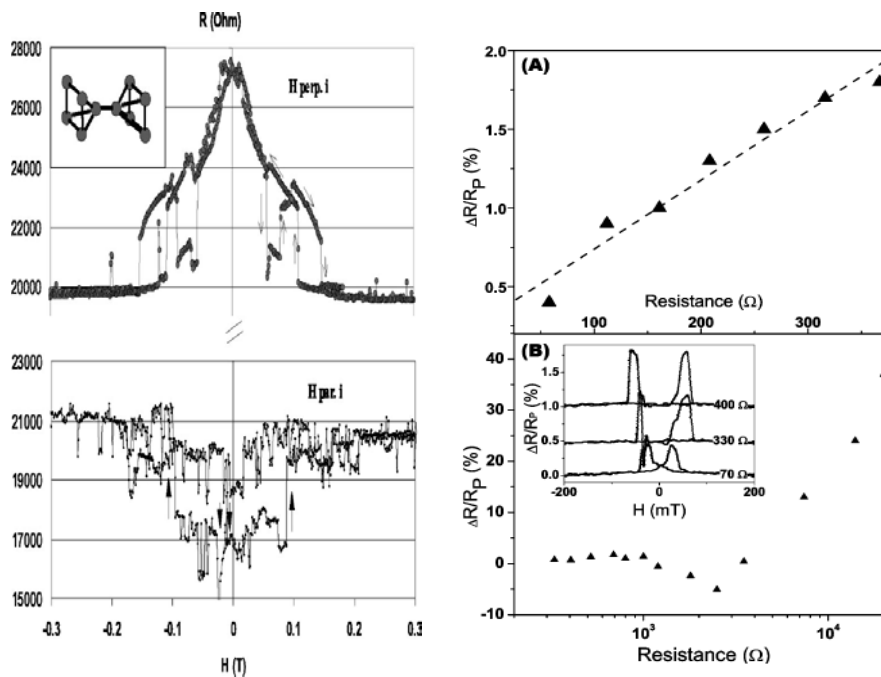
Fig. 2.31 Left – BMR effect in MBJ Ni nanocontacts on parallel and perpendicular geometries [58]; **Right** – BMR effects obtained in Ni electromigrated nanocontacts [59], the largest effects are obtained for conductance around $1G_0$

shown MR effects of maximum 80 % obtained when the sample is having a conductance around G_0, value at which ballistic conduction regime is expected to be dominant. Even for samples done by electrochemistry, the previous spectacular results could not be reproduced. Mallet [62] observed a complete lack of any MR effects while Yang [63] found a maximal value of 70 % (fig. 2.32) for MR under applied magnetic field for Ni electrochemically obtained. Trying to find an explanation for all this discrepancies, Egelhoff [64, 65] conducted experiments on investigating the stability of the electrodes of nanocontacts and the influence of magnetic forces, which can affect

or alter the measured resistance of samples. His initial goal was to find credible evidence to support the existence BMR effect in magnetic nanocontacts. He investigated both thin-film and thin-wire geometries for both mechanically formed and electrodeposited nanocontacts and find no systematic differences between mechanically formed and
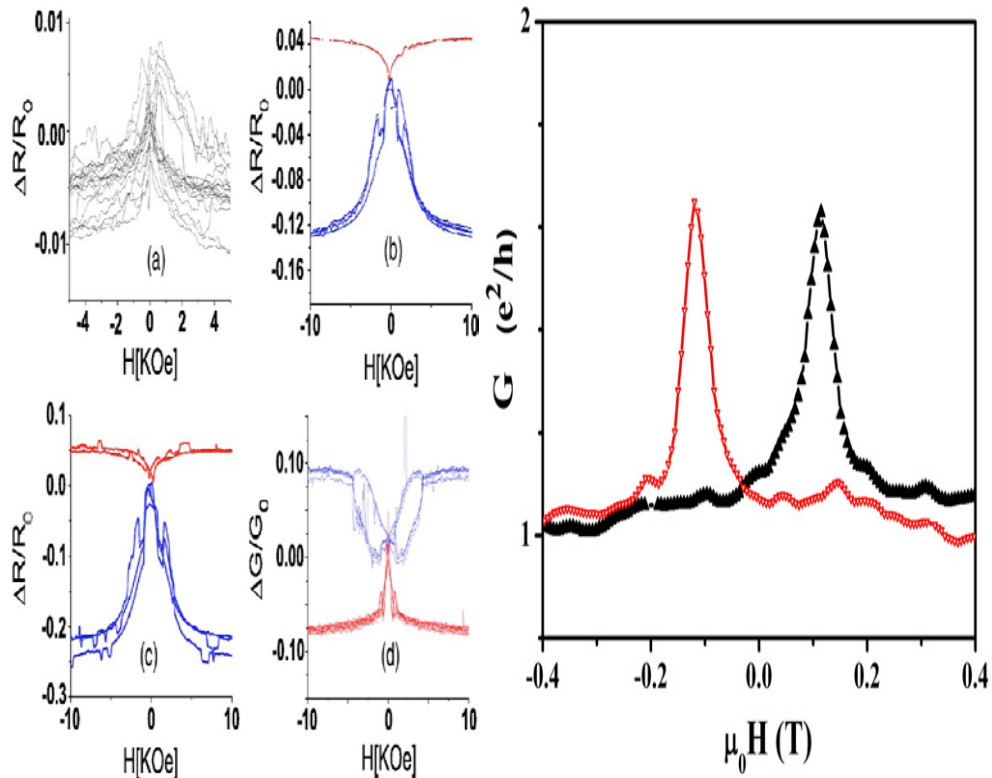

Fig. 2.32 Left – 30 % maximum BMR obtained in Electromigrated junction by Keane **[61]** (perpendicular and parallel geometry);
Right – 70 % BMR obtained in electrochemical Ni junction by Yang **[63]**

 electrodeposited nanocontacts. Egelhoff did not obtain any spectacular BMR effects but instead he did find a number of artifacts due to magnetostrictive, magnetostatic, and magnetomechanical effects that can mimic BMR.

Fig. 2.33 summarizes several possible mechanical artifacts. For 4mm long Ni wires the change in length due to magnetoelastic forces, when passing from parallel to antiparallel alignment was calculated to be around 6-8 nm . Therefore, for an assumed atomic contact with a length of few nanometers this change in length can significantly modify the conductance, essentially opening and closing the contact. Same calculation for a T-shape geometry (fig. 2.33b) indicate changes in length due to magnetostriction
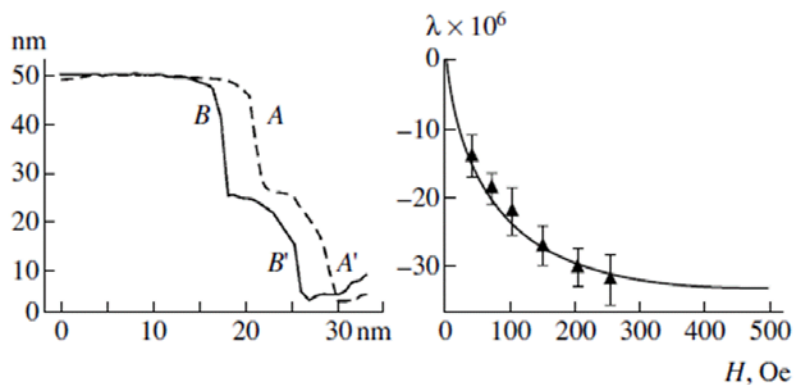
forces in the axial and transversal wires about 100 nm, therefore inadmissible for a presumed "one-atom" contact.
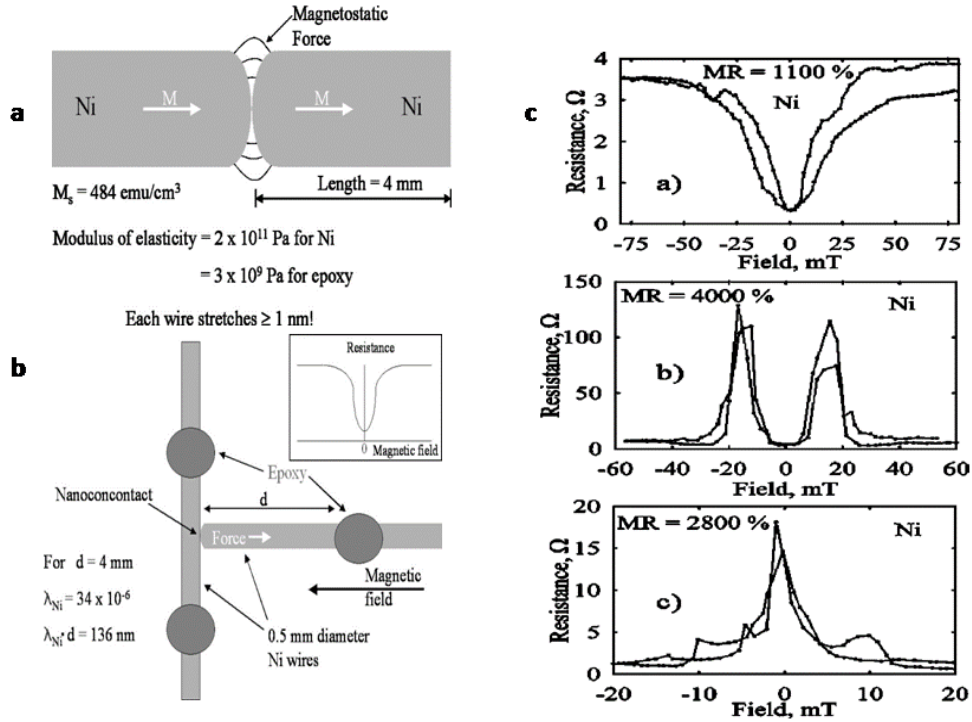
Fig. 2.33 Artifacts that can mimic the BMR **[64, 65]**
a) Magnetostatic forces in linear geometry; b) Magnetostriction forces in T-geometry;c) differences in mounting the sample


Fig. 2.34 left - diagram of the shift of the AFM image profiles upon the magnetic field switching (AA'-field off; *BB'*, field on); **right** - a plot of the experimental values of magnetostriction versus magnetic field **[66]**

Measurements on the influence of magnetostriction forces on the size of nanocontacts (fig.2.35) were also performed by Gatyatov [66] that showed that a magnetic field of 250 Oe changes the gap between two-nickel microwires by several tens of nanometers.

Gabureac [67] performed experiments on NI MBJ junctions and he claimed that even when the magnetic parts of a sample are fixed, the magnetostriction can still affect the geometry of the nanocontact and alter the BMR measurements. He found large resistance changes with the angle between the applied magnetic field and the contact and attributed these to the modifications of nanocontact geometry by magnetostriction (fig.2.35).

In conclusion [28], the magnitude of the MR does not correspond to reported results of amplitude much larger than giant MR ratios, i.e. larger than 100%. Such results confirm the claim of Egelhoff *et al.* that data attributed to very large 'ballistic magnetoresistance' is unlikely to be correct. The shape of the MR curves is in first
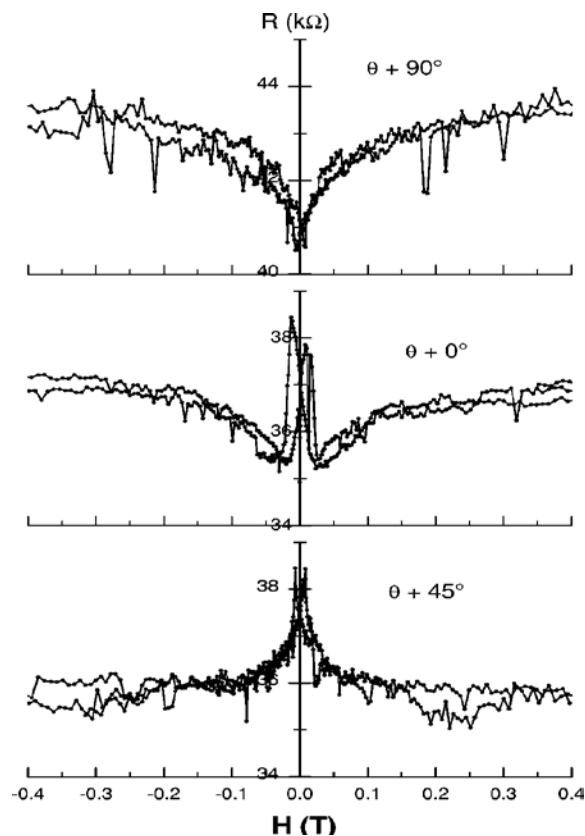
Fig. 2.35. Magnetoresistance curves for different angles between applied field and the contact. Positive and negative behavior can be observed for same sample [67]

approximation similar for all temperatures and types of samples. This is a somewhat surprising result, as the shapes, aspect ratios and environments of the samples are

different, and it is unexpected to find similarities in the magnetic properties. The magnitude of the MR decreases rapidly with decreasing sample resistance. The conductance change under sweeping applied magnetic field is of the order of e^2/h, even though the conductance varies by up to two orders of magnitude. When reaching resistance values corresponding to typical Sharvin's resistance in a metal (several ohms), the expected MR values do not exceed the few per cent range, in agreement with experiments using point contact geometry.

Another set of experiments conducted on ferromagnetic nanocontacts is related to the changes of resistance under the influence of the orientation (angle θ) of the applied magnetic field related to the current passing through the contact. This phenomenon is called ballistic anisotropic magnetoresistance (BAMR) in analogy with the anisotropic magnetoresistance (AMR) – the phenomena appearing in bulk materials. The AMR explanation relies on the Lorentz force exerted on the charge carriers, that can result in different resistivity for directions parallel ($\boldsymbol{\rho}_\parallel$) or perpendicular ($\boldsymbol{\rho}_\perp$) to the magnetization direction. The resistivity follows following relationship:

$$\boldsymbol{\rho}(\boldsymbol{\theta}) = \boldsymbol{\rho}_\perp + (\boldsymbol{\rho}_\parallel - \boldsymbol{\rho}_\perp)\mathbf{cos^2\theta} \qquad\qquad 2.21$$

The AMR ratio is the magnitude of this effect and is defined as :

$$\mathbf{AMR} = (\boldsymbol{\rho}_\parallel - \boldsymbol{\rho}_\perp)/\boldsymbol{\rho}_\perp \qquad\qquad 2.22$$

This anomalous behavior in ferromagnetic systems refers to the internal magnetic field, proportional to the magnetization of the sample. The mechanism by which this field interacts with the current in ferromagnets is the spin–orbit interaction between the electron trajectory and the magnetization. This coupling is at the origin of most anisotropic magnetic properties of materials. The electron spin sees the internal field, and the associate energy of this coupling is of form $E = \lambda\mathbf{L}\cdot\mathbf{S}$.

The AMR mechanism in the ballistic regime is completely different from that corresponding to the diffusive one due to absence of any scattering processes. When passing from bulk to atomic size the orbital moment and the spin moment per atom became larger. Like example for cobalt the orbital moment corresponding to a single atom is 5 times larger, while the spin moment per atom increase from 1.57 (bulk) until 2.08 μ_B (1D-chanell**) [28].** Therefore, this coupling is much stronger in the ballistic regime.

Velev [68] performed ab *initio* calculations for BAMR for Co and Ni while Viret [69] investigated Fe. The calculations of Burton [9] (fig.2.36) shows that the AMR in
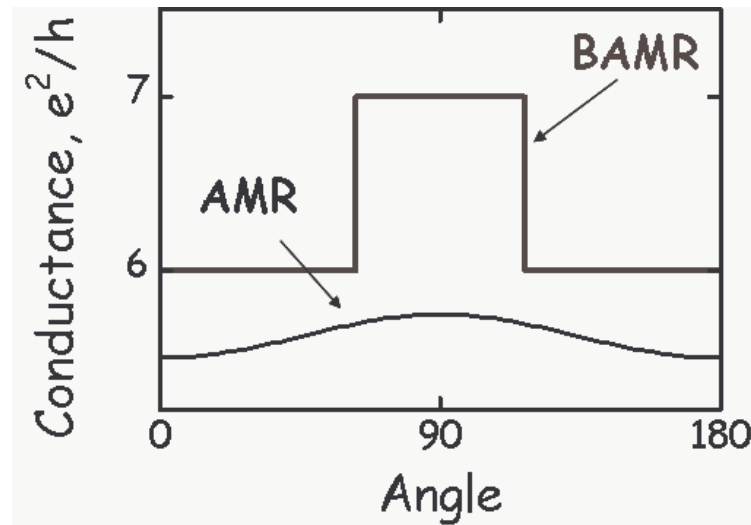

Fig. 2.36 Comparing BAMR in a Ni monoatomic wire and the AMR in bulk Ni [9]

atomic ferromagnetic contacts originates from anisotropy of the electronic structure

Doudin and Viret [28], summarize all the differences between BAMR and AMR as follows:

- BAMR relative magnitude is significantly larger than bulk AMR, with an absolute magnitude of conductance change of the order of e^2/h

- BAMR angular variation should be abrupt, as conduction channels are either open or closed, in contrast with a smooth cos2 variation of bulk AMR

- The sign of the BAMR can be either positive or negative. Calculations usually show that the parallel resistivity is larger than the perpendicular one (similarly to AMR), but there is no fundamental argument prohibiting the opposite, as the sign is mostly determined by the 1D subbands crossing at the Fermi level, which can increase or decrease when lifting the energy degeneracy through spin–orbit interaction.

There are only a few experiments on studying the BAMR in ferromagnetic nanocontacts. For a clean experiment, the samples should be saturated while varying the angle of the field. Note this experimental setup has the advantage of creating a non-ambiguous magnetic configuration on the sample, in the contrast of GMR-type studies, where a model for the magnetic configuration in an atomic-scale contact is necessary. Viret [69] did experiments on MBJ Fe nanocontacts, at low temperature (fig. 2.37). He observed clear two level effect only for samples having the low conductance values around one, two G_0, the maximum effect (top curve) being
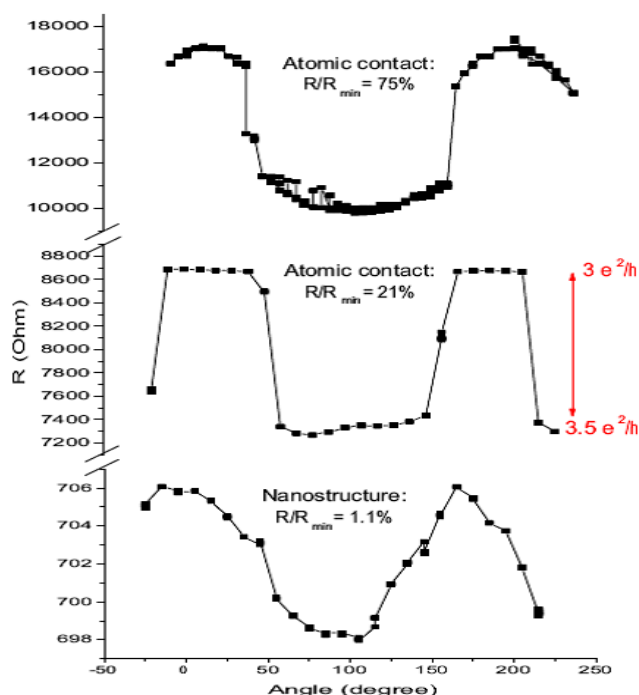
Fig. 2.37 Resistance depending on angle for different atomic Fe contacts **[69]**

measured for one quanta of conductance. As the conductance increases, the AMR effect is approaching for a $\cos^2$ behavior as in bulk materials (bottom curve).

Clearer indications of AMR properties, distinct from the bulk properties were obtained in experiments at room temperature performed by Sokolov **[70]** for electrodeposited nanocontacts of Co (fig. 2.38). He obtained clear abrupt e^2/h changes in conductance when the sample was rotating in magnetic field. Around 10% of samples have shown a change in sign of the AMR (b, c, d curves), illustrating the possibility that the number of bands crossing Fermi level can increase or decrease when the magnetization is changing its orientation. AMR studies appeared to reach some consensus, exhibiting type of behavior for nanocontacts, related to MR not exceeding a few tens of percents. Note however, that Shi **[71]** obtained two level fluctuations due to electrical noise (fig. 2.39) which can easy which can easily mimic a BAMR behavior, thus the experimentalists should be very carefully in eliminating any sources of possible artifacts. This controversy also reveals that difference in MR behavior should remain when compare samples made under very different conditions and investigated at different temperatures. Most importantly, the environment changes from UHV to concentrated ions in polar solvents.
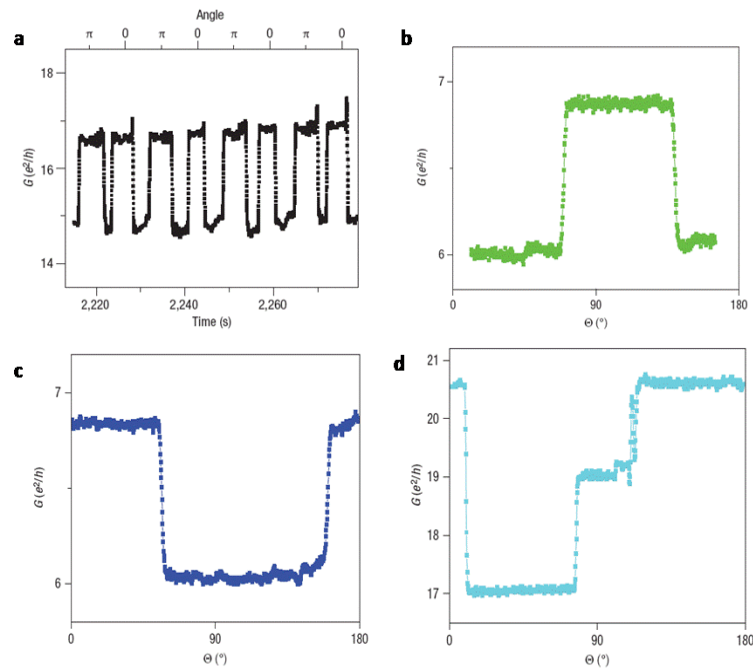
Fig. 2.38 BAMR effect obtained in Ni electrodeposited nanocontacts **[70]**;
a – evolution of the conductance in time; **b,c,d** – switching between states having conductance
values integers of (e^2/h)
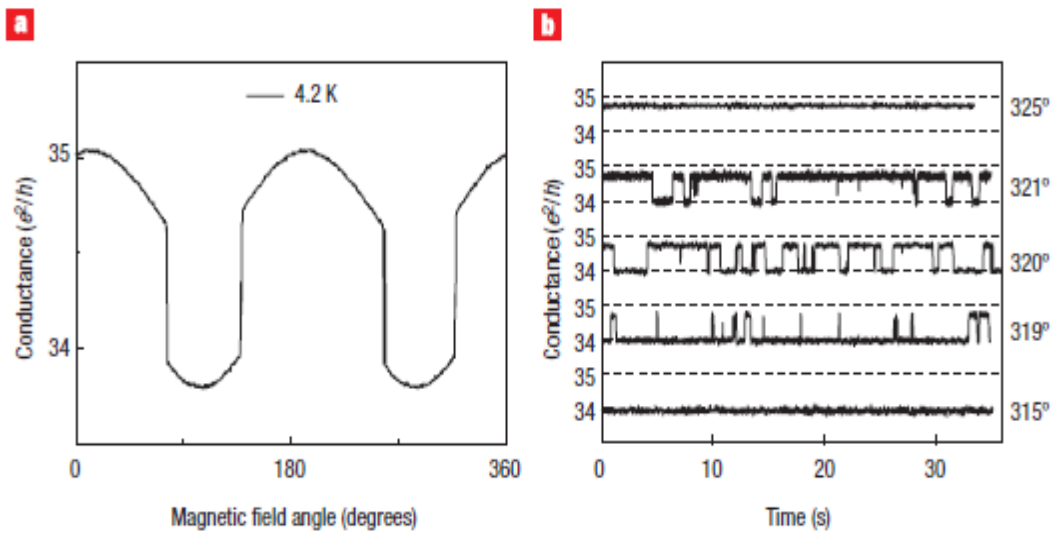
Fig. 2.39 Abrupt conductance changes in a nanoscale Ni contact at 4.2 K. **a**. Conductance as a
function of magnetic field angle, for a field magnitude of 800 mT. The field is rotated in the
sample plane. **b**, Conductance as a function of time at several fixed field angles, for the same
sample as in a. At field angles in the vicinity of the conductance steps in a, we observe two-level
conductance switching owing to atomic motion **[71]**.

Summarizing the present chapter, I can surely affirm that the topic of electric transport through nanocontacts is far from being closed. There are still many unanswered questions and many controversies that must be solved. The experiments should be improved especially in the atomic stability part and new theoretical models including possible new approximations might be necessary.

Bibliography

[1] A. Sommerfeld und H.Bethe, *Elektronentheorie der Metalle*, 1933, Springer Verlag, Heidelberg

[2] J. C. Maxwell, *A Treatise on Electricity and Magnetism, 1904,* Clarendon, Oxford

[3] Y. V. Sharvin, *Zh. Eksp. Teor. Fiz.* **48**, 984, (*Sov. Phys. JETP*, 1965, **21**, 655)

[4] J. A. Torres, J. I. Pascual, and J. J. Saenz, *Phys. Rev. B*, **49**, (1994)**,**16, 581

[5] G. Wexler, *Proc. Phys. Soc. London,* **89**, (1966)*,* 927

[6] R. Landauer, *Phil.Mag.*, **21**, (1970),863

[7] B. J. van Wees, H. van Houten, C. W. J. Beenakker , J. G. Williamson, L. P. Kouwenhoven, D. van der Marel, and C. T. Foxon, *PhysLett*, **60,** (1988), 848

[8] B. J. van Wees, L. P. Kouwenhoven, E. M. M. Willems, C. J. P. M. Harmans,J. E. Mooij, H. van Houten, C. W. J. Beenakker, J. G. Williamson, and C. T. Foxon, *Phys. Rev. B*, **43**, (1991), 12431

[9] J. D. Burton and E. Y Tsymbal, 2010, Magnetoresistive *phenomena in nanoscale magnetic contacts.* In Oxford Handbook of Nanoscience and Technology, vol.1,eds. A. V. Narlikar, and Y. Y. Fu, Oxford, UK, Oxford Univ. Press, 677-718

[10] T. N. Todorov and A. P. Sutton, *Phys. Rev. Lett.,* **70**, (1993), 2138.

[11] M. Brandbyge, J Schiøtz, M. R. Sørensen, P. Stoltze, K. W. Jacobsen, J. K. Nørskov, L. Olesen,E. Laegsgaard, I. Stensgaard, and F. Besenbacher, *Phys. Rev. B,* **52**, (1995), 8499.

[12] H. Ohnishi, Y. Kondo, and K. Takayanagi, *Nature*, **395**, (1998), 780

[13] J. M. Krans, J. M. van Ruitenbeek, V. V. Fisun, I. K. Yanson and L. J. de Jongh, *Nature,* **375,** (1995), 767-769.

[14] J. M. van Ruitenbeek, *Naturwissenschaften,* **88** *, (*2001), 59-66*.*

[15] J. M. Krans, C. J. Muller, I. K. Yanson, Th. C. M. Govaert, R. Hesper , J. M. van Ruitenbeek, *Phys Rev B*, **48**, (*1993), 14721

[16] E. Scheer, N. Agrait, J.C. Cuevas, A. Levy Yeyati, B. Ludoph, A. Martin-Rodero, G. Rubio Bollinger, J.M. van Ruitenbeek, C. Urbina, *Nature* , **394**, (1998),154–157

[17] N. Agrait, A. L. Yeyati, J. M. van Ruitenbeek, *Physics Reports*, **377,** (2003), 279

[18] J. Moreland, J. W. Elkin, *J. Appl. Physics*, **58**, (1985), 3888-3895

[19] C. J. Muller, J. M. Ruitenbeek, L. J. de Jongh, *Physica C*, **191**, (1992), 485-504

[20] J. M. Krans, J. M. van Ruitenbeek, *Phys. Rev. B*, **50**, (1994),17569

[21] H. Park., A. K. L. Lim, A. P. Alivisatos, J. Park and P. L. Mceuen, *Appl, Phys. Lett*, **75**, (1999), 301

[22] M. Z. Wu, M. Steinacher, R. Huber, M. Calame, S. J. van der Molen, C. Schonenberger, Appl. *Phys. Lett.,* **91***,* (2007), 053118-3.

[23] R. Hoffmann, D. Weissenberger, J. Hawecker, D. Stoffler, *Appl. Phys. Lett.,* **93,** (2008), 043118-3.

[24] E. A. Osorio, T. Bjørnholm, J. - M. Lehn, M. Ruben*,* and H. S. J. van der Zant, *J. Phys.: Condens. Matter*, **20**, (2008), 374121

[25] K. I. Bolotin, F. Kuemmeth, A. N. Pasupathy and D. C. Ralph, *Appl. Physics Letter*, **84**, (2004), 3154

[26] D. R. Strachan, D. E. Smith, D. E. Johnston, T - H. Park, M. J. Therien, D. A. Bonnell and A. T. Johnston, *Appl.Phys.Lett*, **86**, (2005), 0413109

[27] M. L. Trouwborst, S. J. van der Molen and B. J. van Wees., *Journal of Applied Physics*, **99**, (2006), 114326

[28] M. Bowman, A. Anaya, A. L. Korotkov and D. Davodovic, *Physical Review B*, **69**, (2004), 205405,

[29] B. Doudin and M. Viret, J*. Phys.: Condens. Matter,* **20**, (2008), 083201

[30] A. F. Morpurgo, C. M. Marcus and D. B. Robinson, *Appl. Phys. Lett.,* **74***,* (1999), 2084

[31] Educator's Reference Guide for Electrochemistry, Pine Instrument Company Grove City, Pennsylvania, 2003

[32] Sergio Trasatti, *Pure & Appl. Chem*., **58**, **7**, (1986), 955 - 966

[33] www.ktf-split.hr/glossary/image/standard_hydrogene

[34] http://www.jesuitnola.org/upload/clark/Refs/red_pot.htm

[35] Y. Kashimura, H. Nakashima, K. Furukawa, K. Torimitsu, *Thin Solid Films,* **438**, (2003), 317–321

[36] Q. Qing, F. Chen, P. Li, W. Tang, Z. Wu, and Z. Liu, *Angew. Chem*., **117**, (2005), 7949 –7953

[37] C. -S. Yang, Ph. D. thesis, University of Nebraska at Lincoln, 2004.

[38]. J. Xiang, B. Liu, S. -T. Wu, B. Ren, F. -Z. Yang, B. -W. Mao, Y. L. Chow, and Z. -Q. Tian, *Angew. Chem*., **117**, (2005), 1291 –1294

[39] S. Boussaad and N. J. Tao, *Appl. Phys. Lett*., **80**, (2002), 13

[40] A. Bagrets, N. Papanikolaou, I. Mertig, *Phys. Rev. B,* **70**, (*2004*), 064410.

[41] D. Jacob, J. Fernandez-Rossier, J. J. Palacios,*Phys Rev B ,* **71,** (2005), 220403.

[42] T. Ono, Y. Ooka, H. Miyajima and Y. Otani, *Appl. Phys. Lett*., **75**, (1999),1622

[43] F. Elhoussine, S. Matefi-Tempfli, A. Encinas, L. Piraux, *Appl. Phys. Lett.,* **81**, (2002), 1681-1683*.*

[44] F. Komori, K. Nakatsuji, *Materials Science and Engineering B*, **84**, (2001), 102-106

[45] V. Rodrigues, J. Bettini, P. C. Silva, D. Ugarte, *Phys. Rev. Lett.*, **91,** (2003), 096801

[46] *S.* Blugel, *Phys. Rev. Lett. ,* **68,** (1992), 851

[47] M. R. Calvo, M. J. Caturla, D. Jacob, C. Untiedt, J. J. Palacios, *IEEE Transactions on Nanotechnology,* **7**, (2008),165*.*

[48] A. Smogunov, A. Dal Corso, E. Tosatti, *Phys. Rev. B ,* **70**, (2004), 045417

[49] A. Bagrets , N. Papanikolaou, I. Mertig, *Phys. Rev. B ,* **75,** (2007), 235448

[50] C. Untiedt, D. M. T. Dekker,D. Djukic, J. M. van Ruitenbeek, *Phys. Rev. B,* **69**, (2004)*,* 081401*.*

[51] R. H. M. Smit, Y. Noat, C. Untiedt, N. D. Lang, M. C. van Hemert, J. M. van Ruitenbeek, *Nature,* **419,** (2002), 906-909

[52] N. Garcia, M. Munoz, Y.-W. Zhao, *Phys. Rev. Lett.,* **82**, (1999), 2923*.*

[53] N. Garcia, G. G. Qiang, I. Saveliev, *Appl. Phys. Lett.,* **80**, (2002), 1785-1787

[54] S. H. Chung, M. Munoz, N. Garcia, W. F. Egelhoff, R. D. Gomez, *Phys. Rev. Lett.,* **89**, (2002), 287203.

[55] J. J. Versluijs, M. A. Bari, J. M. D. Coey, *Phys. Rev. Lett.,* **87**, (2001), 026601

[56] H .D. Chopra, Z. S. Hua, *Phys. Rev. B,* **66**, (2002), 020403

[57] N. Garcia, H. Wang, H. Cheng, and N. D. Nikolic, *IEEE Transactions on Magnetism*, **39**, (2003), 5

[58] Z. S. Hua, H. D. Chopra, *Phys. Rev. B*, **67**, (2003), 060401

[59] M. Viret, S. Berger, M. Gabureac, F. Ott, D. Olligs, I. Petej, J. F. Gregg, C. Fermon, G. Francinet, G. Le. Goff, *Phys. Rev. B*, **66**, (2002), 220401

[60] K. I. Bolotin, F. Kuemmeth, N. Pasupathy Abhay, D. C. Ralph, *Nano Letters,* **6**, (2005),123-127*.*

[61] *Z. K.* Keane, L. H. Yu, D. Natelson, *Appl. Phys. Lett.*, **88,** (2006), 062514-3

[62] J. J. Mallett, E. B. Svedberg, H. Ettedgui, T. P. Moffat, W. F. Egelhoff, *Phys. Rev. B,* **70,** *(*2004), 172406

[63] C. -S. Yang, C. Zhang, J. Redepenning, B. Doudin, *Appl. Phys. Lett.*, **84,** (2004), 2865-2867

[64] W. F. Egelhoff Jr, L. Gan, H. Ettedgui, Y. Kadmon, C. J. Powell, P. J. Chen, A. J. Shapir, R. D. McMichael, J. J. Mallett, T. P. Moffat, M. D. Stiles, E. B. Svedberg, *J. Appl. Phys.*, **95**, (2004), 7554-7559

[65] W. F. Egelhoff Jr, L. Gan, H. Ettedgui, Y. Kadmon, C. J. Powell, P. J. Chen, A. J. Shapir, R. D. McMichael, *Journal of Magnetism and Magnetic Materials,* **287**, (2005), 496-500

[66] R. Gatiyatov, P. Borodin, A. Bukharaev, D. Bizyaev, *Technical Physics Letters,* **32**, (2006), 857-859.

[67] M. Gabureac, M. Viret, F. Ott, C. Fermon, *Phys. Rev. B* , **69,** (2004), 10040

[68] J. Velev, R. F. Sabirianov, S. S. Jaswal, E. Y. Tsymbal, *Phys. Rev. Lett.*, **94**, (2005), 127203

[69] M. Viret, M. Gabureac, F. Ott, C. Fermon, C. Barreteau, G. Autes, R. Guirado-Lopez, *The European Physical Journal B - Condensed Matter and Complex Systems,* **51,** (2006), 1-4.

[70] A. Sokolov, C. Zhang, E. Y. Tsymbal, J. Redepenning and B. Doudin, *Nat. Nanotechnology,* **2,** *(*2007), 171

[71] S. F. Shi and D. C. Ralph, *Nat. Nanotechnology*, **2, (**2007), 522

Chapter 3

Sample preparation

The following chapter describes the process of samples fabrication, starting for a bare silicon oxide wafer and ending with a pair of gold electrodes spaced by few tens of nanometers. This involves multi step process with several top-down fabrication techniques: optical lithography, E-Beam lithography, Focused Ion Beam Milling. Each technique used is briefly described and the particularities are given. A detailed description of fabrication steps for the PDMS electrochemical cell follows. A part of this chapter is dedicated to the lab on chip approach used in my thesis. Hence, in the end of this chapter, the reader has a general idea of how the samples are build and how they are integrated in the measurement circuit.
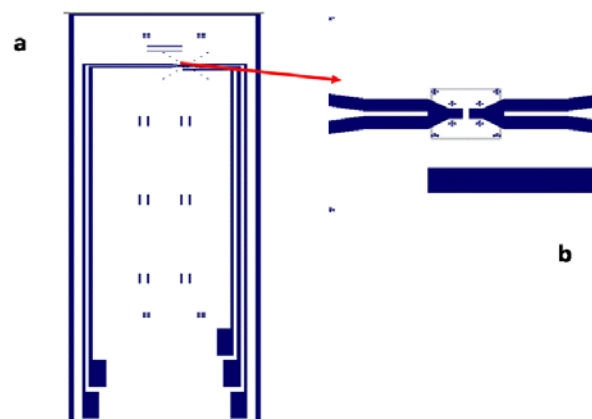
3.1 Patterning initial electrodes

The process of nanogap fabrication is starting from a bare silicon wafer and is ending with a pair electrodes separated by tens of nanometers, used like starting electrodes in the electroplating process. This part is a well defined succession of steps, each step involving different techniques and different apparatus. Most of this preparation work was done in StNANO's facilities. The main methods involved in the preparation of the samples used in this thesis research are: Optical Lithography, Electronic Beam Evaporation, Focused Ion Beam Milling and Electron Beam Lithography.

Optical Lithography

The Si/SiO$_2$ wafers from Si-Mat were initially cut in 2 by 2 cm pieces, a convenient size for subsequent processes. Four small circuits were patterned on these Si pieces. The goal is to make four contact separated by 5 micrometers for e-beam lithography or a line of 50 X 5 micrometers for subsequent FIB. The wafers were covered with AZ5214 resist, spin coated at 2000rot/min for 45 seconds and then baked for 120 s at 120^0 C on a hot plate. A special mask from Femto-ST (fig.3.1) was used in a Suss MJB4 submicron mask aligner to transfer the pattern on the wafer.
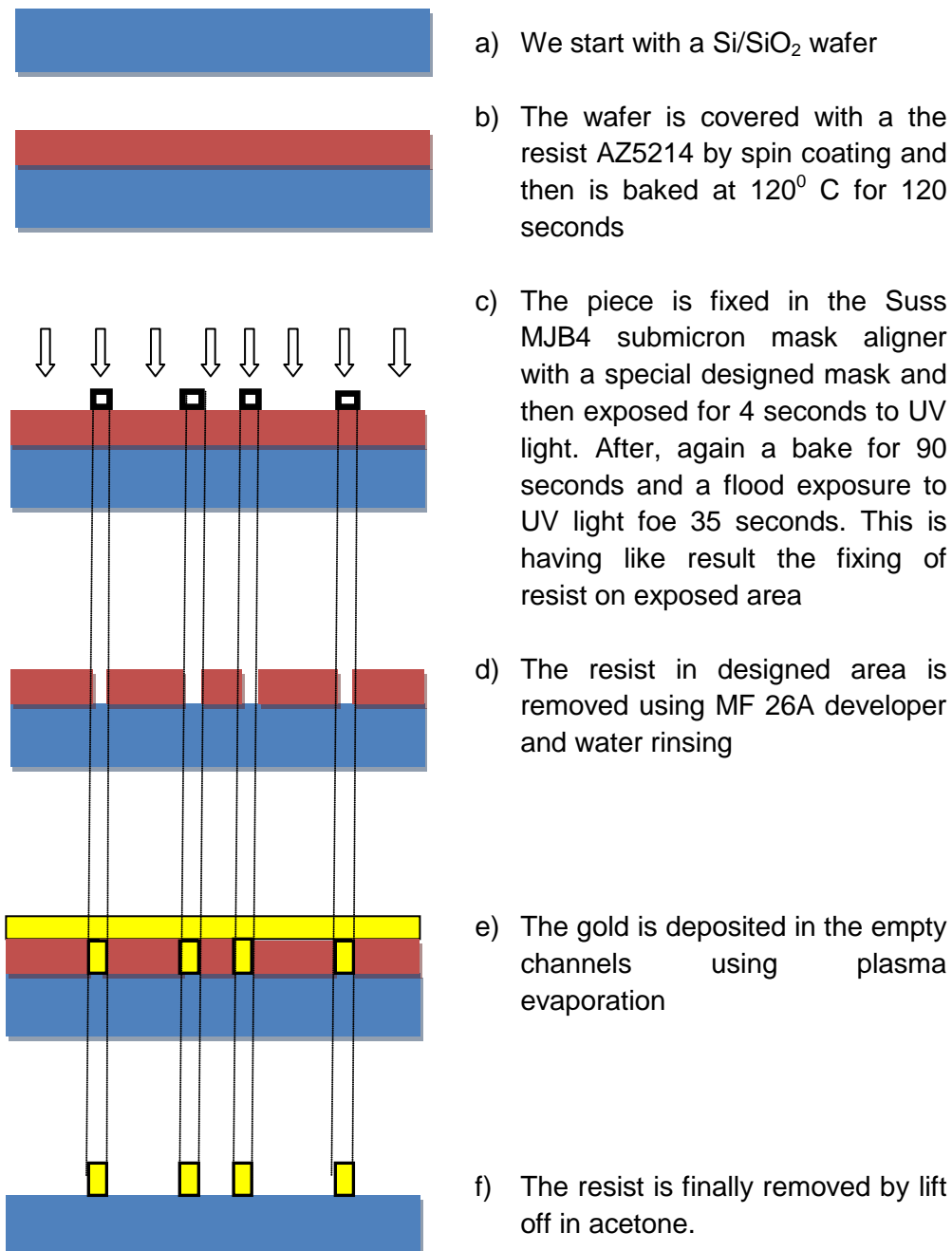

Fig. 3.1 Mask used in Suss MJB4 submicron mask aligner
a) complete view; b) zoom in the nanocontact area

The wafer, covered with resist was exposed to UV light with energy of 32 mJ, then again baked at 120^0 C for 90 seconds and again flood exposed to UV light for 35 seconds. The last step is then cleaning the samples in a special remover for the resist during 30 seconds and in water for one minute. By doing these, the final product of this step is the Si wafer covered with hard baked resist. The wafer is not fully covered, some channels, following the exact pattern of the masks used, being

a) We start with a Si/SiO_2 wafer

b) The wafer is covered with a the resist AZ5214 by spin coating and then is baked at 120^0 C for 120 seconds

c) The piece is fixed in the Suss MJB4 submicron mask aligner with a special designed mask and then exposed for 4 seconds to UV light. After, again a bake for 90 seconds and a flood exposure to UV light foe 35 seconds. This is having like result the fixing of resist on exposed area

d) The resist in designed area is removed using MF 26A developer and water rinsing

e) The gold is deposited in the empty channels using plasma evaporation

f) The resist is finally removed by lift off in acetone.

Fig. 3.2 Different processes involved in sample preparation and the successive stages of samples

resist free; therefore on those area the Silicon is exposed. A detailed flow chart of all this processes is shown in fig 3.2

E-BEAM Evaporation

After the final flood exposure to UV light and the use of remover the samples are introduced in the evaporating chamber of an E-Beam evaporator (Fig. 3.2d).The principles of E beam evaporation are well known so I mentioned them briefly.

This method is a Physical Vapor Deposition, performed under vacuum and at low temperature. The main part of the evaporator consists in the powerful electron guns (tens to hundreds of kV). The electron beam, generated by thermionic emission or field electron emission are accelerated under high electric potentials and bombards the targets.
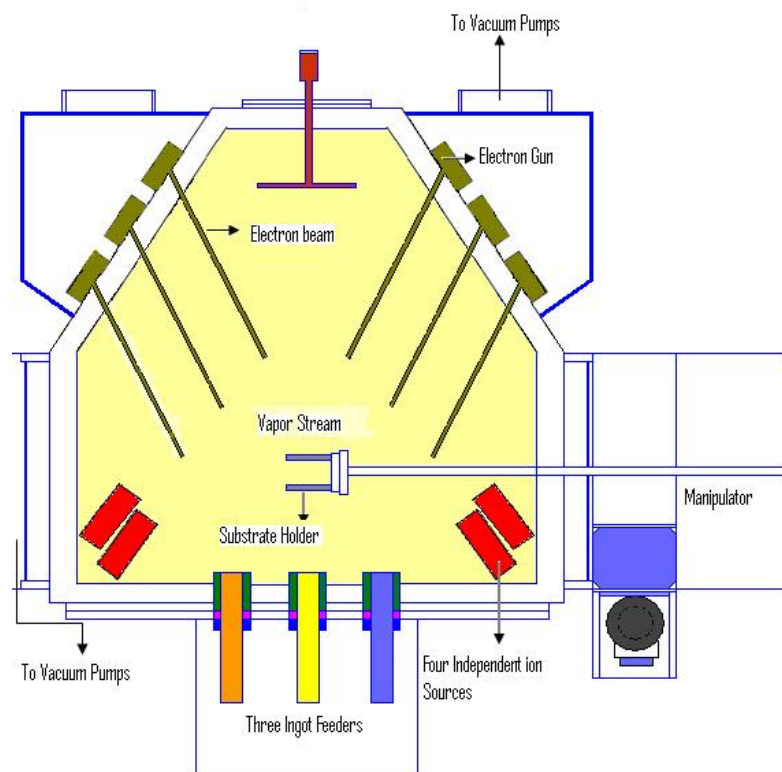
Fig.3.3. General Schematic of an E Beam Evaporator **[1]**

These targets, constituted from the materials to be deposited, evaporate under the vacuum due to the thermal energy furnished by electronic beams.

The substrates, consisting in Silicon partially covered with resist after the optical lithography described before, are fixed on a substrate holder situated in front

of the target to be evaporated. The distance between the holder and the target can be modified depending of the deposition regime desired. For assuring a good uniformity of film deposited the sample holder is rotating during evaporation. A negative DC voltage of few hundreds of Volts is applied on the holder to ensure a needed geometry of electrical field inside of deposition chamber.

In CNRS Strasbourg cleanroom, an E-beam evaporator dedicated to lift-off technique (Plassys MEB 550) is used. It is used to deposit various materials like Au, Ni, Pt, Cr, Ti, etc. It is fully automatic, controlled by software. It was calibrated for different deposition rates of different materials so the operator is just choosing the best thickness for his needs. This evaporator has an ion gun also, mainly used for the primary cleaning of the substrates. Deposition rates varying from few Angstroms by seconds to micrometers by minutes can be obtained.

We deposited first a 5 nm thin layer of Titanium and then the Gold, being well known that the directly adherence of the Gold on SiO_2 is not so good. Depending of the further processes we obtained two different of samples with different geometry shape of electrodes (Fig.3.4.). The height of deposited gold layer is 50 nm; hence one can have an idea about roughness from this figure.
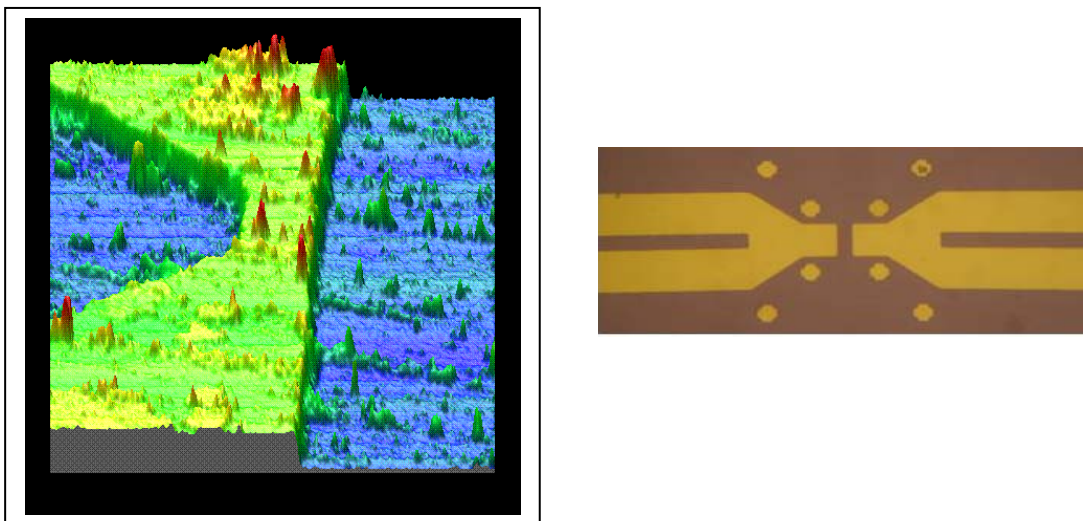

Fig. 3.4 Samples after E beam evaporation;
left –AFM image for a sample prepared for subsequent FIB;
right – optic image for a sample prepared for subsequent E-Beam

Electron Beam Lithography

Electron Beam Lithography uses a focused beam of electrons to irradiate a resist following a preprogrammed pattern. It simply draws the pattern over. A high resolution results from the short wavelength of the 10 – 50 keV energy of the electron beam and it limits damage on a thin resist. It is a mask less process, the pattern being directly realized by the electron beam. A typical EBL system consists of the following parts (fig 3.5):

1) an electron gun or electron source that supplies the electrons;

2) an electron column that 'shapes' and focuses the electron beam;

3) a mechanical stage that positions the wafer under the electron beam;

4) a computer system that controls the equipment, in particularly being able to turn "on" and "off" electrostatically the focused e-beam.
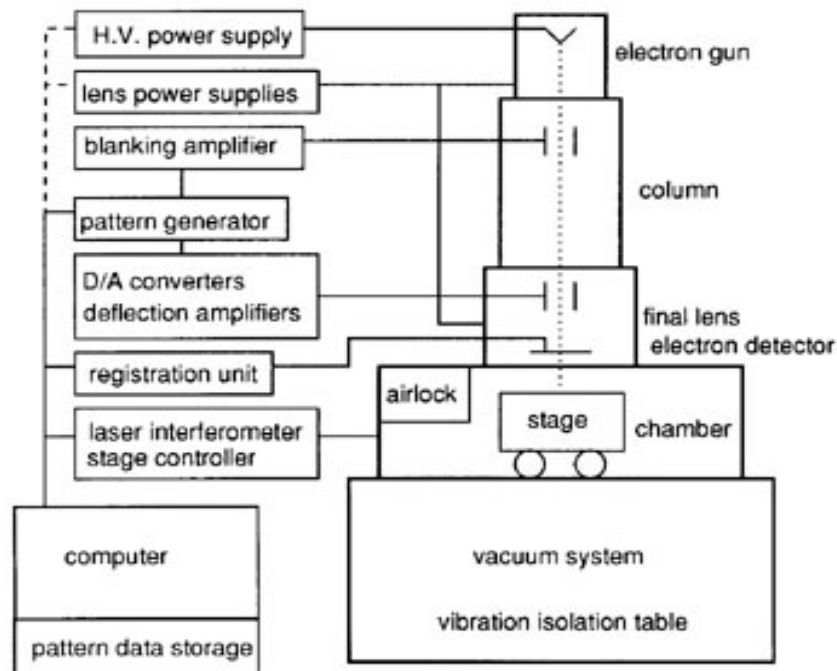

Fig. 3.5 Bloc diagram for an EBL setup **[1]**

This technique can be used to fabricate gaps down to 5 nanometers or even less, being preferred especially because is a "no mask" process **[2, 3, 4]**

The E-Beam lithography was performed in the eFab facilities of IPCMS. A high tech E beam – SEM setup from Zeiss is the main endowment of this lab. It is a ZEISS SUPRA 40 SEM with GEMINI technology integrated. A beam booster is an

integral part of the GEMINI® electron optical column (fig.3.6). The beam booster always maintains high beam energy throughout the entire column, regardless of the electron beam energy selected by the operator. Only after passing through the scanning system is the electron beam decelerated to its selected landing energy. The electron beam path has been designed to eliminate crossover of beam electrons between source and specimen Furthermore, the high beam energy throughout the column ensures that the GEMINI® column is extremely well protected against stray magnetic fields, even when operated at very low voltages. The tolerable stray magnetic field limit is therefore independent of the selected voltages. An electromagnetic, multi-hole aperture changer is incorporated close to the electron source, in combination with a magnetic field lens to select the optimum beam aperture angle and to tune the probe current. The combination of the high beam energy and cross-over free electron beam path also minimize the statistical Coulomb interactions between beam electrons, which tend to reduce the brightness and hence the resolution limit of the microscope **[5].**
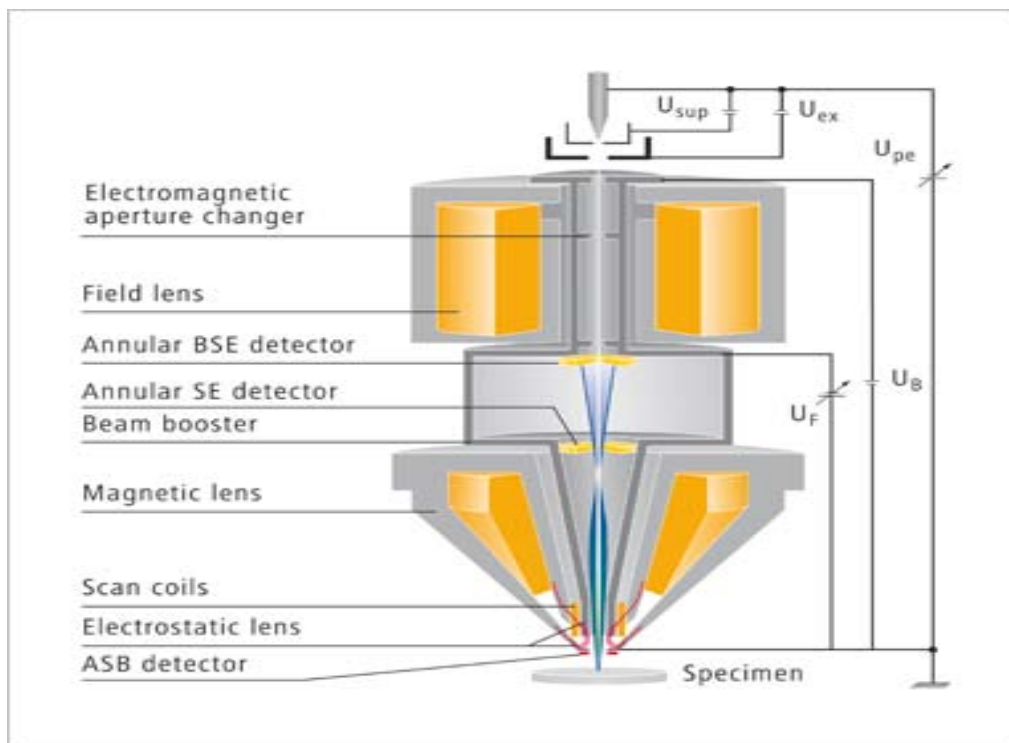

Fig. 3.6 Operating principle of the GEMINI® field emission column **[1]**
U1 - extractor voltage at first anode; U0 - accelerator voltage at second anode; UB - booster voltage

For our sample the e-beam lithography is performed with a Zeiss Scanning Electron Microscope (SEM) and a Raith EBL tool. A double resist layer system is spun on the sample. The first layer is MMA EL 9 (MethylMethAcrylate) resist from Microchemical spun at 8000 rpm and baked at 150°C for 2 minutes. The second layer is PMMA A3 (PolyMethylMethAcrylate) resist from Microchemical also spun at 8000 rpm and baked at 180°C for 2 minutes. This ensures the recessed shape of the resist after development, optimized for subsequent metal layer lift-off process. Then the system is relaxed for at least 30 minutes. SEM parameters are: an extraction voltage of 30kV, a diaphragm aperture of 30µm and a working distance of 8mm. EBL parameters are a current around 0.30nA, an area dose of 450µC.cm^{-2}, an area dwell time of 0.02nm. The pattern used (fig. 3.7 a) is two tips face to face separated by a 50nm gap. Development time is 40s in MethylIsoButylKetone/isopropanol (MIBK/IPA: 1/3) and 20s in IPA. This double layer system allows the patterning
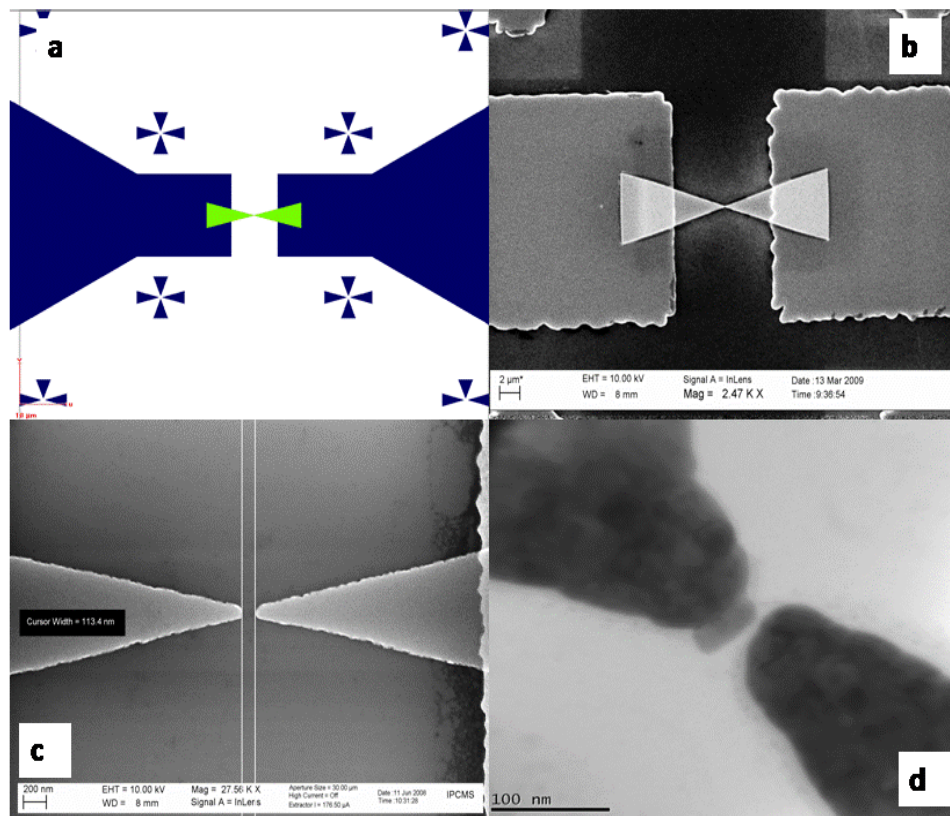

Fig. 3.7 a – Mask used in E-Beam Lithography; b – The nanogap after Lithography, SEM image, 2 microns scale c– The nanogap after Lithography, SEM image, 200 nm scale; d – The nanogap after lithography, TEM image, 100 nm scale;

of reproducible nanogaps around 30nm. Due to proximity effects, the MMA layer is dissolved in the insulated part as well as in the 30nm gap. The PMMA layer is dissolved only in the insulated part forming a PMMA bridge over the substrate. Substrate is then introduced in the load lock of a Plassys e-beam evaporator and the procedure of cleaning, metal evaporation and lift-off are the same than those described for the UV lithography step. In the end a gap with a separation around 30 nm is obtained as depicted in fig.3.7

Focused Ion Beam Milling
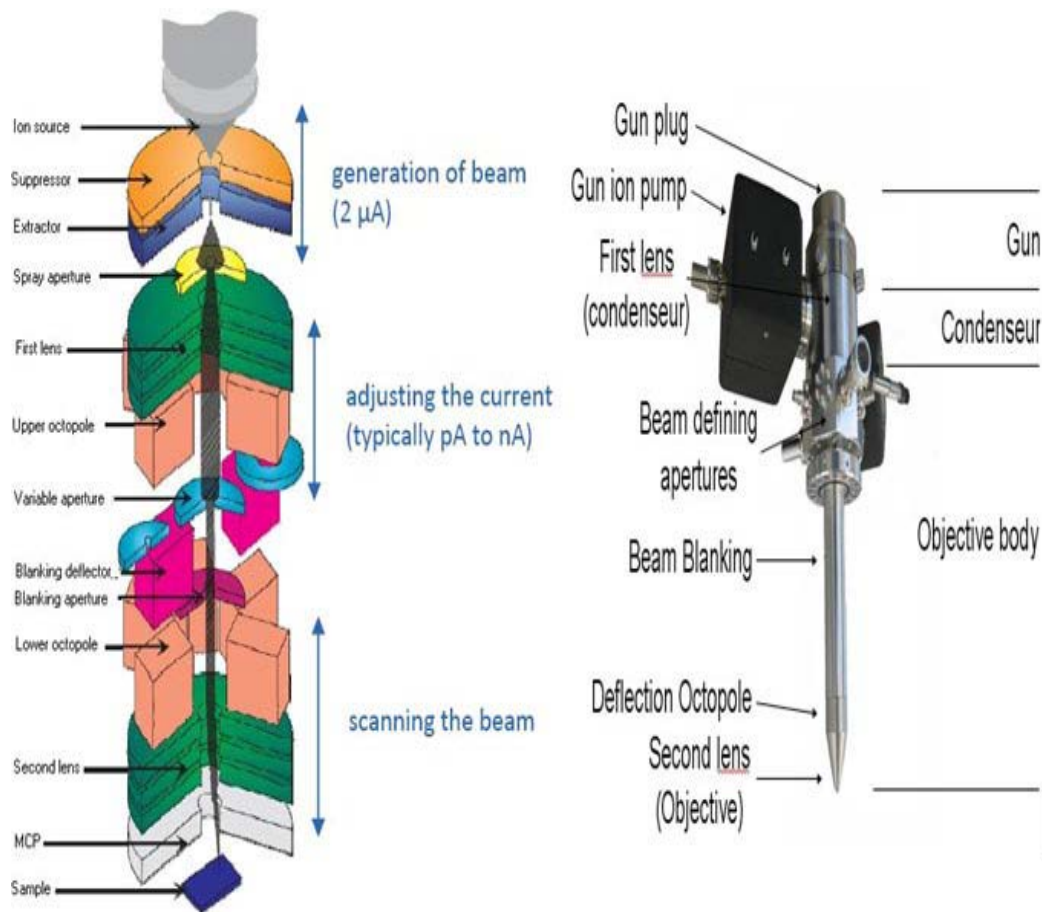
Fig.3.8 Diagram of a FIB setup **[1]**

Focused ion beam, also known as **FIB**, is a technique used in materials science fields for site-specific analysis, deposition, and ablation of materials. Usually FIB is typically using Ga ion beams. These ions are accelerated to energy of 5-50

keV and focused onto the sample by electrostatic lenses. FIB is very similar in functioning with a SEM but is using ions instead of electrons (fig.3.9). The ions are larger, heavier and slower than electrons, hence they interact less with core atom electrons; they have more momentum in interactions and are milling materials within a sputtering process (fig. 3.9). This milling technology is used wide nowadays to obtain gaps down to tens of nanometers, depending on the resolution of the primary ion beam **[6, 7, 8]**.
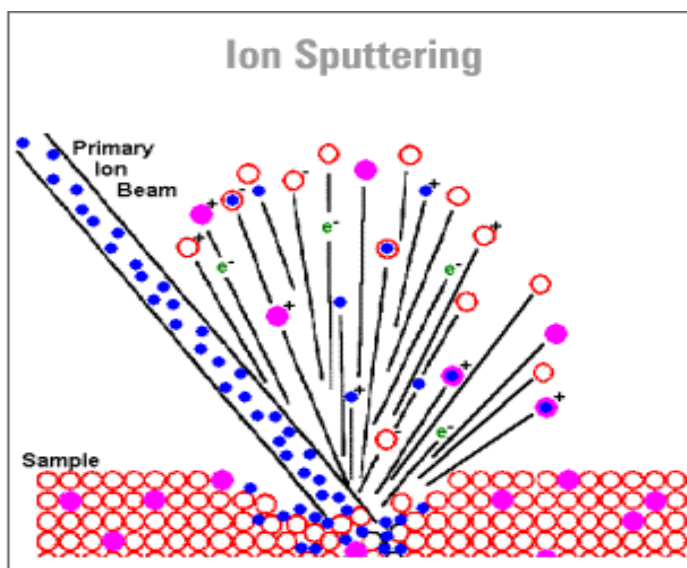

Fig.**3.9** FIB principle: Gallium (Ga+) primary ion beam hits the sample surface and sputters a small amount of material

In this work a FEI Dual Strata Beam 235 FIB (5nm)-SEM (1nm) from ISIS (Institute de Science et d'Ingénierie Supramoléculaires Strasbourg) was used. This FIB, composed by a 30 keV gallium ion beam column was used to fabricate the nanogaps. The ion current used for milling was 50 pA. Nanogap electrodes are milled in a two-step process (Fig.3.10.), firstly formation of two triangular shaped electrodes (conjoined), and secondly, a thin horizontal cut is made to separate the electrodes. Reproducible nanosized gaps of 40-50 nm (fig.3.10) were successfully fabricated. Scanning electron microscopy imaging and measurements of leakage current below 1 pA at several volts applied bias were used to quantify and check the initial gaps fabrication.
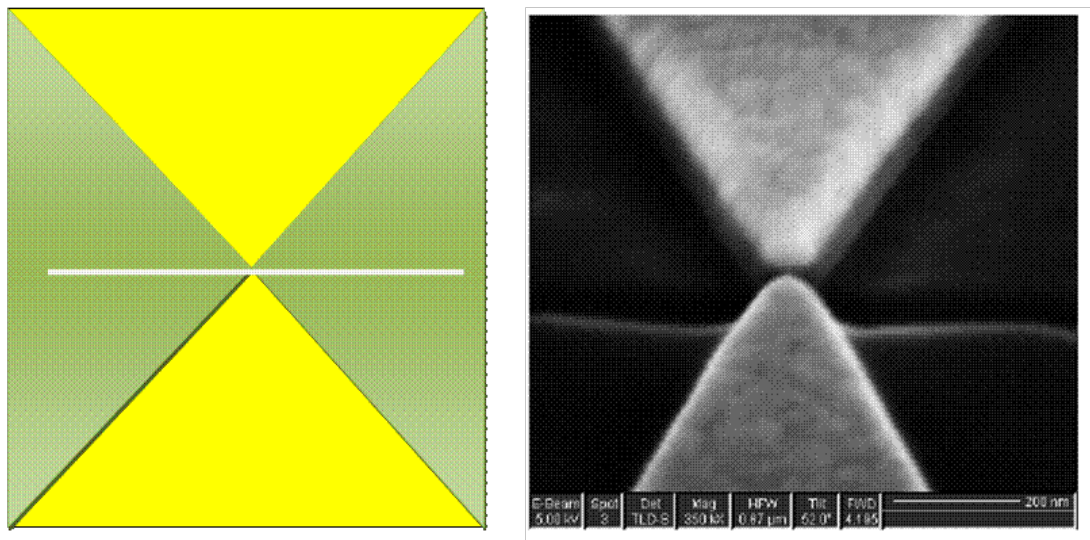
Fig.3.10.Left-the pattern used in the milling process. In green are the areas which will be milled by FIB; Right-the gap obtained after FIB,SEM image

One significant concern for gallium ions milling is the implementation of the substrates with ions, resulting potentially in leakage currents between electrodes. We discarded that this possible effect could harm significantly samples of final impedance Z<1MΩ, but cannot exclude spurious effects when investigating the molecular transport between electrodes.
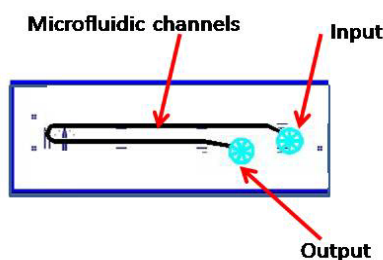
3.2 Preparing microfluidic system

Microfluidic consists, as the name clearly said, in systems providing small flow channels for liquids and gases. The first microfluidic device was built in 1976 in **[9]**. Since then, the development of microfluidics devices exploded, especially in the fields of biology, chemistry and microelectronics. A list of applications of microfluidics is well documented in **[10]**. Early devices were done using glass or silicon. These materials are quite expensive and required sometimes complicate processes especially when one tries to seal the devices. Processes involve high temperatures, high voltages and often necessitate a cleanroom environment.

In last decades new materials were studied and used for fabricating microfluidic devices **[11]**. Polymers are attractive, due to their properties, to their relatively low prices and flexibility in processing. PDMS (Polydimethylsiloxane) is the most popular choice and well suited for our setup. It has the following advantages **[12, 13]**:

- it seals reversibly and irreversibly to different substrates relevant for our applications (especially silicon and glass)
- channels with sizes below 100 micrometers can be easily fabricated using PDMS
- it is compatible with aqueous solutions and the electrolytes used in my work

Fabrication of PDMS starts by doing a master in SU-8 using optical lithography. The inverse of desired pattern of our microfluidic channels is patterned on SU-8 is deposited on a Silicon wafer (fig. 3.11)
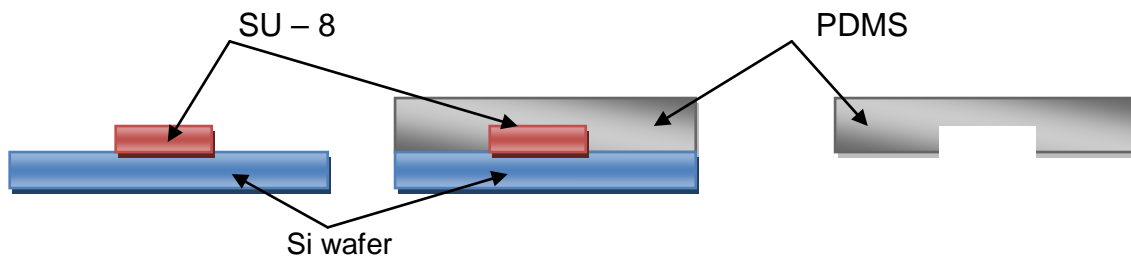

**Fig. 3.11**. The master of microfluidic system patterned in SU-8

We used a standard PDMS elastomer, Sylgard 184 from Dow Corning –USA that is poured over the SU-8 master. The elastomer is mixed with a baking agent in 10 to 1 ratio and the mixture is introduced in desiccators for removing bubbles air.

The pressure is reduced from atmospheric value to 1 mbar 4 or 5 times until no air bubble is remaining inside of the material, avoiding possible block or obstructions on the channels. We used thickness ranging from 200 micrometers to 1 cm. When cover the master with PDMS, curing at 65 C for one hour, after the replica is peeled out from the master. A scalpel is cut to right size and then the holes for inserting the tubing are done using a biopsy punch (fig.3.12)
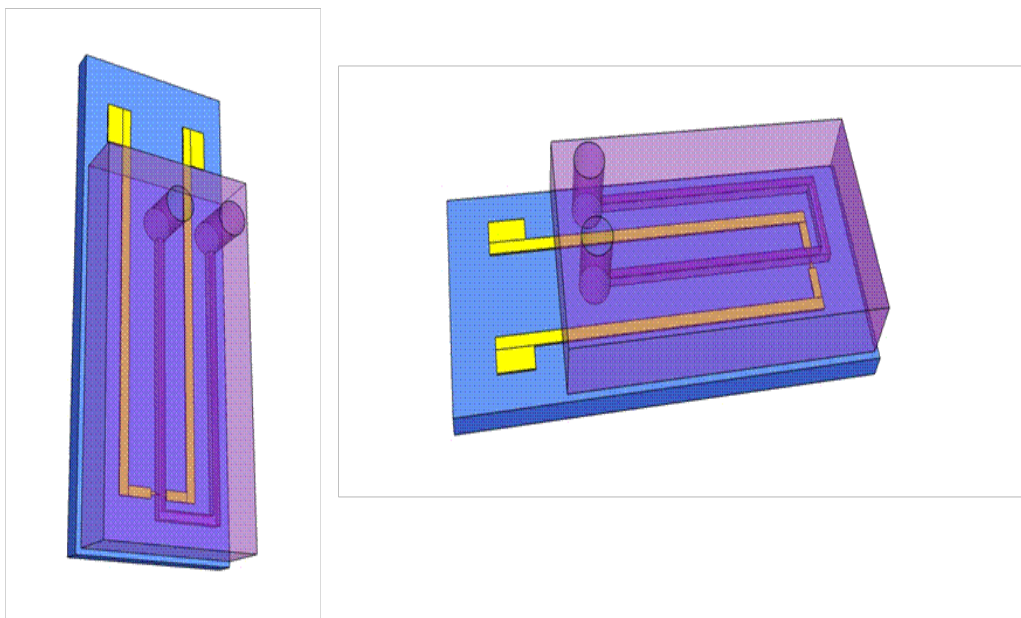
Fig. 3.12. Two different views of PDMS stab after being cut and punched

The most critical step is the bonding the microfluidic PDMS on the silicon. The oxygen plasma is used to activate chemical bonds, both in PDMS and in Silicon **[14]** ensuring sticking when they are put together. There are many studies about the

quality and strength of the bonds between PDMS and various compatible substrates **[15]**. Another important role of plasma activation is changing the PDMS from hydrophobic to hydrophilic, helping the wetting of the small channels.

More precisely we activate the two components of our system in Oxygen plasma under RF power of 32W for 20 seconds. The alignment of the microfluidic inlet channel with the patterned gold structure on Si/SiO$_2$ was performed manually under binocular. Further annealing at 100 °C, for 20 min on a hotplate under a pressure of 10kPa enhance the bonding between the PDMS and. Finally, plastic tubes were introduced in the access holes using UV polymerizing glue if liquid leaks occur.

The flowing of electrolyte in our system is ensured by a syringe pumping system correlated with an external valve system, as detailed explained in the next chapter. If faster exchange of electrolytes is needed a pneumatic valve system built in PDMS can be added. This kind of valves starts to be used nowadays **[16]** especially in the field of nanobiology where fast exchanging of solutions is needed. Using this system the exchange time can go down to microseconds.
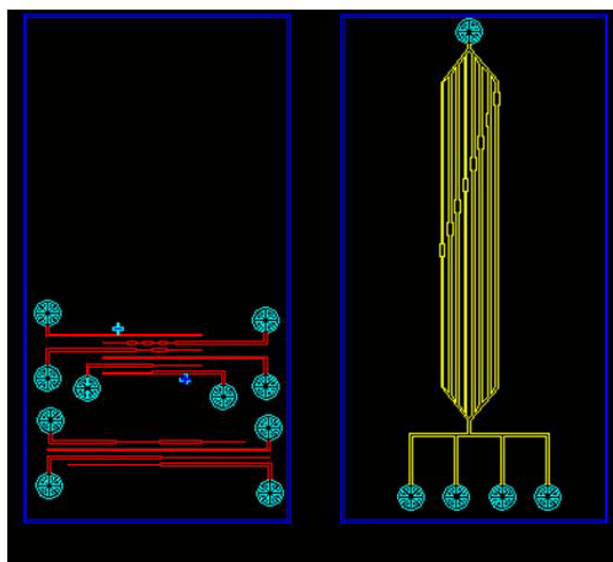
Fig. 3.13. SU-8 masters for fabricating PDMS pneumatic valves
left – the master for air flowing channels
right – the master for electrolytes flowing

The method consists in using two or more layers of PDMS with different patterned channels (fig. 3.13). There are aligned one on top of the other and then both sticked on the patterned gold. By flowing air or other gases under pressure the channels through liquid solutions are flowing can be blocked or opened (fig.3.14).
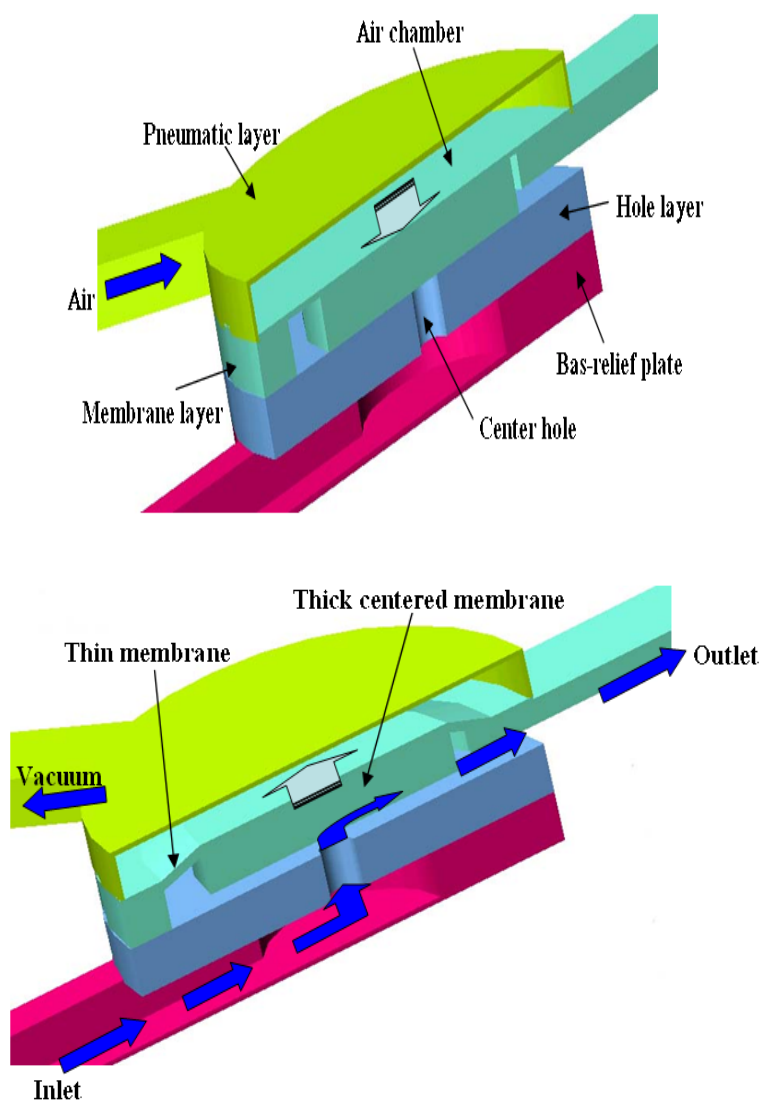
Fig. 3.14 Schematic and operation of the thick centered valve.
top - Closing of the valve by compressed air,
bottom - opening of the valve by vacuum **[17]**

We didn't use this pneumatic system for this thesis because a very fast exchange of electrolytes is not imperious necessary and the processes is quite challenging. Anyhow we made essays and the results are promising. We will maybe implement it for further experiments

3.3 The lab on chip approach

A **lab-on-a-chip** integrates one or several laboratory functions on a single chip of only millimeters to a few square centimeters in size. This term appeared after the apparition of microtechnology, back in the middle of 50's, and the first lab on chip was a gas chromatograph was built in 1975 at Stanford University. The boost in the development of lab on chip approach came in 90's with the introduction of PDMS molding technologies, which simplified the essential needs of "micro-plumbing", implementing easily construction of network of micro channels with the sizes of tens of micrometers. There is a very wide range of applications of this new technology **[18, 19]**, with an emphasis in Biology, Genetics, Chemical Analysis and more. The main advantages of Lab on Chip Technologies are:

- low fluid volumes consumption (less waste, less required sample volumes)
- faster analysis and response times due to short diffusion distances
- better process control because of a faster response of the system
- compactness of the systems due to integration of much functionality and small volumes
- relatively lower fabrication costs, allowing cost-effective disposable chips

In our work we identified this technique for reliability and versatility motivation. In this way our sample can be easily handled, lowering the possibility of damaging our fragile nanocontact, and also protecting it from the influence of external environment.

The chips with the PDMS layer are attached on a home designed Copper sample holder covered with a printed circuit board (PCB) with gold pads linked to small coaxial female connectors. One end of the PCB is U-shaped with pads wire bond to the chip. A wire-bonding machine with 25 micrometers Aluminum wire provided connection wire between our chip and the pads from PCB. The whole assembly can be fixed on the apex of the cold finger of a cryostat, where it can be placed in a magnetic field, and/or cooled down. A general picture is presented in Fig 3.15. There we can easily distingue the microfluidics circuits and the electrical connections via white (in this figure) special coaxial micro connectors.
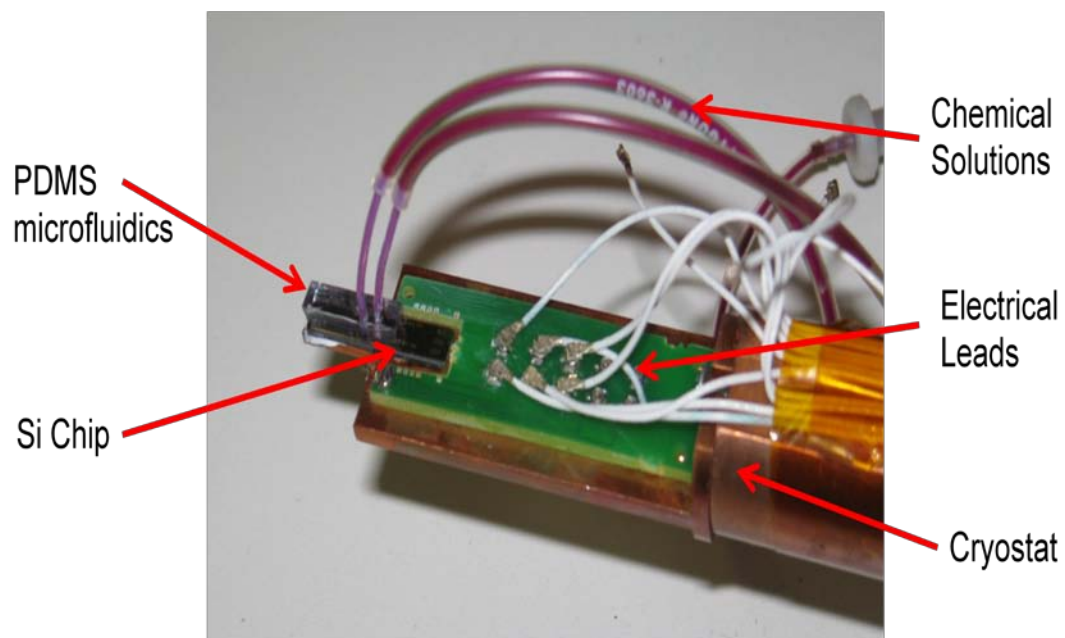
Fig. **3.15** Experimental lab on chip setup.

.

Bibliography

[1] http://en.wikipedia.org

[2] T. Blom, K. Welch, M. Strømme, E. Coronel and K. Leifer, *Nanotechnology,* **18**,(2007), 285301

[3] M. Nagase and H. Yamaguchi, *Journal of Physics: Conference Series*, **61**, (2007), 856–860

[4] M. Nagase and H. Namatsu, *Jpn. J. Appl. Phys.*, **43**, (2004), 4624-4628

[5] http://www.zeiss.com

[6] S. Kronholz, S. Karthauser, A.van der Hart, T. Wandlowski, R. Waser , *Microelectronics Journal*, **37**, (2006), 591–594

[7] M. I. D. Fischbeina and M. Drndić, *Applied Physics Letters*, **88**, (2006), 063116

[8] C.- S. Ah, Y. J. Yun, J. S. Lee, H. J. Park, D. H. Ha, and W. S. Yuna, *Applied Physics Letters*, **88**, (2006), 133116

[9] S. C. Terry, J. H. Jerman, J. B Angel, *IEEE Trans.Electron.Devices*, **ED-26**, (1979), 1880 – 1886.

[10] J. C. McDonald, D. C. Duffy, J. R. Anderson, D. T. Chiu, H. Wu, O. J. A. Schueller and G. M. Whitesides, Electrophoresis, **21**, (2000), 27 – 40.

[11] N. L. Jeon, D. T. Chiu, C. J. Wargo, H. Wu, I. S. Choi, J. R. Anderson and G. M. Whitesides, *Biomedical Microdevices,* **4:2**, (2002), 117-121.

[12] A. Mata, A. J. Fleischman and S. Roy, *Biomedical Microdevices,* **7:4**, (2005), 281–293,

[13] M. Liu, J. Sun, Y. Sun, C. Bock and Q. Chen, *J. Micromech. Microeng*, **19**, (2009), 035028

[14] D. C. Duffy, J. C. McDonald, O. J. A. Schueller, and G. M. Whitesides, *Anal. Chem.*, **70 (23)**, (1998), 4974-4984

[15] K. C. Tang, E. Liao, W. L. Ong, J. D. S. Wong, A. Agarwal, R. Nagarajan and L. Yobas, *Journal of Physics: Conference Series,* **34**, (2006)*,*155–161

[16] J. A. Weaver, J. Melin, D. Stark, S. R. Quake and M. A. Horowitz, *Nature Physics*, **6**, (2010), 218 - 223

[17] J. Y. Baek, J. Y. Park, J. I. Ju, T. S. Lee and S. H. Lee, *J. Micromech. Microeng.*, (2005), **15**, 1015–1020

[18] H. Andersson, A. van den Berg, *Sensors and Actuators B,* **92**, (2003), 315–325

[19] P. Abgrall and A.-M. Gue, *J. Micromech. Microeng.*, **17**, (2007), R15–R49

Chapter 4

Experimental setup.

4.1 Electrical circuit

4.2 Fast rotating and sweeping magnetic field

4.3 Microfluidic circuitry design

Our experimental setup is designed to realize nanocontacts by electrochemical deposition with in situ characterization of magnetoresistive properties. It is a complex system that was completely designed and built in our laboratory in the first part of my thesis. The idea of doing magnetic nanocontacts by electrochemistry was first given by Morpurgo **[1]** and then more work in this field, described in **[2]**, was done by Kervennic.

We add here the in situ magnetic measurements, following previous work **[3]**. We carefully characterized electrochemistry part, combining this with microfluidic tools. The system is designed for being wet chemistry compatible. This imposed significant restrictions of the whole experimental design, for example imposing non-convenient geometry for applying an external field.

4.1 Electrical circuit

Our experimental setup is designed to achieve two main goals
- ensure that the deposited metal is of high quality
- use in situ measurement to monitor the impedance of nanojunctions

We use an electrochemical cell to carry out the deposition of the metals. As shown in fig 4.1 and described in chapter 3 our cell consists of two working electrodes and a counter electrode. The electrodes are made by depositing gold onto a Si substrate. Besides these electrodes, a fourth electrode, the reference electrode is also inserted in circuit, for assuring controlled reactions at the working electrodes **[4]**.
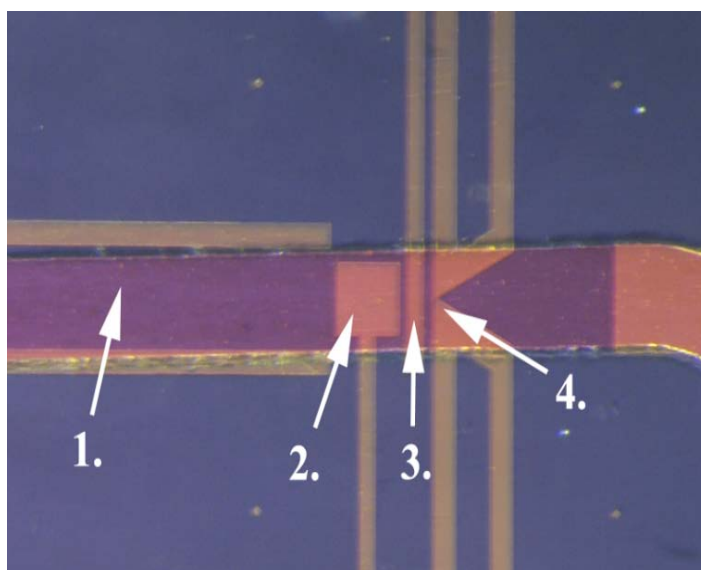
Fig.4.1 Micro electrochemical cell.1.Microfluidic channel (50 mm); 2. Counter electrode; 3. Reference electrode; 4. Working electrodes

The main part of the electrodeposition circuit is a HEKA potentiostat (model PG340), whose main role is to apply the desired deposition potential at the working electrodes, by controlling the potential difference between working and the reference electrodes **[5]**. The voltage across the cell and the deposition current are monitored via Potpulse software provided by HEKA. Additional filters, necessary for low noise and for eliminating low noise and perturbation are also provided. The external input mode is used for the potentiostat, using a voltage signal generated by home designed software via a data acquisition card from National Instruments to impose the potentiostatic value of the HEKA system.

The second part of the electrodeposition circuit monitors the impedance of nanojunction. It consists mainly of an Elmayer SR750 Lock-In Amplifier connected in circuit, able to indicate accurately the changes in impedance and phase in our circuit. The output of the lock in provides a small ac excitation in our circuit and the inputs are used in differential voltage mode, measuring the voltage drop across a series 1 kilo ohm resistor related to the current flowing through the impedance separating the two sides of the nanocontact (W_1, W_2 in fig. 4.2). We first tried to measure the voltage drop directly across the gap **[6]** but this wasn't a good way to do it due to the loosing of some valuable phase information.
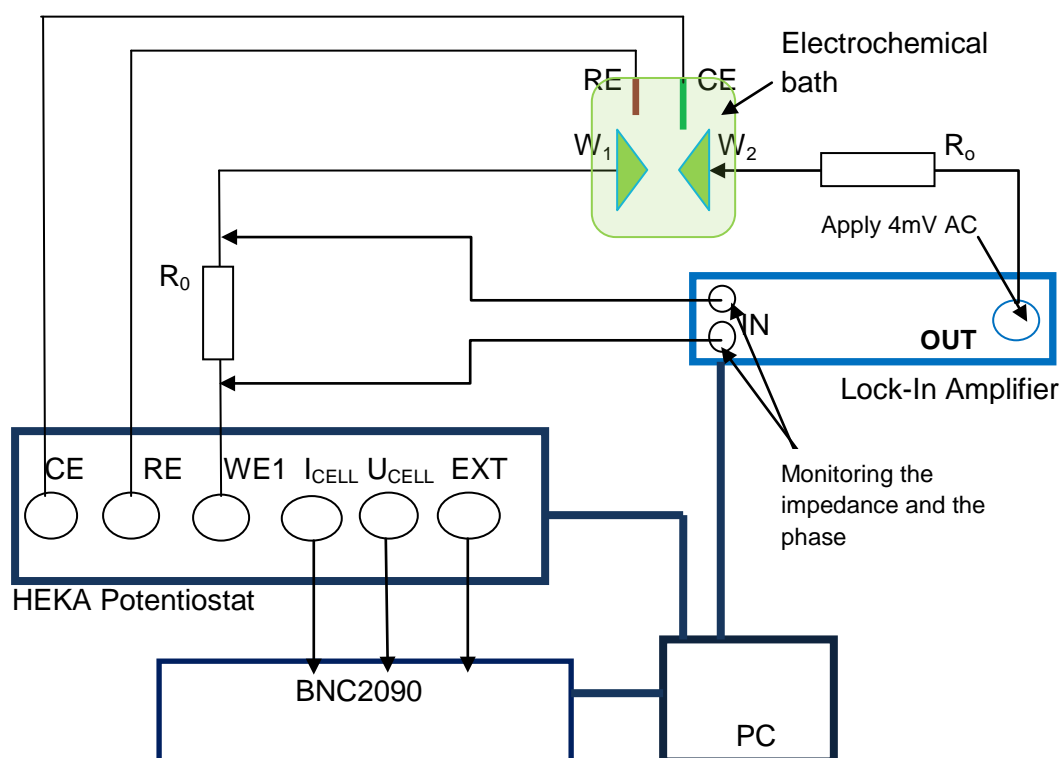

Fig.4.2. Detailed block-connection diagram of the electrical setup

In fig.4.2 the whole assembly of electrical circuit is shown. As you can see the PC is gathering data from:

1. Lock in amplifier
- the magnitude of the voltage drop across the resistor
- the phase of the voltage drop across the resistor
2. Potentiostat
- the electrodeposition voltage
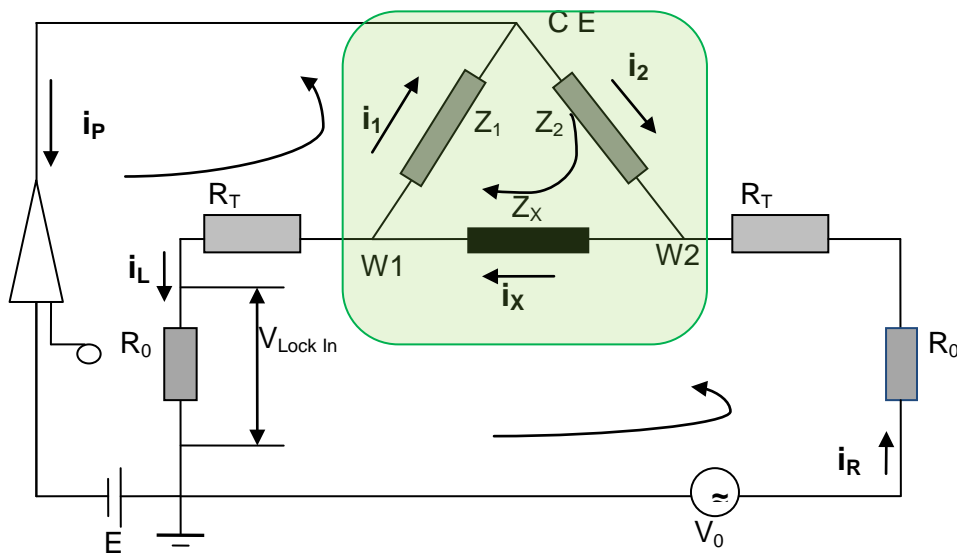- the deposition current

3. BNC DAQ - parameters from deposition

The computer also controls:

- the AC signal amplitude and frequency, the time constants of the reading and other filter settings
- the potentiostat – send the desired deposition potentials
- the BNC –DAQ

Equivalent electrical circuit.

The electrical diagram of our circuit is presented below in fig 4.3

Fig.4.3. Electrical circuit

Where:

E – the DC potential , provided by the potentiostat , used for deposition or dissolution;

V_0 – the AC excitation, supplied by the Lock In;

R_0 – 1 kΩ resistors – used for limiting the current in the circuit. We are using two of them to ensure symmetry of the two working electrodes circuits;

R_T – gold tracks resistance –having values of 200 Ω (for E-beam samples) up to 1700 Ω (for FIB samples); These values, comparable with other resistances from the circuit can't be neglected;

Z_1, Z_2 – the bath impedances between counter electrode and WE_1, WE_2 respectively;

Z_X – the impedance between the two working electrodes – this is our parameter of main interest;

$V_{Lock\ in}$ – the voltage across the resistor.

Our goal is to carefully measure the Z_X between two working electrodes during the deposition/dissolution processes. This would be vary in a range from hundreds of kilo ohms (when the junction is open) till ohms when the junction is closed. For finding Z_X the electrical circuit should be solved applying the circuit's laws.

In 3 loops and 4 nodes the Kirchoff laws of circuit are:

$$i_1 = i_P + i_2 \tag{1}$$

$$i_X = i_L + i_1 \tag{2}$$

$$i_X = i_2 + i_R \tag{3}$$

$$i_R = i_L + i_P \tag{4}$$

$$i_1 Z_1 - i_L R = 0 \tag{5}$$

$$i_2 Z_2 + i_1 Z_1 + i_X Z_X = 0 \tag{6}$$

$$V_0 = i_R R + i_X Z_X + i_L R \tag{7}$$

where

$$R = R_0 + R_T \quad \text{and}$$

$$V_X = i_L R_0 \quad \text{the voltage magnitude measured by Lock In}$$

After solving this system and making the assumption of $Z_1, Z_2 = Z \gg R$ we get for our impedance:

$$Z_X = \frac{V_0 R_0 Z^2 - V_X[2Z^2 R + 2ZR^2]}{V_X(Z+R)^2} = \frac{\frac{V_0}{V_X} R_0 Z^2 - 2RZ^2\left[1 + \frac{R}{Z}\right]}{(Z+R)^2}$$

Hence

$$Z_X = \frac{\frac{V_0}{V_X} R_0 - 2R\left[1 + \frac{R}{Z}\right]}{\left(\frac{R}{Z} + 1\right)^2}$$

Therefore we can deduce our impedance Z_x by measuring the voltage drop V_x across a 1 kilo ohm resistor. Also the value is dependent on the R/Z ratio which can be easily approximate; R can be accurately get as 1 kilo ohm resistor in series with the gold track resistance 250 and 1300 ohms. So the final value for R is between 1.2 and 2.3 kilo ohms. The impedance of the bath between one working electrode and the counter electrode, Z, in actual bath condition, can be easily measured using impedance spectroscopy methods (see next chapter). Our measured values were greater than 120 kilo ohms. The following approximation is therefore justified:

$$\frac{R}{Z} \ll 1$$

So our impedance simplify to:

$$Z_X = \frac{V_0}{V_X} \; R_0 - 2R$$

That is essentially a simple voltage divider (V_x, V_0) in a closed loop with two resistances R and Z_x in series.

A first way to check this result is to see what happen in our two extreme cases.

- Junction is completely closed so Z_X is nearly zero

$$V_X = \frac{R_0}{2R} V_0$$

which make perfectly sense, the voltage drop on R_0 resistor depends only on the resistance of whole circuit.

- Junction is open so we have a huge impedance for our contact

$$Z_X \rightarrow \infty \leftrightarrow V_0 \gg V_X$$

so $V_X = 0$ as expected for a open circuit

Our physical property of interest is the conductance or the resistance of the contact so the formula for our use is
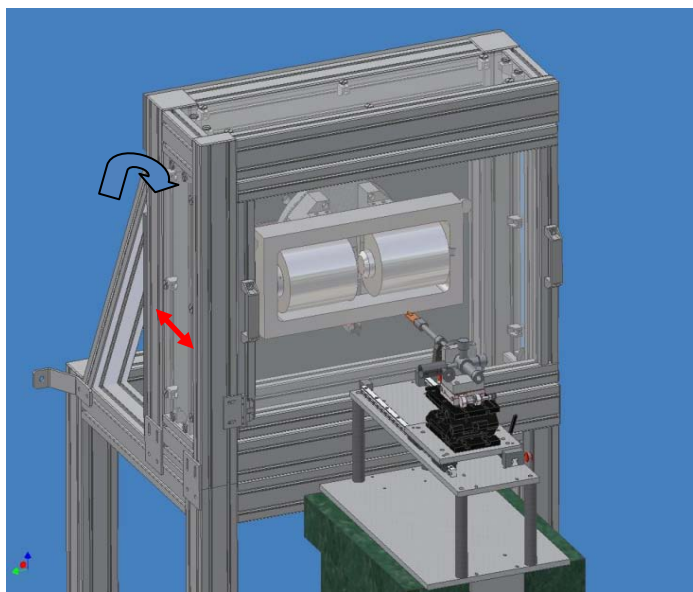
$$G_X = \frac{1}{Z_X} = \frac{1}{\frac{V_0}{V_X} \, R_0 - 2R}$$

or in units of quantum conductance , using $G_0 = 12{,}9 \text{ k}\Omega^{-1}$

$$G_X = \frac{1}{\frac{V_0}{V_X} - 2R} G_0$$

4.2 Fast rotating and sweeping magnetic field

For studying the magnetic effects in our samples a special magnet was designed and built. This was necessary because of the fragility of our samples and

Fig.4.4. The rotating magnet. The cart which move the cold finger with sample attached is also shown

also the short lifetime of the nanojunctions. Fragile samples in a liquid environment necessitated that the sample remain fixed while the magnet is rotated and the short lifetime implied that the magnet had both high speed sweeping and rotation capabilities. A sufficiently high magnetic field was necessary in order to reach the critical fields of some of the materials, sometime exceeding 1 T.

The magnetic system can be described in two main parts; one is the magnet itself, which was built by CAYLAR S.A.S; the second part is the system that rotates the magnet. The magnet, consists of two coils, having a diameter of 125 mm and a height of 160 mm with a power of 38 w each. There are powered using a power supply of 2V-50 A. This source can be driven by a Hall effect field regulator, which ensure a constant magnetic field by applying a constant current. The magnet has 4 pairs of interchangeable polar pieces, with a diameter of 50 mm, which allows different values of field to be reached. The gap between poles can be adjusted in the range of 8 – 30 mm, depending on the size of the samples studied. The cooling

of system is done by natural convection so no complicated fluid cooling installation is needed. The Hall probe is fixed on one polar piece and is measuring the real values of magnetic field the maximal readable value being 20 KGauss with 1Gs error. Assuming, our magnet can provide a field in the ±1.4 T range, depending on the poles what are used. The rate of sweeping rather depends on the DAQ or PC software limitations, a sweep by 1T/s being anyway easy to achieve.

The second part of the system consists of the rotating motor. This was completely designed and built buy our technicians, here at IPCMS. The difficulty in this design was due to high precision needed and the no negligible weight of the magnet – 60 kg approximate. A big difficulty was the necessity of an horizontal rotation axis, constrained by an horizontal sample, compatible with liquids. Rotating with a considerable speed with such a big weight around a very fragile sample with a size in millimeters range was a big challenge. For solving this, a very solid and rigid enclosure was built (fig. 4.4). The motor used is a step motor, each step corresponding to 1/600 of one degree. It can rotate the magnet with a speed by one complete oscillation by two seconds. All is remote controlled by a program which is also integrated in the main software.
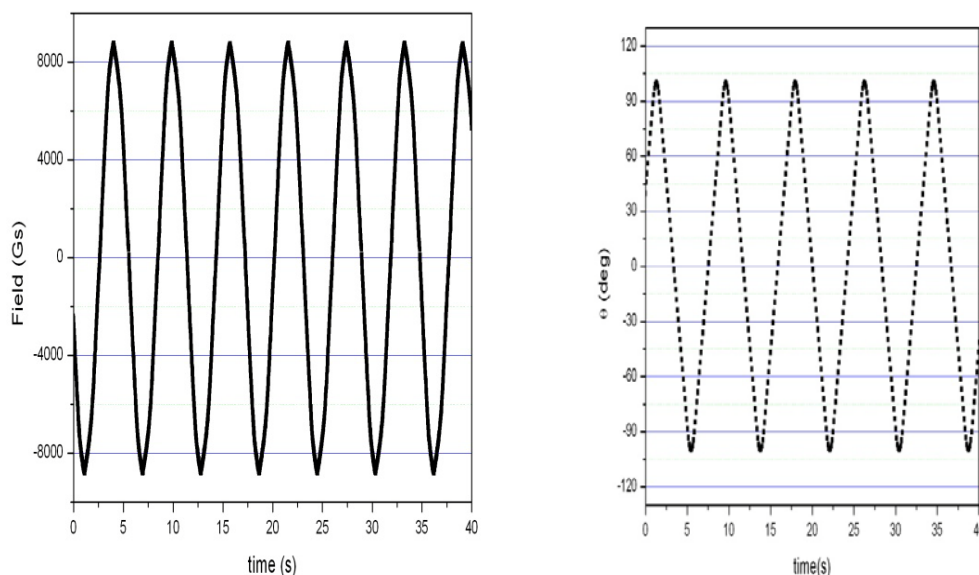
Fig.4.5. The sweeping - rotating magnetic field;
left – the field is swept in a given symmetrical range; **right** – a fixed field is rotating

4.1 Microfluidic circuitry design

To carry out electrodeposition of the metal nanocontacts it is necessary to have ionic solutions in contact with the electrodes of the electrochemical cell. For this we realized a simple but effective system that allows us to control in a precise way the electrodeposition process. The microfluidic system consists in a PDMS cell (described detailed in chapter 3), having 100 microns wide and 50 microns high patterned channels. This cell, placed over the electrodes (fig. 4.6), is connected to
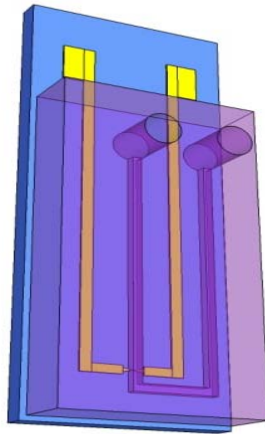
Fig.4.6. PDMS cell stacked on a Si chip. The channel are aligned over the nanojunction

the liquid flowing system using polypropylene small tubes, chemically inert to the flowing electrolytes.

The flow rate of the liquid is controlled using a syringe pump system (Harvard Company). It consists in a syringe whose piston is pushed in an automatic controlled way by a small step motor. With this system we can obtain flow rates starting from 100 of micro liters by hour up to 5 milliliters by minute, depending also on the size of syringe used.
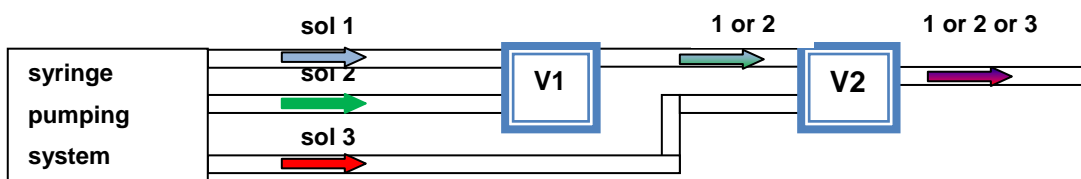
Fig.4.7. Simplified block diagram of the fluidic system

Considering the fact that the electrolyte is also passing through our microfluidic channels (described in a previous section), with a size of hundreds of micrometers, and simply applying continuity law for flowing, we see that the flow rates is an important factor. As an example, for a syringe flow rate of 1 ml/h, in the nanojunction area the electrolyte will move with a speed of approximately 2 cm/s which is noticeable high for a deposition process at nanometer scale. Anyhow the electrodeposition is performed without flowing electrolyte.

The key advantage of the lab on chip approach is the possibility to exchange electrolytes. Our experiments typically involve replacing the electrolyte solution by water for rinsing and N2 for cleaning and drying. Our ambition is to then rapidly cool down the sample, keeping it under inert conditions at all times. The microfluidic technique developed by us is allowing doing all these without moving the sample, only by changing the solution which flows through the nanogap. For this purpose we use a Mate-valve 6 microvalves system from DAGAN Company. This system consists in 6 fully automatic controlled valves (fig 4.6. V1 and V2 are two of them) that permit exchanging between 6 different fluids. One problem is the time lag between valve switch and the effective solution exchange at the nanocontact position. This depends on the length of the tubes used and the syringe flow rate. The last one must be minimal so we have do diminish as much is possible the length – so to bring as close as possible the valves to our sample. One way to solve this is to use the pneumatic on-chip valves referenced in the literature **[7, 8]**. As explained at the end of previous chapter this requires several layers of PDMS patterning. After initial tests the reliability was not satisfactory for our time consuming nanocontact fabrication. Anyhow for further experiments when fast exchanging liquids is needed this direction should be considered.

Bibliography

[1] A. F. Morpurgo, C. M. Marcus, and D B. Robinson, *Appl. Phys. Lett.*, **74**, (1999), 2084.

[2] Y. V. Kervennic, H.S.J.Van der Zant, A F. Morpurgo, L. Gurevich, and L.P. Kouwenhoven, *Appl. Phys. Lett.*, **80**, (2002), 321.

[3] C. -S. Yang, *Ph.D. Thesis*, University of Nebraska at Lincoln, USA, (2004).

[4] K. K. Kasem and S. Jones, *Platinum Metals Rev*, **52**, (**2**), (2008), 100-106

[5] http://en.wikipedia.org/wiki/Electrochemical_cell

[6] N. T. Kemp, H. Majjad, P. Lunca Popa, G. Dalmas and B. Doudin, *ECS Transactions*, **16 (45),** (2009), 3-10

[7] N. L. Jeon, D. T. Chiu, C. J. Wargo, H. Wu, I. S. Choi, J. R. Anderson and G. M. Whitesides, *Biomedical Microdevices,* **4:2**, (2002), 117-121.

[8] M. A. Unger, Ho. -P. Chou, T. Thorsen, A. Scherer, S. R. Quak, *Science*, **(7) 2887**, (2000), 113 - 116

Chapter 5

Experimental results

5.1 Study of the electrodeposition process.

5.2 Monitoring of the sample impedance. Conductance stabilization.

5.3 Magnetoresistance of nanocontacts

5.4 Experiments on mechanical break junctions in electrochemical environment

5.5 Discussion of results and future works.

In this chapter I will present the result of my experiments. Formation and electrical properties of a nanocontact are monitored using a lock-in measurement technique, using the AC voltage signal across one resistor connected in series with the nanocontact. Evolution of the nanocontact impedance during closing and (eventually) opening is monitored. We carefully tune the electrochemical conditions in order to slow down the process and find plateaus in the conductance versus time, which can be interpreted as stabilization of a contact made of a few atoms. Conductance of various metals is successfully measured. Magnetic field effects on electrical transport on ferromagnetic nanocontacts are systematically investigated. Taking advantages of using a lab on chip strategy an important part of experiments is dedicated to studying the influence of electrochemical bath on the transport properties across atomic size contacts. Experiments combining electrochemistry with mechanical break junction are also performed and the results are presented in a dedicated section of this chapter.

5.1 Study of the electrodeposition process

Prior to nanocontacts fabrication, measurements on electrochemical baths were performed to ensure the use of right parameters for electrochemical reactions at the working electrodes. In particular, Electrochemical Impedance Spectroscopy (EIS) studies were done for all baths. This method consists of measuring the impedance of an electrochemical cell while the frequency is swept in a desired range. The baths used in present work (Table 1) have been chosen after a carefully study of previous work in the field **[1-4]**.They were chosen on a criteria of significant literature and/or known quality of the deposits in terms of small granularity or limited strain of deposited films.

Bath	Substance	Chemical Formula	Molecular Weight (g/mol)	Conc. (mol/l)	Mass (g)
Nickel sulphamate	Nickel sulphamate tetra hydrate	$Ni(SO_3NH_2)_2 \cdot 4H_2O$	322.93	1.8	600
	Nickel chloride hexa hydrate	$NiCl_2 \cdot 6H_2O$	237.69	0.05	10
	Boric Acid	H_3BO_3	61.83	0.65	40
Cobalt sulfate	Cobalt(II) sulfate hepta hydrate	$CoSO_4 \cdot 7H_2O$	281.10	0.45	120
	Boric Acid	H_3BO_3	61.83	0.65	40
Platinum	Chloroplatinic acid hydrate	$H_2PtCl_6 \cdot xH_2O$	409.81	0.01	4
	Boric Acid	H_3BO_3	61.83	0.5	32
Silver	Silver Nitrate	$AgNO_3$	169.87	0.001	0.002
	Nitric Acid	HNO_3	63.01	0.1	6
Gold (Commercial bath ECF61 from Metalor)	Gold	Au	196.97	0.05	10
	Potassium sulfite	K_2SO_3	158.26	0.22	35
	Shining E1 agent	-	-	-	4.7ml/l

Table 1 Chemical composition of electroplating baths used in this thesis

EIS was performed using an Autolab PGSTAT302 potentiostat. We investigated the impedance of the cell under a 4 mV AC excitation and DC potentiostatic conditions
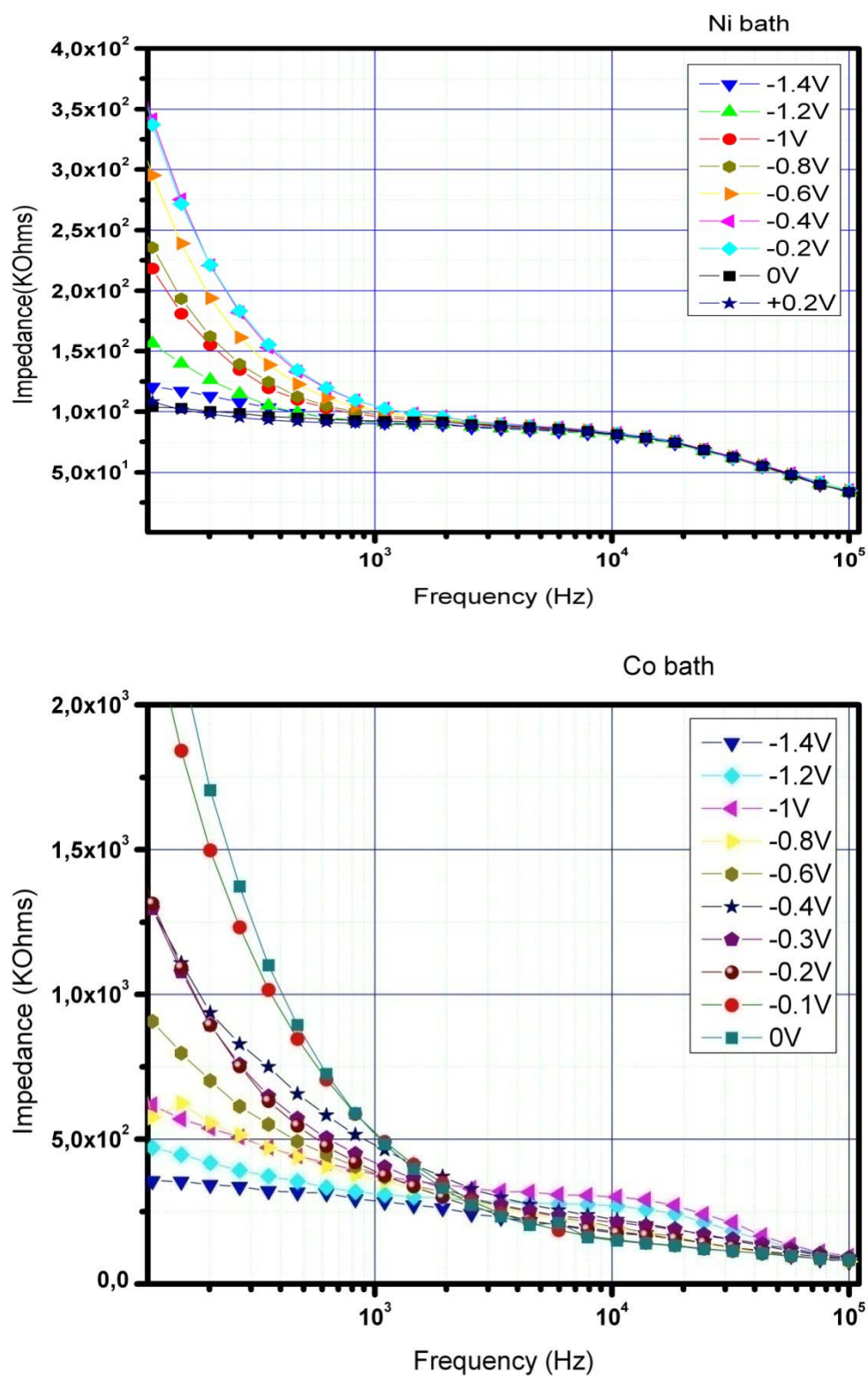

Fig. 5.1 Electrochemical Impedance Spectroscopy data for Nickel (top) and Cobalt (bottom)

in the range of [0 ÷ -1.4 V], related to our subsequent experimental conditions.

Generally the bath impedance depends on the concentration, mobility and the nature of ions present in solution. It also depends on the geometry and the nature of electrodes. For example the electrode area will scale the resistance and the capacity of the cell. The equivalent circuit of our cell is mostly consisting in impedance of the interface in series with the impedance of electrolyte. The results for nickel and cobalt are shown in fig 5.1.The EIS measurements were performed in under conditions similar to those used for electroplating, using the same configuration of the working electrodes. One can observes a decrease of impedance with increasing frequency due to capacitive effects contribution to the bath impedance. Hence the impedance is decreasing from hundreds of kilo ohms at small frequencies down kΩ at 100 KHz. Due to the fact that the geometrical conditions (patterned chip) are the same for all baths, it is clear that the small differences between two different baths depicted are related to the ions contained in the solution. The nickel bath, having a higher concentration of ions (1.8M) is less resistive than the cobalt solution (0.45M). In each graph the first curves from the top are corresponding to small negative plating voltages (0 ÷0.4 V) when no plating and dissolution occurs. The last bottom curves correspond to an over-potential plating regime. The differences became significant at low frequencies, below 1 KHz, as capacitive component not short the current and the ions start to follow the AC voltage. Same characteristics are observed also for all others electroplating resistively baths. Data for gold solution are shown in fig.5.2.

The data shown in fig 5.1 and 5.2 corresponds to the bath between one working electrode and the counter electrode, Z_1 or Z_2 as refereed in section 4.1. As emphasized there, the contact conductance formula was established under the hypothesis that Z_1 and Z_2 are much larger than the 1kΩ, resistance corresponding to gold tracks in series with R_0. Our EIS experiments clearly show that this condition is fulfilled for our working frequencies (200-230 Hz) for all applied potentials. We chose low enough lock-in frequencies to ensure that the baths studied are showing always impedances larger than 100 kΩ in plating experimental condition.

The baths impedances between both working electrodes and the counter electrodes are almost identical due to the symmetry of the electrodes. The experimental measurements confirmed this fact. In fig. 5.3 (left) both impedances are shown for an Au bath in the frequency range used for our experiment. The

differences are relatively no important especially when one compares Z_1 and Z_1 with R_0. For this particular example the impedances are around 200 KΩ for an AC
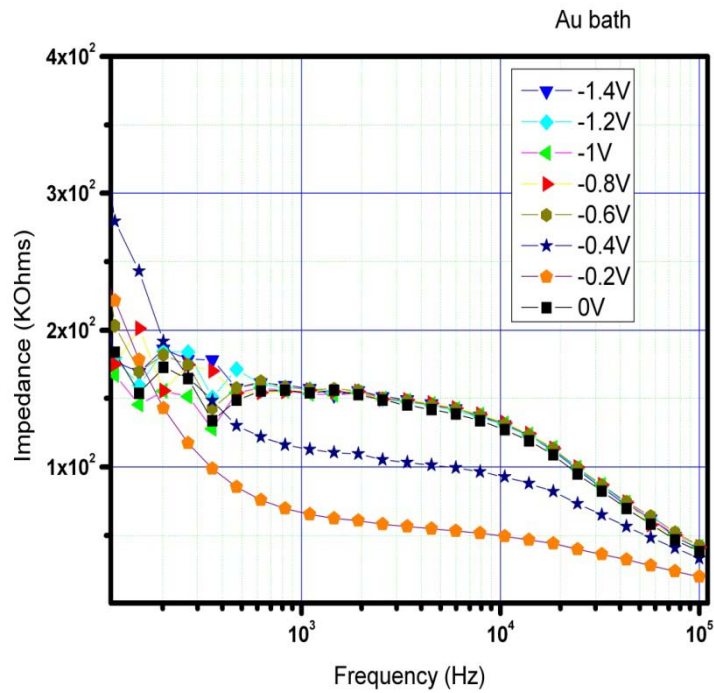

Fig. 5.2 Electrochemical Impedance Spectroscopy data for ECF 61 gold plating commercial bath from Metalor
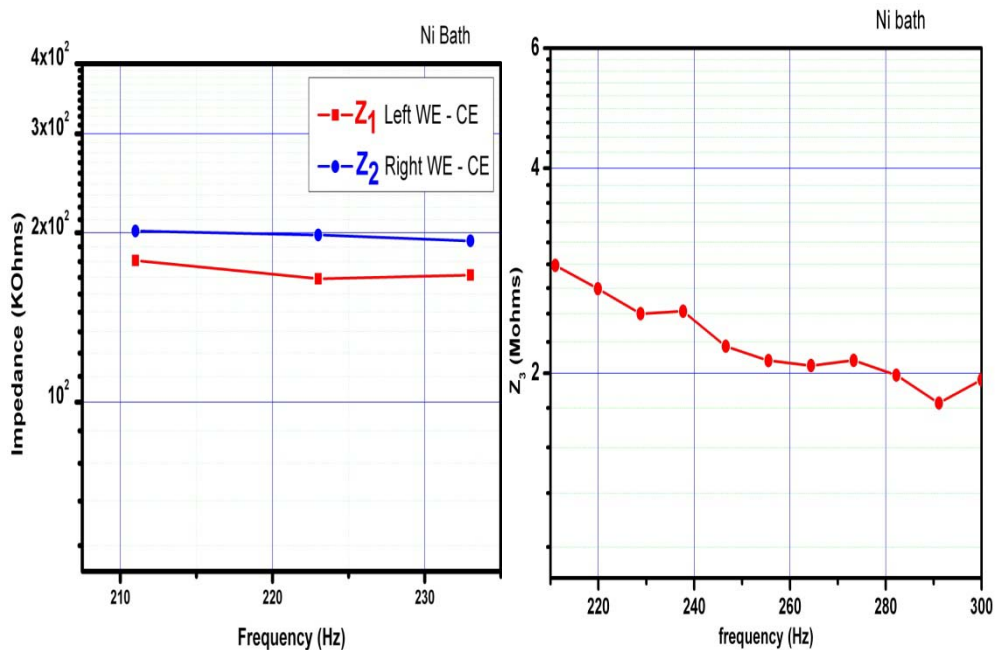

Fig. 5.3 Impedance measurements in work range frequencies (Au bath).
Left: Comparison between Z_1 and Z_2 ; Right: Z_3-between working electrodes

excitation of 4mV. The 10 kΩ difference can be due to the fact that the PDMS channel was not perfectly symmetrically sticked on the junction; hence the working

electrodes areas exposed to the electrode are slightly different. The simplifying hypothesis, $Z_x << Z_1, Z_2$, is therefore well-obeyed when a contact is established.

The impedance of the bath between the two working electrodes, Z_3, cannot be directly investigated, especially when the sample is in the tunnel regime, corresponding to large impedance values (10^6 Ω). Z_3 is decreasing almost linearly when the gap is closing. By my preliminary calculation Z_3 should decrease 10 -20 times while the contact is forming as the gap decrease from an initial value of 20 – 30 nm at 2-3 A and then close. Indication on his initial value can be obtained from the readings of the lock-in when the plating starts. For some general information the impedance of the cell between the two working electrodes was measured by connecting one electrode as a counter and leaving the second one as working. This is not reproducing exactly the plating experiment conditions but again, the aim was obtaining some general information about behavior of electrochemical baths. The results are shown in fig. 5.3 (right). Values of the order of mega ohms were obtained for frequencies of hundreds of Hertz under an oversimplified hypothesis that the impedance scales down linearly with the electrodes separation. The impedance between two electrodes separated by 1 nm should be of the order of 10^5 Ω, still significantly larger than $1/G_0$, and negligible for contacts of a few kΩ.

Before starting the main experiments related to fabricating nanocontacts and studying the transport properties across them, the electrodeposition process was investigated. It is crucial to calibrate the rate of deposit and ideally find the best conditions for improving the quality of deposited films. Electrochemistry at such nanometric scale is quite different from macroscopic scale processes, due to confinement of the electrolyte.

In the beginning we were interested in determining the deposition rate for various materials. The main parameter here is the voltage applied hence experiments involving electroplating were performed under potentiostatic conditions (fig. 5.4.). Systematic AFM measurements were performed for determining the height of deposit, from which a deposition rate was calculated. As depicted in fig. 5.4 for this Nickel sulphamate bath the deposition starts around -0.9V and then increase exponentially with voltage as expected from Nernst law [5]. These values were determined for vertical deposition (on top of electrodes) but the AFM images (fig. 5.5) shows that same length was deposited horizontally (between working electrodes). This data helps us in approximating the time needed for closing one gap.
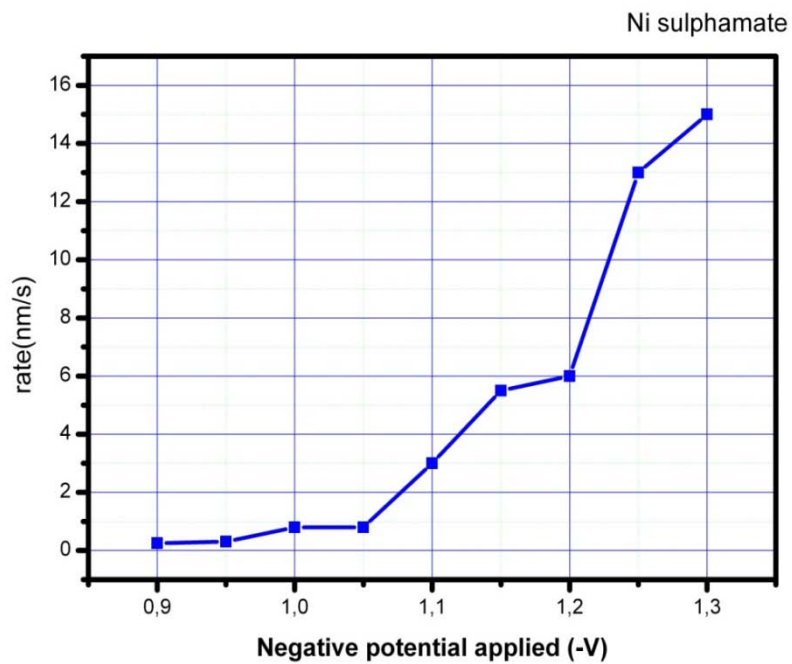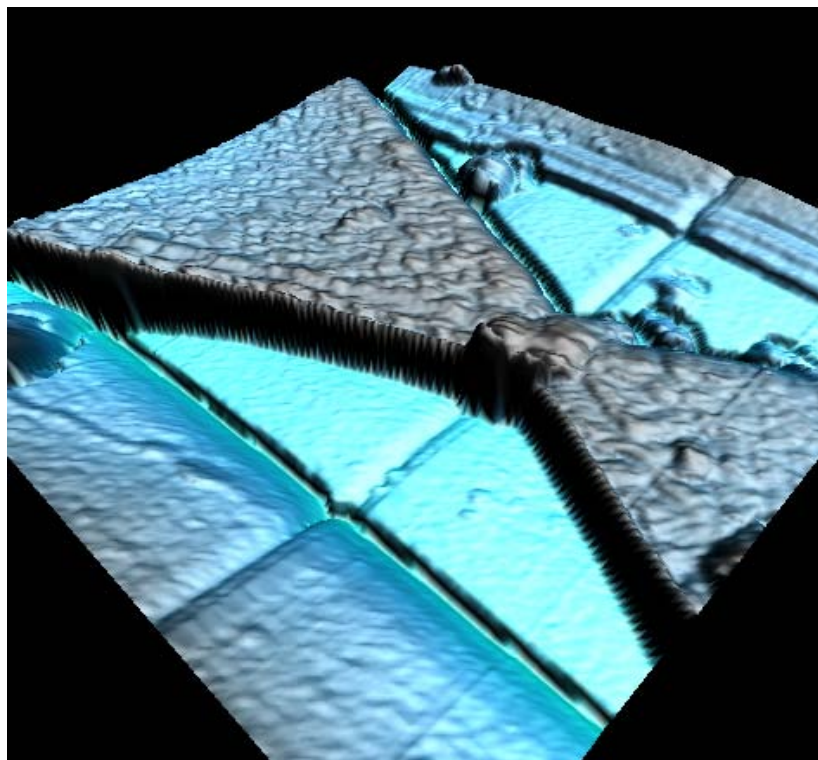
Fig. 5.4 Deposition rate versus applied plating voltage for a Ni bath
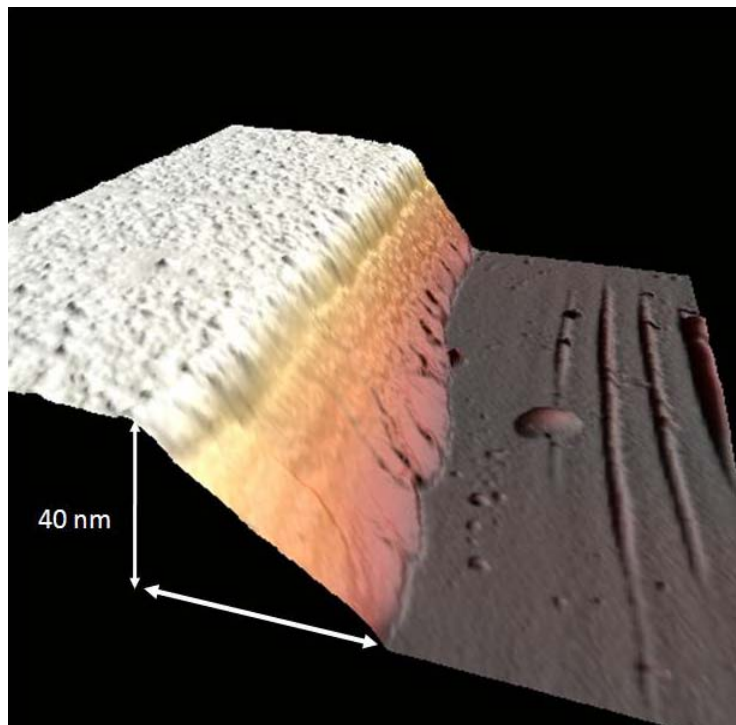
Fig. 5.5 AFM image for Ni deposited on Au substrate. Same length of deposit for the parallel and perpendicular directions

When the plating starts nucleation centers are forming on the substrate. These one grows, forming islands, and finally coalesce for forming the layer.

Fig. 5.6 AFM image for a Ni deposited nanojunction on gold electrodes.

The problem is this layer doesn't have a uniform height due to randomly formation of nucleation centers on the initial surface. The formation of this is related to thermodynamic and mechanical equilibrium laws. Generally, first nuclei are forming on the sharp edges or close to any defect in the crystalline structure of the substrate. Therefore the final layer will have a "mountains aspect" with greater heights where first crystallization nuclei were formed as clearly observed in fig.5.6.

A method often used for improving the quality of deposit is the pulse plating technique **[6]**. This method consists in alternating deposition and dissolution voltage pulses as depicted in fig.5.7. A complete work cycle is composed by two short voltage pulses one which ensure deposition and the other ensuring dissolution. Sometime, a third pulse, corresponding to a voltage where no deposition or dissolution occurs, is also added allowing the system to relax for bringing the ion concentration back to equilibrium.

The length of cycles varies from microseconds to seconds, frequencies of kilohertz being used by some researchers **[7, 8]**. The depositing pulse is longer than removing one (70-95% comparing with 30-5%). During the removing part of the

cycle a "polishing" or a leveling process is taking part and after, when plating again, new nucleation centers are created. A series of experiments are needed to
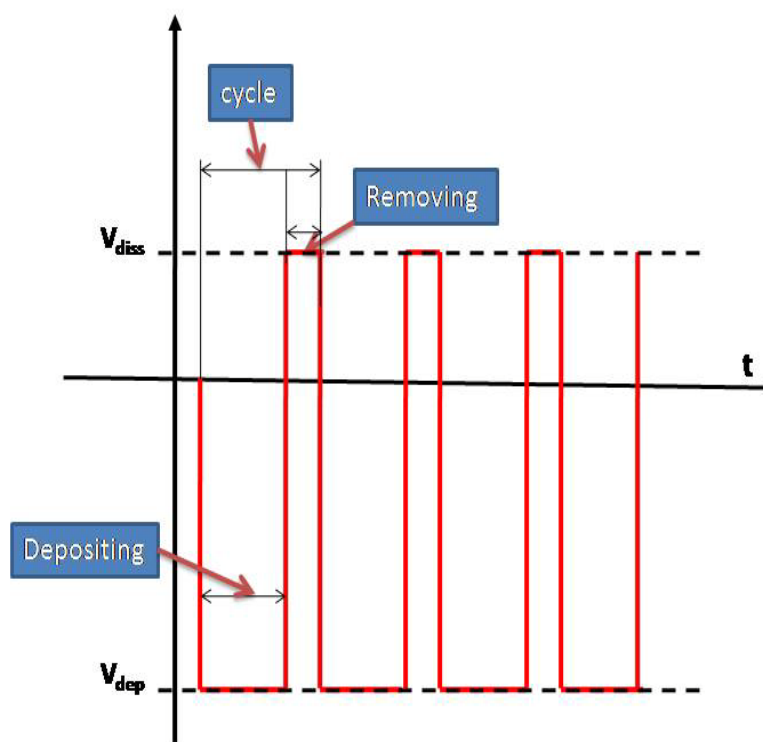

Fig. 5.7 Diagram of a pulse plating process.

determine the optimum parameters for an electrodeposition process. The search for an optimum set of parameters can be a bit time consuming and we mostly took conditions from literature as basis and used then to improve the roughness of our deposits.

The deposits obtained using pulse plating are having a higher adherence on the substrate and are also exhibiting reduced roughness and better uniformity (fig. 5.8). We used this method and after finding the suitable parameters an obvious improvement in the quality of deposits was achieved (fig.5.8). For DC normal plating used in depicted deposits we used voltage of -1.4 V. For pulse plating deposits we used the following parameters: frequency 70 KHz, plating voltage = -2.5 V, applied during 90 % of the cycle and dissolution voltage = + 0.25 V applied during 10 % of the cycle. In these experiments, dedicated to improve the quality of deposits, we used a two-step layer deposition strategy, where the initial growing was performed under pulse plating conditions, and then use normal potentiostatic conditions for the closure or the opening of the nanocontact.

However we didn't observe significant changes in MR behavior between samples pulse plated or not. This is not fully surprising as the transport within
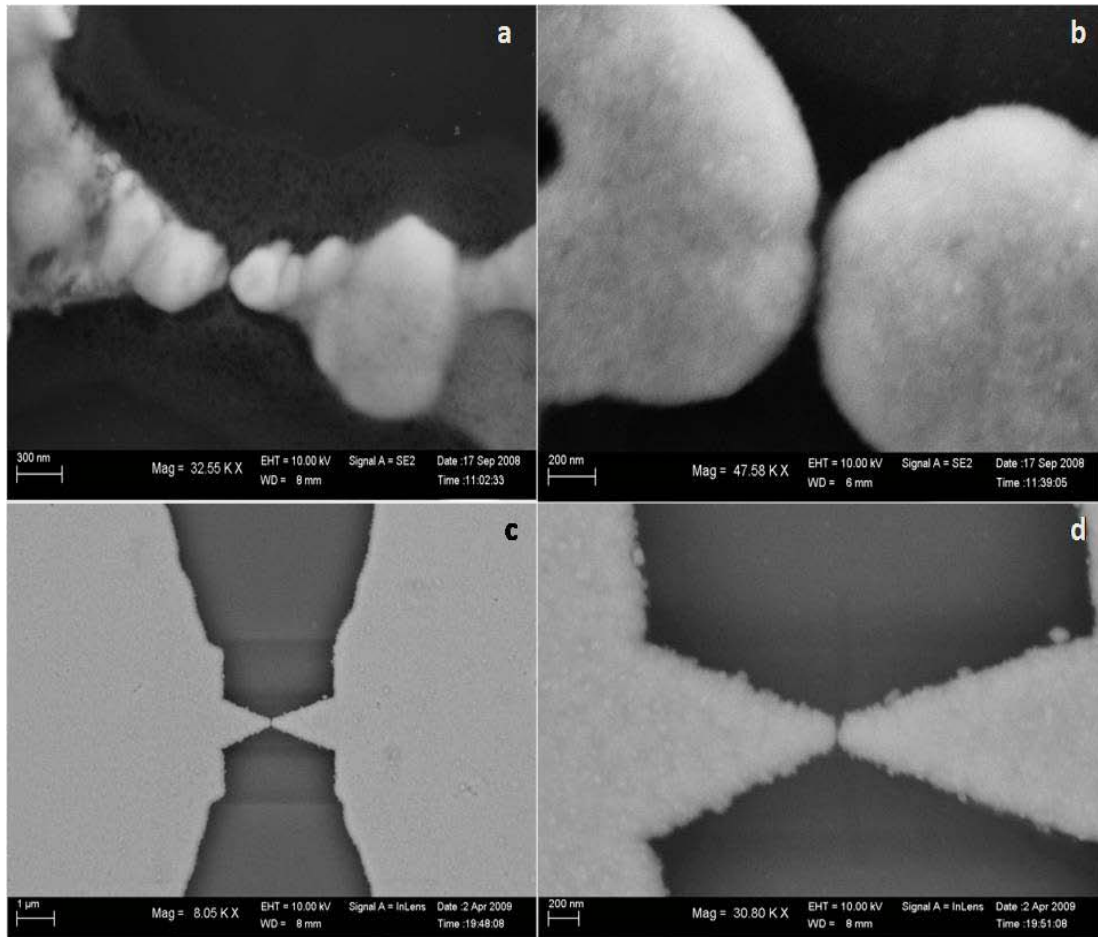
Fig. 5.8 SEM images for nickel deposited on Au initial electrodes using DC plating (a, b) or pulse plating (c, d)

nanocontact is given by the last few atoms deposited, which literally close the contact. Diminishing the grain size of the deposited is affecting only the general morphological aspect of the deposit **[9]**. Pulse plating was therefore used in a few experiments only, especially because this was very CPU time-consuming, resulting in a visible decrease of data acquisition speed, mainly due to the hardware limitations.

5.2 Monitoring of the sample impedance. Conductance stabilization

The experimental key information, directly related to the impedance of the nanocontact are the magnitude and the phase of the AC voltage drop across the 1 kilo ohm connected in series with our contact. This information is correlated with others related to the magnetic field and to electroplating process. In fig.5.9 one typical full set of data is shown, corresponding to simultaneous acquisition of
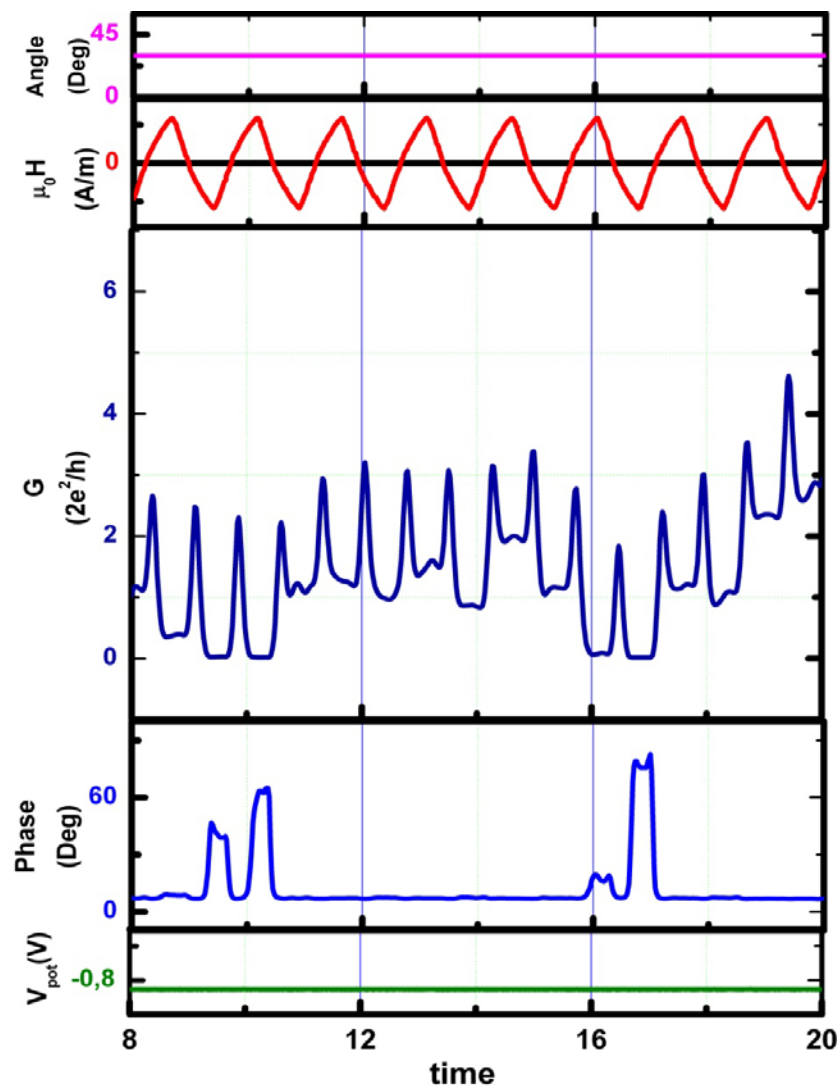
Fig. 5.9 A full set of data acquired during the experiment. Besides the conductance of the sample, related to the magnitude of samples impedance the phase of the voltage drop through the shunt resistor is shown. Simultaneous acquisition of the magnetic field amplitude and orientation and the plating potential are also recorded.

magnetic field magnitude and direction, the conductance of the sample and the phase of current under a given potentiostatic control V_{pot} .

The key advantage of using a lock-in is the simultaneous detection of magnitude and phase of the AC voltage across R_0 (see description of the circuit – fig 4.3) as depicted in fig 5.10
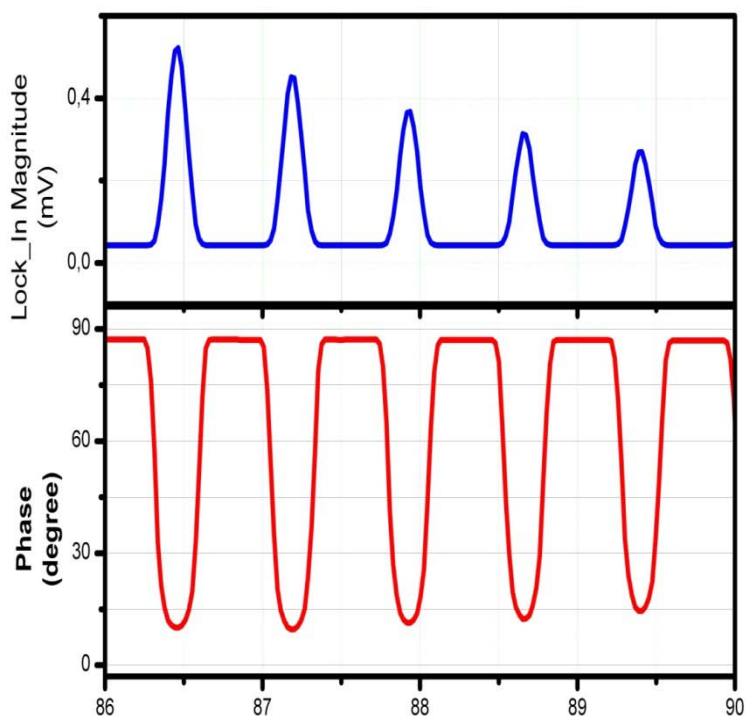

Fig. 5.10 Lock-in Detection of voltage amplitude and phase

Before the contact between the two working electrodes is established establish the current in the circuit is almost zero. Hence the voltage drop is very small. The circuit is having a predominant capacitive behavior due to electrochemical bath; therefore the phase shift is far from zero. When a contact is formed the impedance of circuit diminishes significantly and the current is increasing. The circuit becomes resistive, as indicated by the phase shift to values around 0 degrees. The forming and breaking of the contacts is obtained by switching the DC electroplating potential as previously explained in chapter 4.

The lock-in magnitude aquatinted is processed to calculate the conductance of the nanocontact using the formula deduced in chapter 4

$$G_X = \frac{1}{\frac{V_0}{V_X} - 2R} G_0$$

A graph with time evolution of the nanocontact conductance is provided in real time during the electroplating process as depicted in fig 5.11
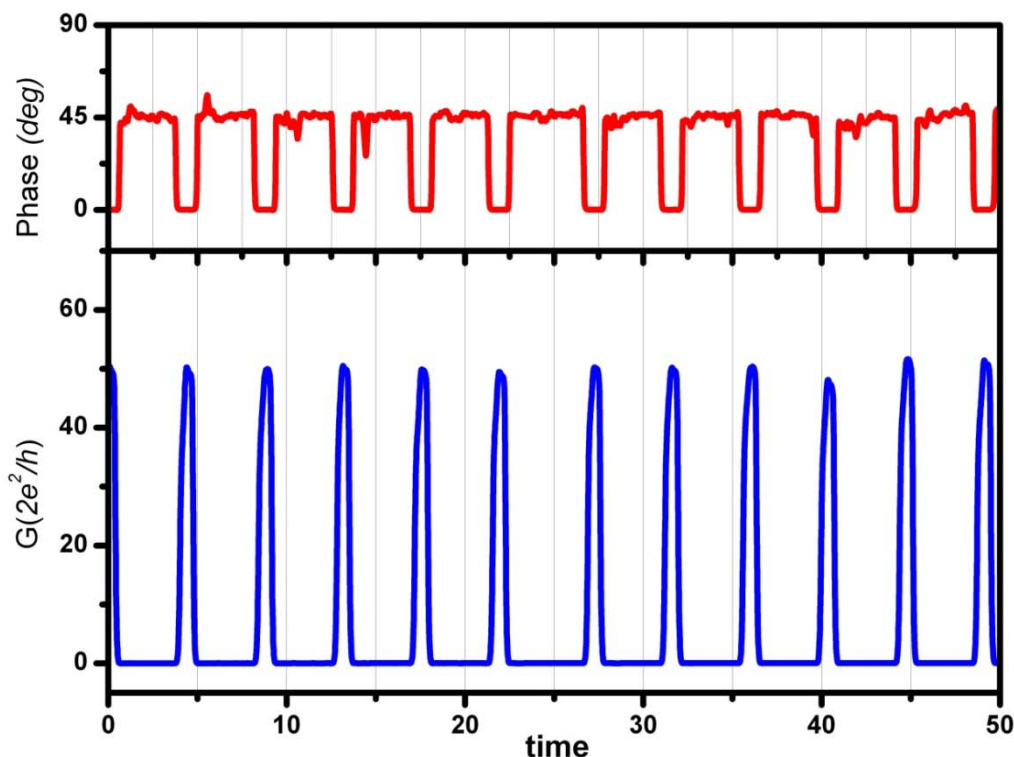
Fig. 5.11 Opening and closing of a Ni nanocontact. When the contact is closed (G>0) the zero phase is corresponds to a pure resistive behavior**.**

Steps and plateaus of conductance were observed for all metals deposited. Stabilizing contacts with a conductance of a few quanta conductance indicates occurrence of a contact made of a few atoms only **[10]**.

For experiments dedicated in observing conductance plateau were performed, the plating potential was conveniently tuned in order to obtain a slow plating regime. In this way we have a small deposition rate, hence a small number of atoms are coming to contacts and the change in conductance is slow. A key goal was to obtain a large time span for the plateaus of conductance, as we want them to persist during a time long enough for performing magnetic field sweeping or rotation.

In fig 5.12 and 5.13 the closure of a nickel, respectively cobalt nanocontact is shown. For nickel, plateaus of conductance close to $1G_0$ and $2 G_0$, lasting several tens of seconds were obtained.
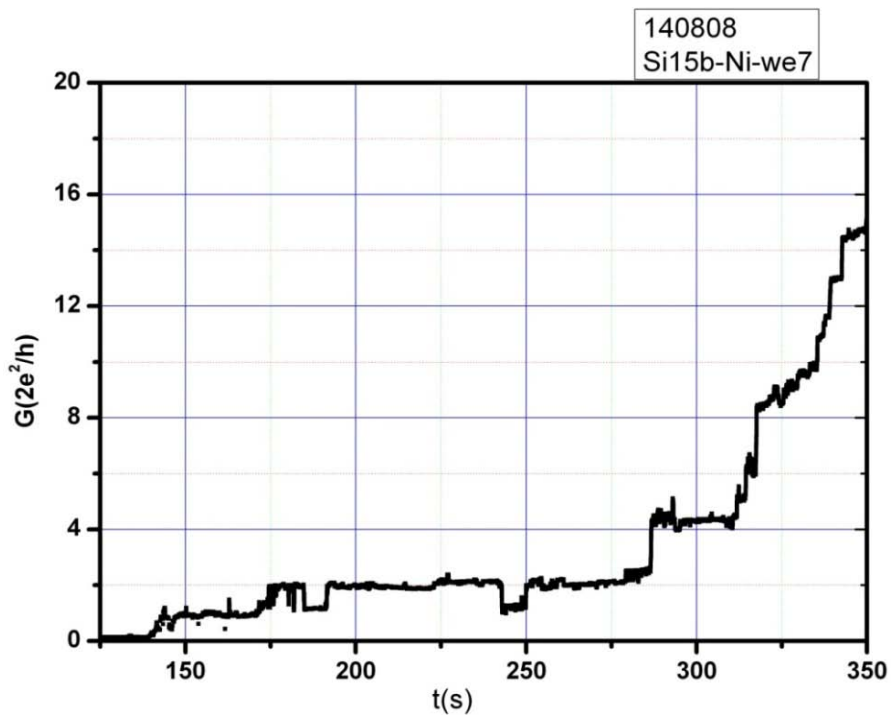
Fig. 5.12 Conductance time evolution for a Nickel nanocontact
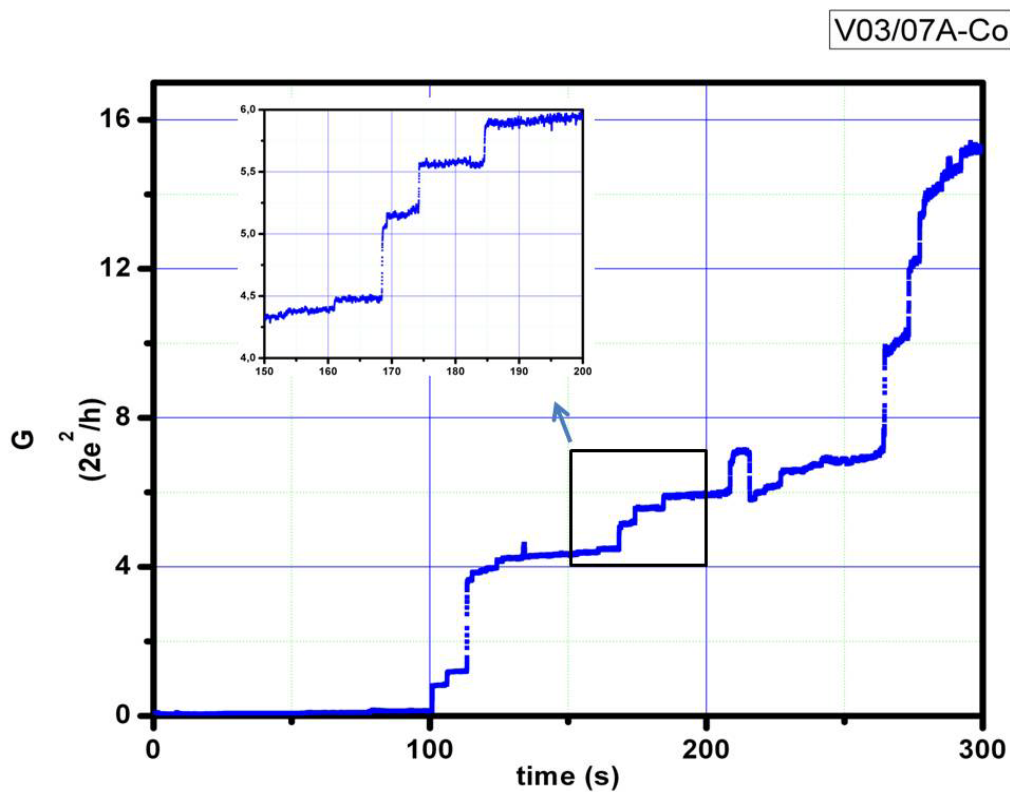

Fig. 5.13 Conductance time evolution for a Cobalt nanocontact.

For cobalt the steps in conductance are also observed, long plateaus being obtained for conductance values close to 4 G_0 and 6 G_0. Note that switching between plateau-like structures can be found. This is not surprising if we recall that a few atoms only ensure the contact stability.

More detailed experiments were performed in the case of silver (fig.5.14)that we used as a bench mark material. It is known that silver is having stable low conductance atomic configurations and exhibit plateaus of simple multiples of G_0. We tried and succeed in reproducing Xie [4] experiments, related to switching between two silver low conductive states.
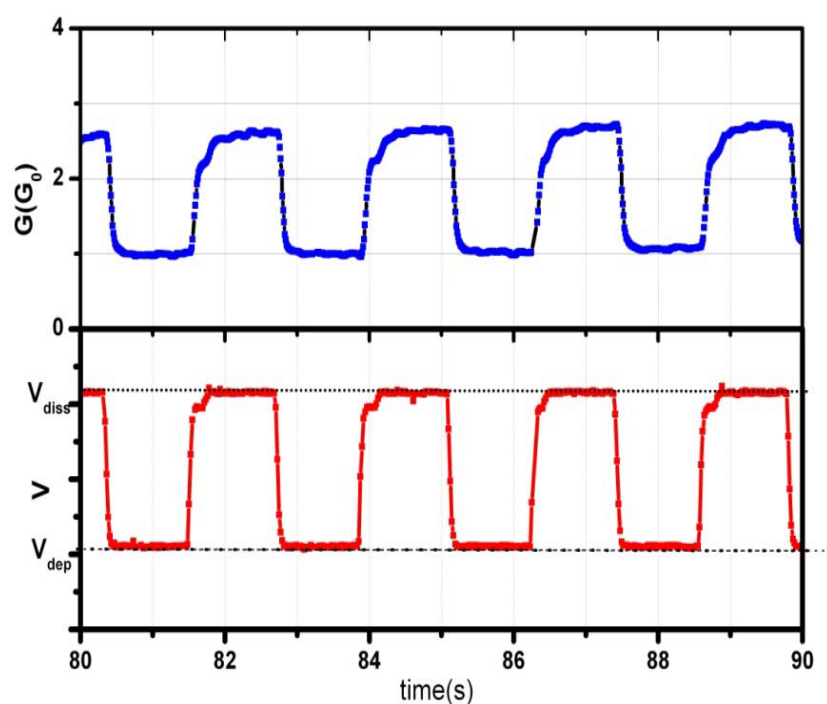
Fig. 5.14 Quantum conductance switches between two low conductive states of a silver atomic contact. The switch is controlled by changing the plating potential. The glitch corresponding to V=0 V is due to potentiostat software

Both experimental [11] and theoretical [12] investigations of atomic-scale silver wires indicate that a monatomic chain exhibits a conductance of approximately 1 G_0 and that the electronic transport through atomic-scale silver chains is free-electron-like. Therefore silver can be expected to behave similarly to the alkali metals and also to gold, leading to a conductance of integer multiples of G_0 for the lower conductance levels. As depicted in fig 5.14 we succeed in obtaining a reproducible atomic switch between approximate 1 and 2 G_0 only by changing the potential applied.

These experiments, related to the observation of plateau conductance, as well as the one related to atomic quantum switch in silver were used as validations for our experimental setup. We obtained a large body of experimental indication of occurrence of conductance plateau, of reproduced experiments on silver, providing us confidence in fabrication of nanocontacts made by a few atoms only.

5.3 Magnetoresistance of nanocontacts

For investigating magnetic effects on the conductance of nanocontacts the magnetic field was swept or rotated while the metal is slowly deposited or dissolved. By choosing adequate plating potential we managed conductance plateau stabilization lasting tens of seconds. This is easier to realize especially for higher values of conductance, while for contacts of few quanta of conduction maintaining the stability is challenging. All data presented in this chapter are for experiments where repeated sweeps for magnetic fields could be performed. Reproducible MR behavior is considered as fundamental necessary condition for presenting data.

The magnetic field rotation axis is in the plan of the substrate, perpendicular to the electrodes axis. The sweeping rate was between 0.06 and 0.75 Hz with maximum amplitude of 1.4 Tesla. For rotation the maximum speeds was π rad/s, but smaller speeds, around 0.01π rad/s or even lower were used if the time span of the conductance plateau allowed. Low speeds were preferred because our setup is
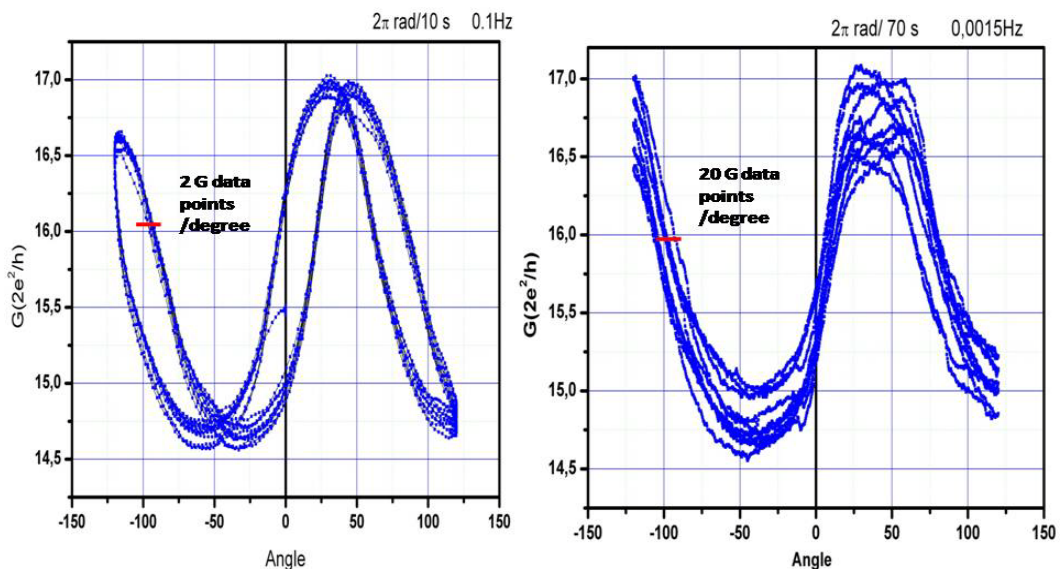
Fig. 5.15 The influence of speed rotation of the magnet on the shape of recorded data. The hysteresis is due to a delay between lock-in and magnetic field acquisitions artificial resulting from the integration time of the lock-in data

exhibiting a lag in data acquisition at higher rates as depicted in fig. 5.15

For most of the data presented in this thesis the AC excitation had 4 mV amplitude and a frequency in the range of [211-231] Hz. This 4mV is small enough

for ensuring similar electrochemical conditions at the two sides of the contact as several tens of mV is usually needed for plating/dissolution conditions we used. A few AC cycles are necessary to obtain reasonable lock-in data. Typical integration time was set to 50 ms.Except where mentioned, the data was taken *in situ*, in the presence of the electrochemical bath or of the electrolyte. This fact is having a major importance as emphasized at the end of this chapter.

The work of this thesis was mainly focused in study of magneto-resistance effects in nickel nanocontacts but also others metals (as cobalt, gold, silver and platinum) were studied and the results are presented further. As described in chapter two, previous studies on magnetoresistive effects on nickel nanocontacts reports values of magnetoresistance in a very wide range, from the complete absence up to one million percent. Our experimental results for these effects also reflect this huge range of magnetoresistance values. After all results will be presented we are thinking we found a plausible answer for this problem, which is the key work of this thesis.

I will start by presenting the experiments that didn't show any magnetic effect with sweeping or rotation of magnetic field. In fig 5.16 are presented the time evolution for contacts conductance when the field was swept between -1 and +1 T (left) or rotated: 1T magnitude with $2\pi/10s$ (right). As depicted those ones were sample for which we succeed in maintaining a stable plateau of conductance for almost 100 seconds or even more
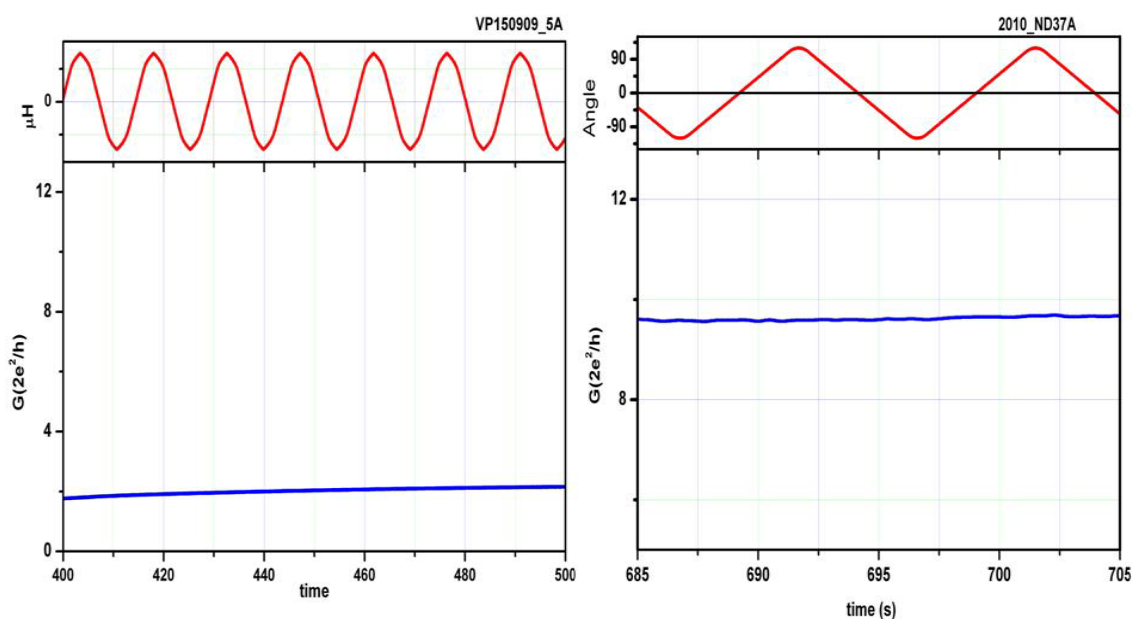
Fig. 5.16 MR and AMR curves for nickel nanocontacts in a ballistic regime of conduction. No dependency on magnetic field is present.

 magnetic field. This behavior was met for almost 30 percents of all our samples. What is interesting to be mentioned here is this absence of any magneto-resistive effects were common for a whole batch of four pre-patterned samples. As described in the chapter related to the sample preparation, on one silicon substrate are prepared concomitant, by optical and e-beam lithography, four gold nanojunctions. This similar magnetic behavior, with 0% magnetoresistance, for all nanojunctions from the same substrate induced the idea that the problem is possible related to fabrication process. Even we have open and close the contact few times for rearrange the atomic configuration still no effect was observed for these samples.

The next set of results is related to experiments where the magnetoresistive effects were in agreement with previous work **[13-17]**, and theoretical simplest estimates **[18, 19]**. According to valence band model, in atomic size contacts of nickel the electric transport is characterized by five conduction channels with the transmission probabilities between 0 and 1. The opening or closing of one or more of these channels results in changes in MR of 10-70 % for low conductance values as most frequently reported in literature **[20, 21].**

 Our experiments did not show indications of spin valve behavior, or domain-wall MR effects. All data found when sweeping field can be interpreted by an AMR model. At low field values the change in resistance is attributed to a deviation of the average magnetization from saturation magnetization. The key experimental indication is a similar magnitude of MR and AMR and the change of MR sign when modifying the angle by 90 degrees.

In figure 5.17 an example of MR effect around 8-10 percent is presented. A magnetic field with amplitude of 0.75 Tesla was swept with a frequency of 0.6 Hz. The data was taken while closing the contact, as a slightly time increase of conductance can be seen in the up figure. The resistance is presenting two symmetrical minimums around 0.35 Tesla. The results have a good reproducibility, if we omit the variances on conductance due to the closure of the contact and the position of the conductance peaks remains stable for many sweeps of magnetic field

Fig. 5.17 MR effect in a nickel nanocontact. Top: Time evolution of conductance. Bottom: The corresponding G vs magnetic field curve.

Anisotropic magnetic resistance measurements showing similar amplitudes are presented in fig 5.18. A 1.2 T magnetic field was rotated with a frequency of 0.15 Hz in a plane perpendicular to the junction .The conductance was switching between 10 and 11 G_0 under the field. The shape of the curves is rather close to a $\cos^2$ behavior
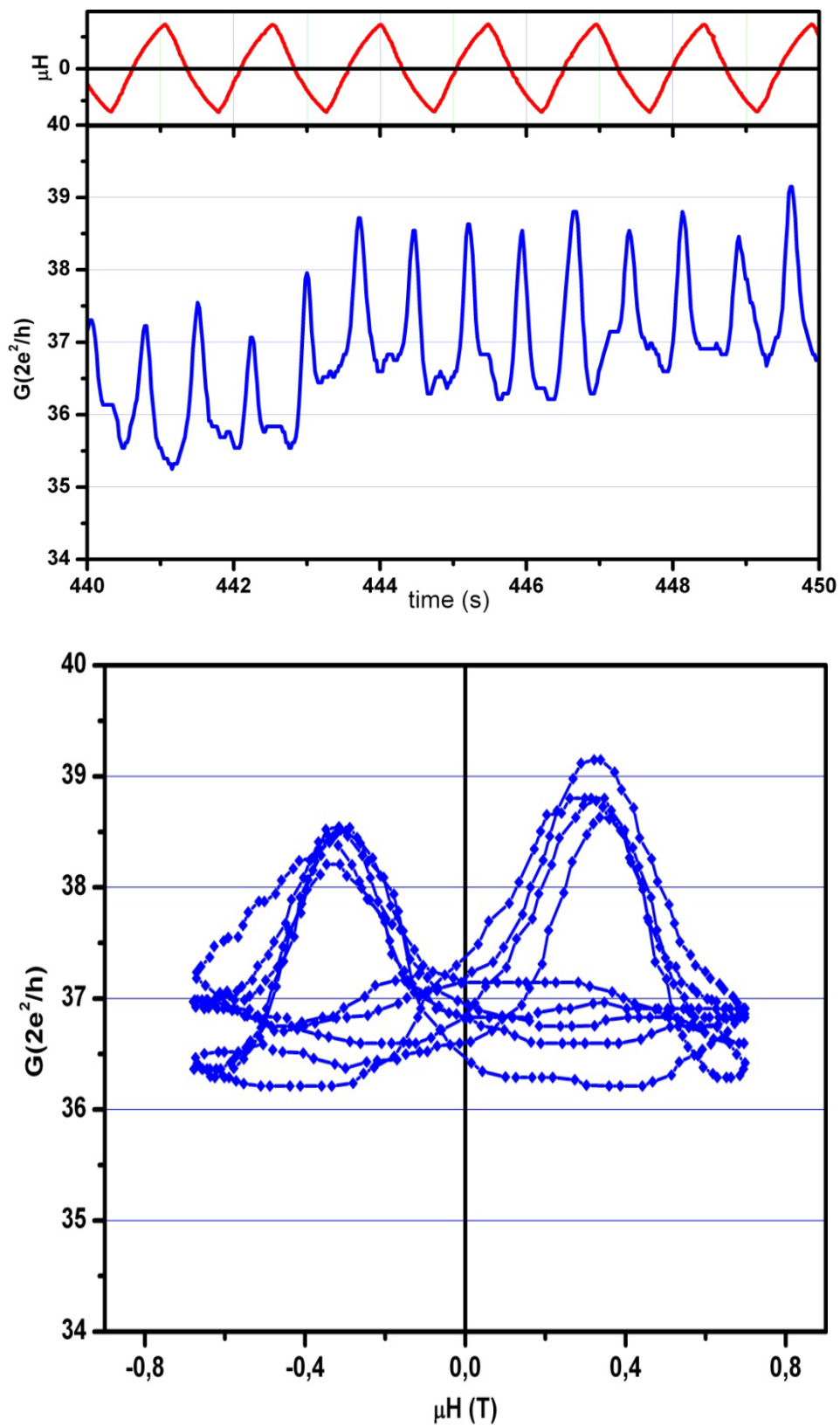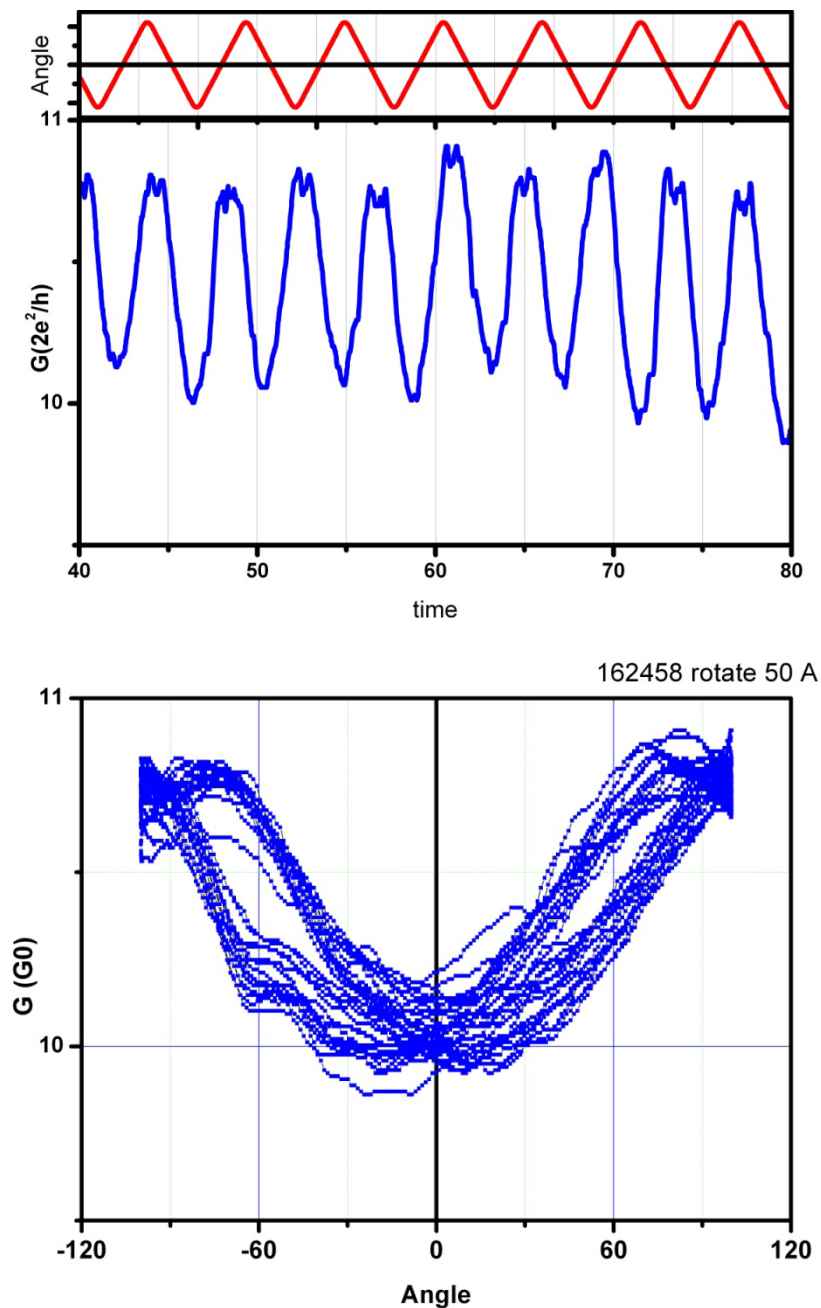

Fig. 5.18 AMR effect in a nickel nanocontact. Top: Time evolution of conductance. Bottom: The corresponding G vs magnetic field curve

About 30% of the samples exhibited values for MR in 10 -70 % range. The remaining 40% showed spectacular MR or AMR effects, greater than 100 %. We can't explain why this difference between samples prepared in a very similar manner. It may be related to small, uncontrollable variations in the preparation process or, more probably, to the electrochemical environment.

First spectacular results were obtained for a FIB pre-patterned sample, depicted in fig. 5.19. The amplitude of magnetic field was 0.3T and this field was swept and rotated. 600 % MR was observed for values of magnetic field around 300 Gauss. AMR values around 400 % were obtained while rotating the field. The data was taken while the electrolyte was flowing with a rate of 0.5 ml/hour. As shown the conductance jumps between two finite values, hence here is not an open-close switch but between two conductive states. The AMR shape very "peaked" around 90
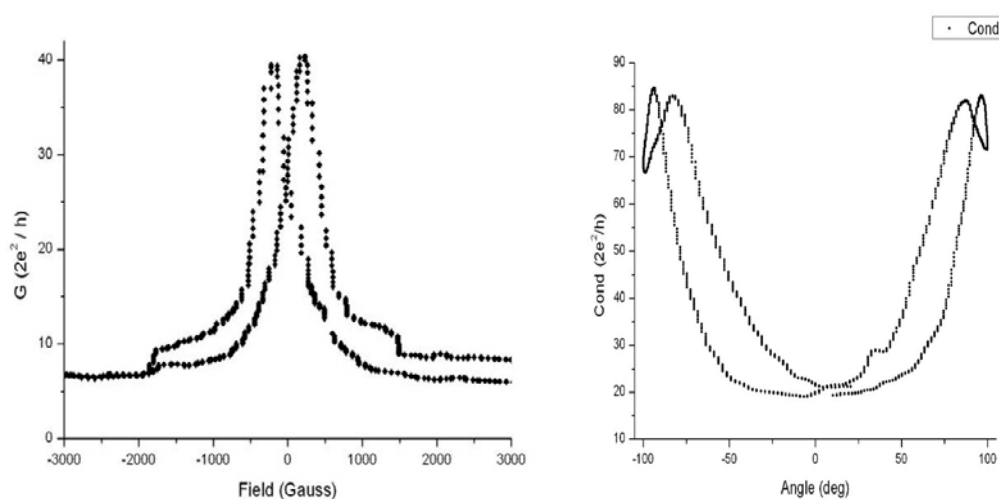
Fig. 5.19 600% MR and 400% AMR in a nickel nanocontact

degree is probably caused by a lack of saturation of the sample with a limited field of 0.3T applied.

One of the most comprehensive data obtained from a sample whose conductance remains quite stable for a long period of time, allowing us to sweep the magnetic field for different angles and then to rotate the field is shown in fig.5.20 for a Nickel nanocontact. Due to the fragility of samples these kinds of results are very difficult to obtain. The key factor is to find the right plating voltage where neither deposition nor dissolution takes place. As seen in upper graph the data looks very reproducible, a

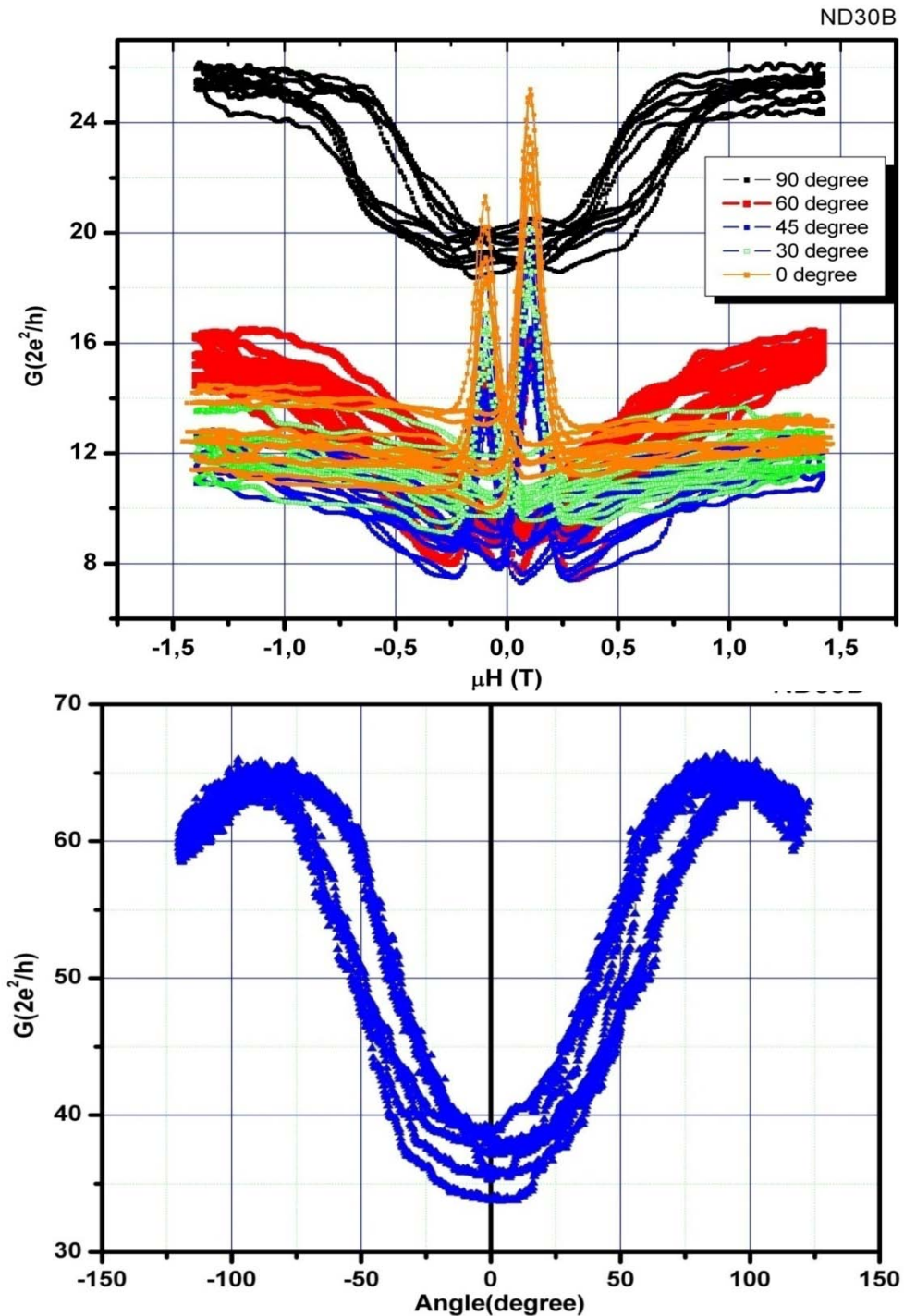**Fig. 5.20** Top: MR curves for different angles. Bottom: AMR curve

clearly indication of the stability of the contact. The conductance jumps between 8-10 G_0 to 20-24 G_0, hence a MR effect around 120% at a magnetic field of approximate 0.2 T. The angle between the direction of the field and the direction of the current was fixed at 0, 30, 45, 60 and 90 degree and for each angle several MR

curves was taken. The peaks for conductance were positioned at same value of the field for every angle and the shape of curves evolves from a flat appearance for 0 degree till a typical one at 90 degree. AMR studies are presented in the bottom graph of fig. 5.20. A field with a magnitude of 1.4 T was slowly rotated (2π rad/1min). A small hysteresis can be observed. The AMR ratio was about 100 %, obtained for quite high values of conductance as it shifted when we went from MR to AMR measurements.

When performs experiments on lower conductance samples with only few quanta of conduction, the problem is again related to the instability of the samples.
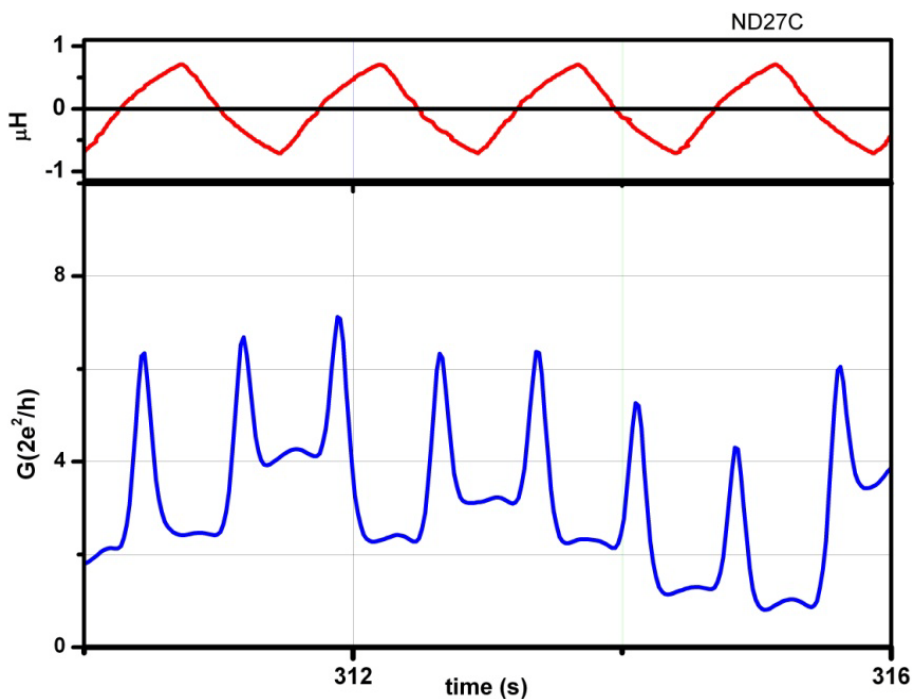
Fig.5.21 Time evolution for a low conductance Ni nanocontact under sweeping magnetic field

In general contacts formed by a few atoms are very hard to be maintained stable. It should be emphasized that the studies are performed at room temperature, where stability of atomic junctions can be significantly altered by thermal fluctuations. Anyhow we succeed in perform MR studies on low conductive samples taking advantage of high speed acquisition data of our system. The data are presented in fig. 5.21. The magnetic field, having amplitude of 0.8T, was swept at 0.75Hz. The conductance was jumping between 2 and 6 G0, hence a MR ratio of 300% was observed.

Almost all measurements performed in this thesis were performed in situ. The electrolyte was always present on the nanocontact area and the data was acquired, under a fixed plating voltage that ensures equilibrium between dissolution and deposition. We tried to flush out the electrolyte, pump the system and cool down the sample in order to perform lower temperatures measurements. As previously described in chapter 2, our system is designed to be cryogenic compatible. We checked that the PDMS enclosure is not modified by thermal (4K-300K) cycling. Anyhow, for low conductance samples, we didn't succeed in performing ex situ or low temperature experiments. As soon as we flush the electrolyte and try to pump down the cryostat the contact was destroyed. More work and many tries are still needed to resolve this problem.

For low resistive sample we succeed in performing ex-situ experiments and the results are presented in fig.5.22. After the contact was fabricated, the electrolyte was flushed out, the sample was rinsed and dried by flowing in the microfluidic channels distilled water and nitrogen respectively. Then, carefully watching the integrity of the contact by monitoring the conductance, the enclosure was sealed, pumped down and cooled using liquid helium. The data was taken using slow rates for sweeping and rotating the field.

The AMR curves corresponding to 300 and 5 K (left) look quite similar. The metallic nature of the contact was confirmed by the increasing of conductance with decrease of temperature. A 1 % value of observed AMR is what is expected for the bulk case.

Same order of magnitude was obtained for MR effects on this sample. The behavior is the same for both RT and LT, with conductance peaks for a magnetic field around 0.3 T. The conductance is obeying significant "high" fields' variations that are rather mysterious. Such behavior is unclear, departs from Lorentz type bulk- magnetization (with a parabolic decrease of conductance verusu magnetic field) and maybe cause by samples oxidation Anyhow, as mentioned before, more work is still needed for doing ex situ measurements, especially for low conductance sample.
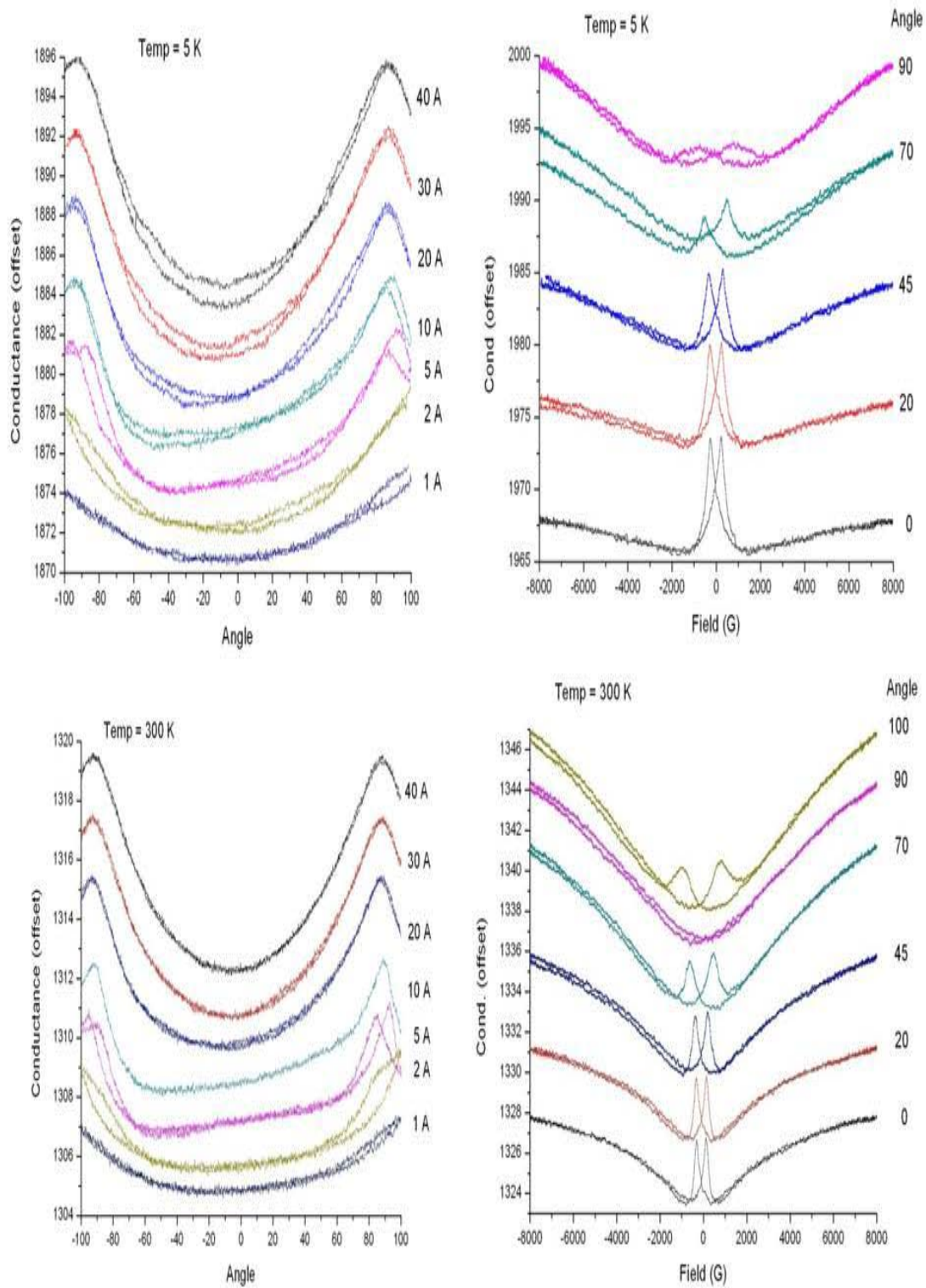
Fig.5.22 Comparison between MR curves for a diffusive regime of conduction in Ni at different temperatures. The curves are offset for clarity. The AMR curves are taken for different values of applied magnetic field. The correspondence between field and current values can be found in appendix 1

In situ experiments in an acidic bath prevent samples oxidation. As evidenced in the chapter describing our experimental setup we are able to change rapidly the electrolytes flowing through the microfluidic channels. This is a new approach limiting mechanical disturbances in order to prevent low conductive junctions to be destroyed.

When implementing a procedure of cleaning and drying the sample with limited detrimental effects, we characterized MR properties under the modification of electrochemical environment. We performed this type of experiment on several samples exhibiting huge change in resistance under applied magnetic field. One example is provided in fig. 5.23 where an open-closure of the sample is observed under swept field.

Oscillations between 0 and 40 G_0 were found with this last upper limit having a slightly tendency of increasing due to continuing plating. The voltage was decreased at -0,85V when a continuous switching behavior of conductance between two fixed values was obtained. This is depicted in the left graph from the bottom of fig. 5.23. As observed for this interval of time the conductance is jumping between an open state and 50 G_0 for very reproducible values of the magnetic field. The graph is symmetrical with respect to zero magnetic field value. It is not a switch between two finite values of conductance; therefore we can consider the MR as infinite in this case.

At t = 75 s we stopped flowing the nickel sulphamate solution and replaced it with the boric acid buffer electrolyte. Typically 20 seconds are needed for the new solution to reach the junction. We used minimal flow rates in order` to avoid huge velocities of the liquid in the microfluidic channels and therefore possible mechanical damage to the contacts (see Appendix 2). At this time of experiment the electromechanical valve system was very distant from the sample, as we intended to cool down the whole system.

As soon as the boric acid is reaching the junction area the oscillations of conductance are disappearing (middle region of upper graph). It should be clearly mentioned that the plating potential conditions remained, avoiding Nickel dissolution (- 0.4V with the peak at - 0.1V) and preventing oxidation. The opening of the gap can be due typical mechanical instability and the absence of Ni ions from solution impedes reconstruction of the contact.
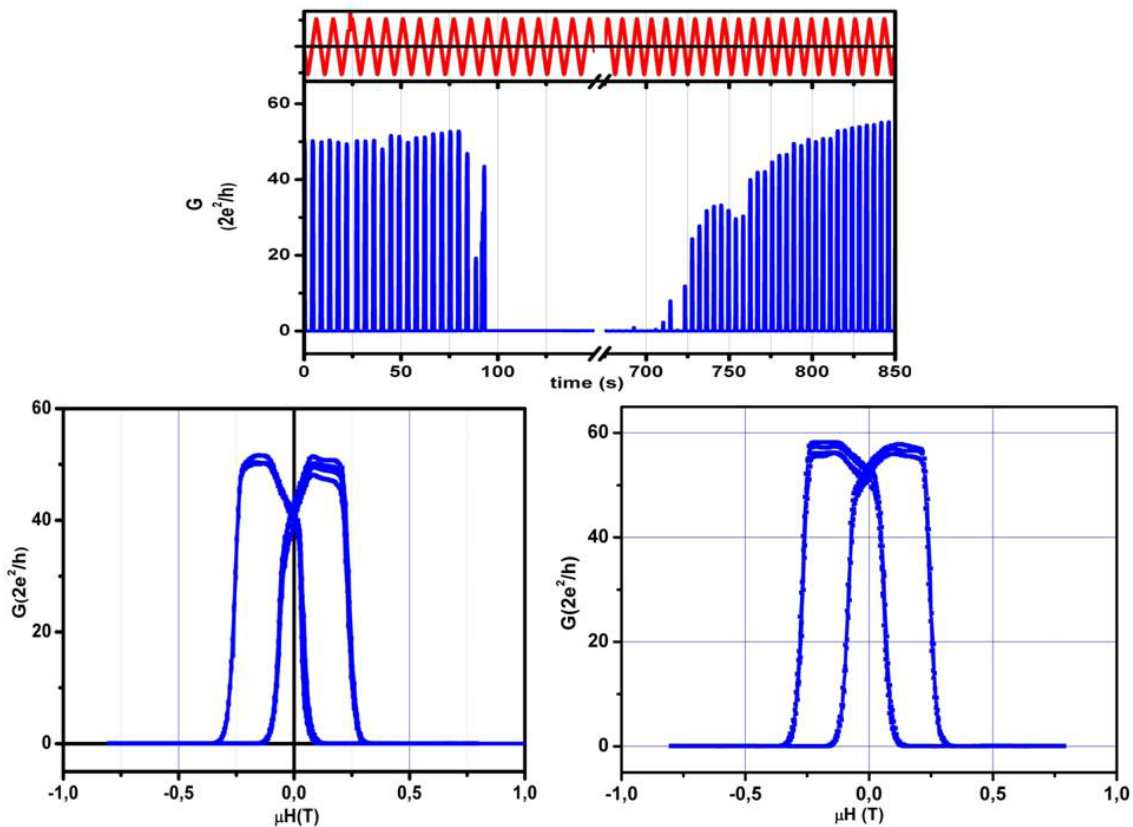
Fig. 5.23 Influence of chemical composition on the MR of a Nickel nanocontact.
Top: time evolution of conductance during the whole experiment.
Bottom: MR curves corresponding to first and last time interval, when Ni ions are present in solution. For the middle period, where no Ni ions are in the solution no switches in conductance are present

When the nickel sulphamate is reinserted in solution the oscillations restarts (bottom right-zone 3) and the MR curves are remarkably recovered. The shapes are almost identical; hence we can affirm that the contact behaves in exactly same manner on both initial and final stages of experiment.

This experiment raised some questions related to the influence of the electrolyte on the transport properties. The main question is what is determining the opening the closing of the gap when Ni ions are present in the solution? The applied voltage is at the onset of reducing Ni ions in solution and quite far from Ni dissolution potential. Keeping boric acid electrolyte prevents the Ni from oxidizing. (ph = 4.3 for boric acid, ph = 3.8 for nickel sulphamate). Data is showing unambiguously opening and closure under applied field. These results are similar of those obtained by Garcia and Chopra [22, 23], where huge values of thousands % for MR were reported. As detailed explained in chapter two these results were attributed to mechanical artifacts [24]. However our experimental conditions are

different, as the free standing length of the sample is reduced below 50 nm. The only way to reconcile a mechanical artifact would be to suppose that the patterned lines are detached from the substrate. Optical microscopy and scanning e-beam images did not shown any indication of such behavior.

The precise values of magnetic for which the jumps in conductance take place indicate unambiguously that these ones are related to the field. For clarifying the aspects related to electrolyte we needed an experiment with a stable, finite value of the conductance in absence of nickel ions. Such occurrence is seldom as we generally observed a contact opening when exchanging the electrolyte. A good compromise is to perform the perfusion when a rather robust contact is made, exceeding 100 G_0. The resulting graphs for this experiment are presented in fig. 5.24. The chemical solution used was the same nickel sulphamate which was exchanged for the middle stage of experiment with a boric acid electrolyte. The amplitude of the field was 1T and the rotating speed was 0.5π rad/s. Rotation was permanently maintained for whole experiment. The initial plating voltage was -1V, which was reduced at -0.8 V when the contact starts to form and kept at this value during time frame of fig. 5.24.

The upper graph of fig. 5.24 is showing the whole time evolution of the conductance. In the initial time range, when nickel sulphamate solution is present, the conductance was jumping between 0 (open contact) and 130 G_0. These jumps are clearly following the magnetic field as depicted in bottom left graph. Around t = 180 s the electrolyte is exchanged. The conductance drifts when the bath composition is modified and the oscillations disappear when the solution is presumably completely exchanged. The most important thing is that the conductance remains stable at a FINITE value. Close inspection of the AMR curves for this part of the (bottom middle graph) revealed a 3% AMR ratio, which is expected for a diffusive regime of conduction in nickel. We consider this data as evidence of absence of mechanical artifacts. This is very important because the influence of these artifacts was always invoked when high values of AMR ratio were obtained.

When we exchange back the nickel solution the oscillations reappeared. The corresponding AMR curves have (bottom right) similar shape with those ones related to zone 1 although a hysteresis is differentiating them.
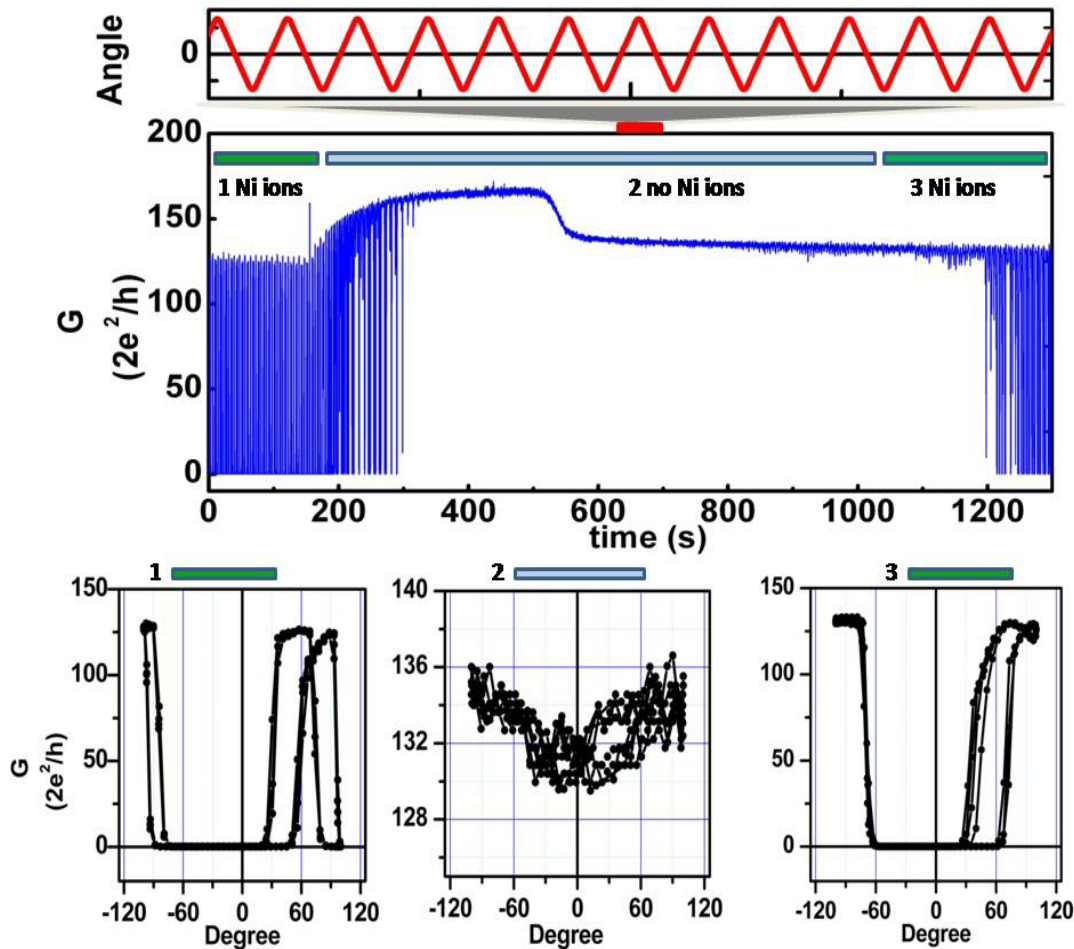
Fig.5.24 Influence of electrolyte on the AMR of a nickel nanocontact.
Top: time evolution of conductance during the whole experiment.
Bottom: AMR curves corresponding to three different stages of experiments.

This experiment clearly opens a new perspective on explanation of huge MR effects characterizing electrodeposited nanocontacts. The fact that the spectacular AMR is present only when the electrolyte contains Ni ions and disappears completely thereafter, allows us to claim that these ions are responsible for spectacular AMR values.

One more argument about the dependency of MR effect on the Ni ions from solution was brought by the experiments where a continuously changing of MR ratio was observed when the concentration of ions was also changing. When the solutions were exchanged the switch was not done suddenly but gradually. It seems the MR ratio follows this change in ions concentration in solution (fig. 5.25)
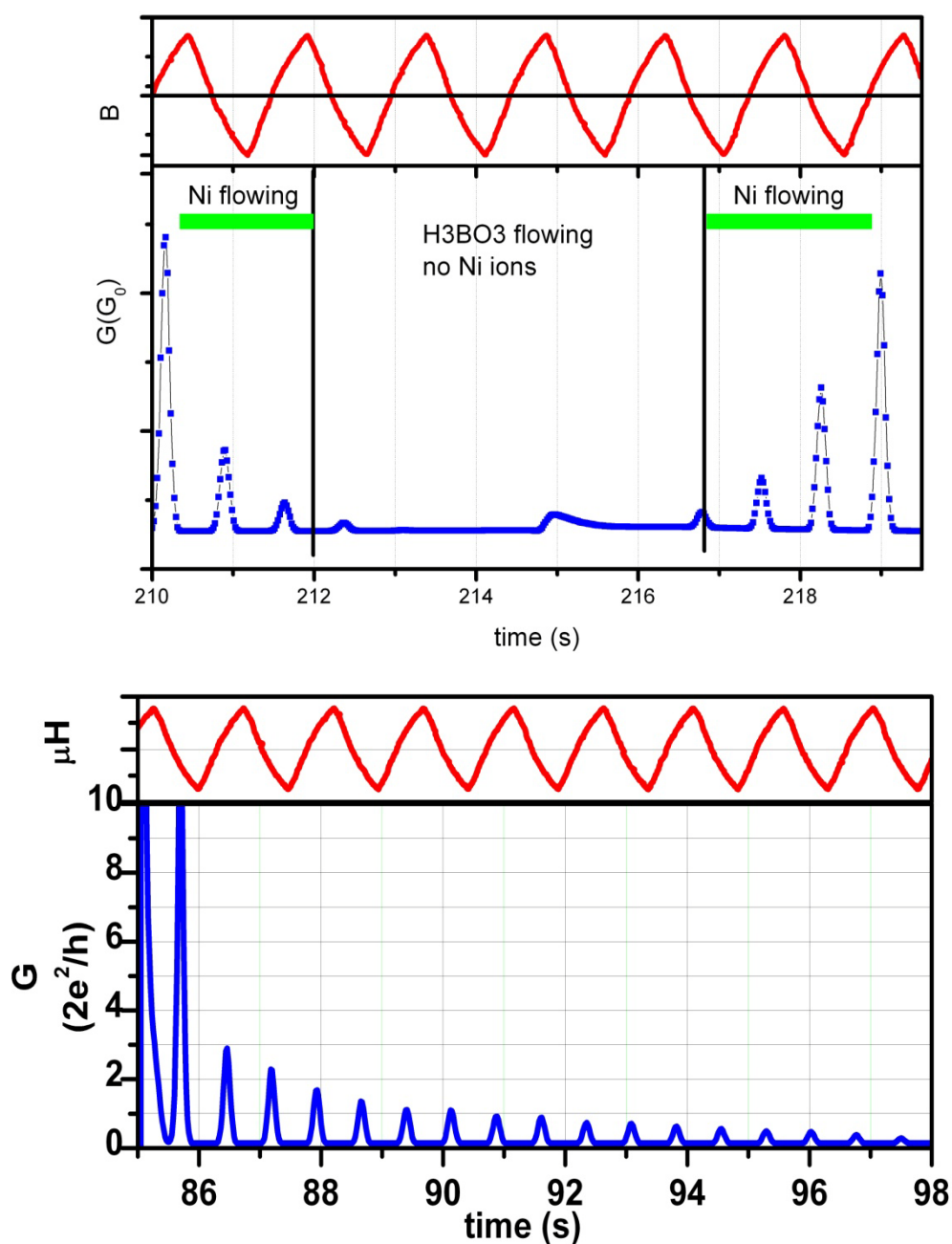
Fig.5.25 Influence of ion's concentration from electrolyte on the AMR of a Nickel nanocontact. When Ni concentration decreases/increases the MR ratio is decreasing/increasing continuously

A few attempts were made for fabricating nanocontacts using other metals than nickel. Because of difficulty in stabilizing the conductance but also due to the lack of time and samples experiments for other metals were not so many. Our priority was first to try to understand the effect for nickel and then extend our studies for other metals. Spectacular magnetoresistance effects were also observed in

cobalt contacts and one corresponding example is shown in fig.5.26. The cobalt was deposited a cobalt sulfate solution (Table 1) at -1.2 V. The magnetic field, having amplitude of 0.6 T was swept at a frequency of 0.4Hz. The data shows a 20 % MR
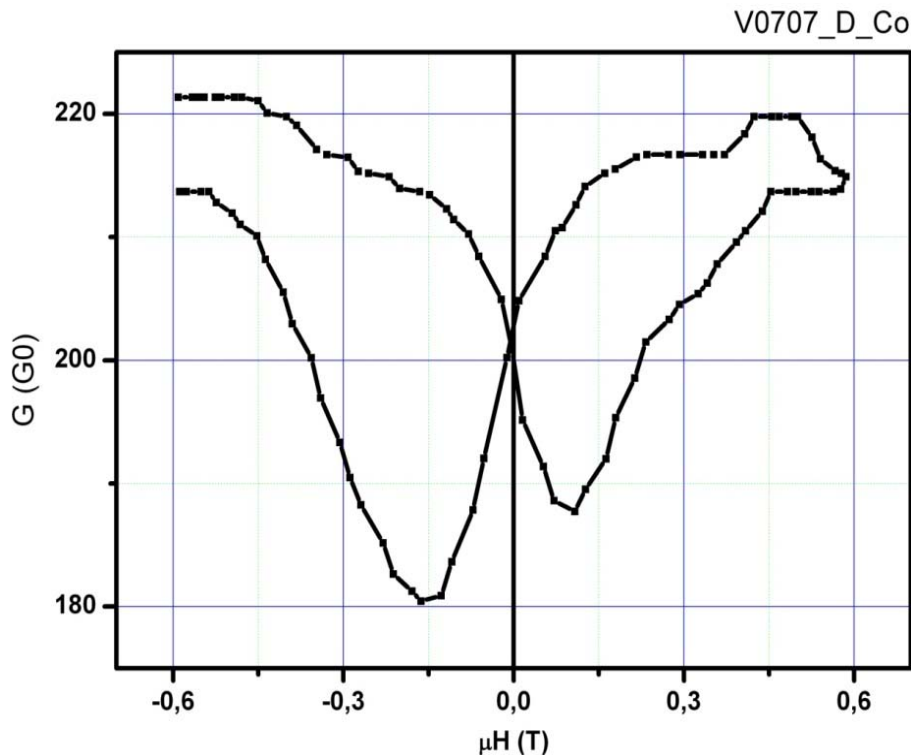
Fig.5.26 MR effects in cobalt contact in the presence of the electrolyte.

ratio, unexpected for this level of conductance (~200 G_0). What is remarkable is the sign of the ratio; opposite to the case of nickel, the cobalt manifests a positive MR (the resistance is decreasing for small magnetic fields.). Again we think such MR values and the MR behavior are related to the presence of transition metal ions in the electrolyte.

Platinum nanocontacts were also fabricated. Platinum is a nonmagnetic 5d metal, at the onset at itinerant ferromagnetic properties. Tosatti **[25]** suggested that 1D platinum nanowires exhibit significant exchange interaction that can lift the spin degeneracy. Platinum is also of interest due to its chemical stability. The deposition was performed using a chloroplatinic acid solution under applied potential ensuring a slow deposition rate. The magnetic field was permanently swept at a frequency of 0.12 Hz for two amplitudes: 0.4 T (upper graphs) and 0.12 T (bottom graphs). The curves from fig.5.27 show a switching of conductance between 0 and 20 G_0 at magnetic field values around 5 mT. The sharp peaks obtained for the lower field can

be a indication that the sample is not saturating in this case. The data corresponding to lower field (bottom) are more interesting because the conductance is switching between two finite values.
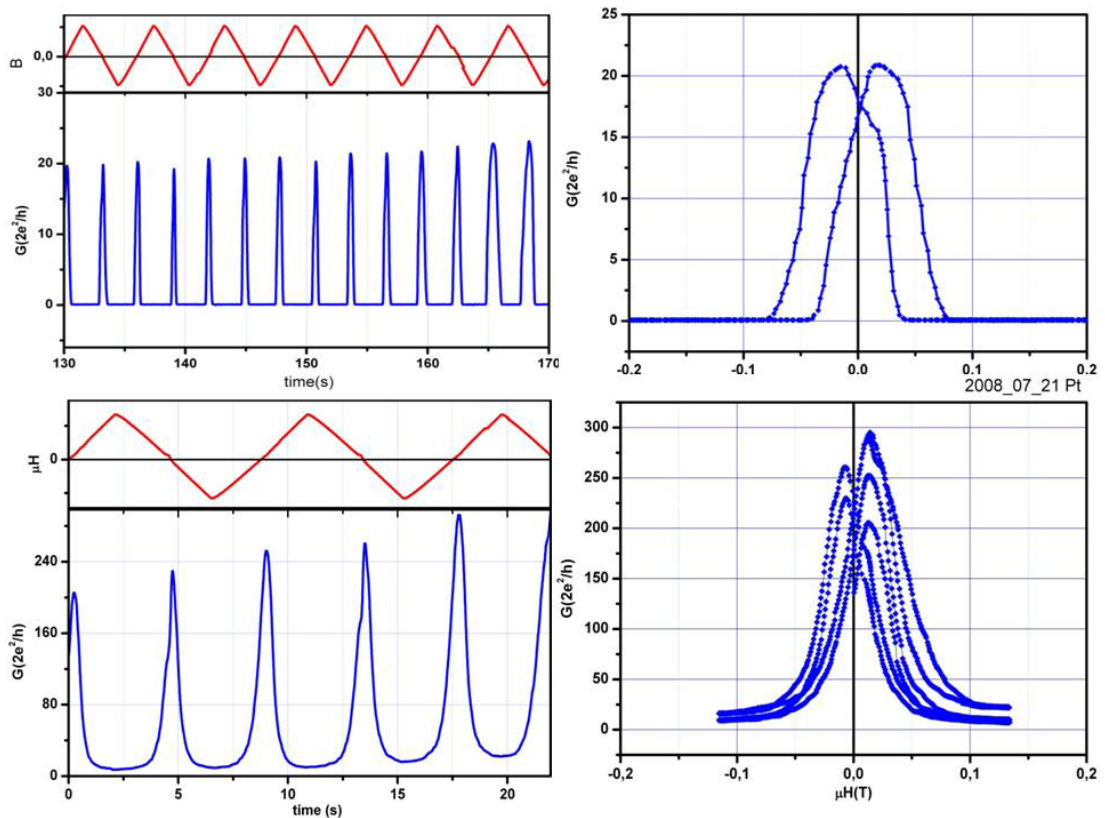
Fig.5.27 Magnetoresistance effects, in platinum nanocontact, in the presence of electrolyte, Applied magnetic field amplitude: Top: 0.4T; Bottom 0.12T
Time evolution of conductance (left) and corresponding MR curves (right)

Indeed the lower value of conductance is increasing from an initial non-zero value. The MR ratio observed in this experiment was up to 2500 %, a huge value, never reported. We can associate this extraordinary value with the presence of electrolyte in the vicinity of the contact.

In summary, for about one third of the samples, MR ratios much larger than those reported on MBJ or ECJ can be observed in nickel nanocontacts. Using the microfluidic setup, we can show that the origin of such behavior relates to the paramagnetic Ni^{2+} (Ni^+) ions in solution, trapped in a very narrow gap between ferromagnetic electrodes.

Such new properties were also observed for cobalt and platinum. These spectacular findings are quite surprising and depart significantly from results

obtained with nanocontacts made by other methods. In order to prove that the observed behavior relates to the medium and not directly to the nanoelectrodes fabrication methods an ideal test of these new ideas is to perform experiments on EMJ or MBJ immersed in an electrolyte.

The data can even correspond to on/off MR behavior related to changes of a few orders of magnitude. Such huge changes were previously reported in the literature, but were essentially discarded by the community, under the assumption of mechanical displacements of the electrodes. We have experimental evidence that the explanation might be different and involve paramagnetic ions in the solution

5.4 Experiments on mechanical break junctions in electrochemical environment

A set of experiments performed for this thesis was dedicated to combine the electrochemistry with mechanical break junctions. This new strategy consisted in first mechanically breaking the junction and then to close it by electrochemistry. A slightly different variant consists in first again mechanically breaking, electroplate for a given time and then close it back mechanically. These experiments were performed in collaboration with the group of prof. M. Viret from CEA Saclay. The initial patterned electrodes were deposited on a flexible kapton substrate (fig.5.28) and the PDMS electrochemical cell was sticked over the metallic lines patterned on this substrate.

I will present here only preliminary results. Combining these two methods is quite time-consuming due to many difficulties in adapting samples to the tow methods. One of the most important problems arises from sticking the PDMS enclosure to the sample. Even covered with SiO2, the kapton had proven not to be a good adherent substrate. The geometry of electrodes obtained by MBJ is different from our samples, special designed for the use of microfluidics. Hence, problems related to the flow of electrolytes through the microfluidic channels occured. Another
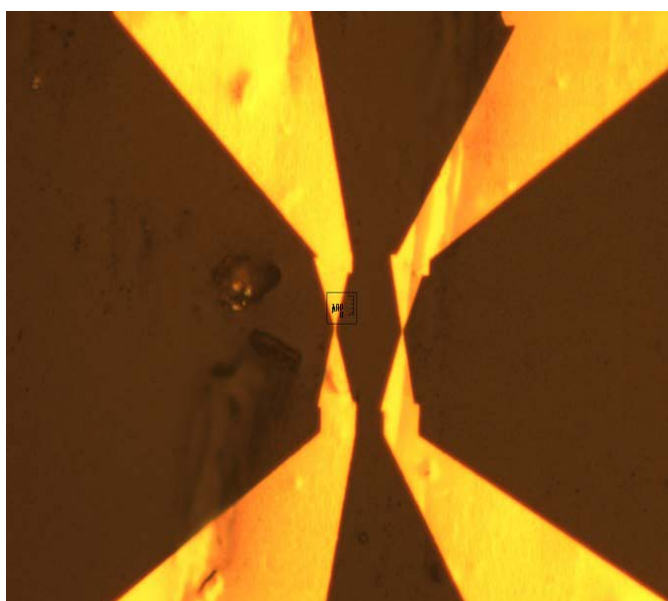
Fig.5.28 Gold electrodes deposited on a kapton flexible substrate for MBJ

problem is related to the size of the setup. We had to insert between the poles of the magnet a sample holder including a system used to mechanically break the junction (fig.5.29). Therefore the applying of large magnetic fields was severely limited..
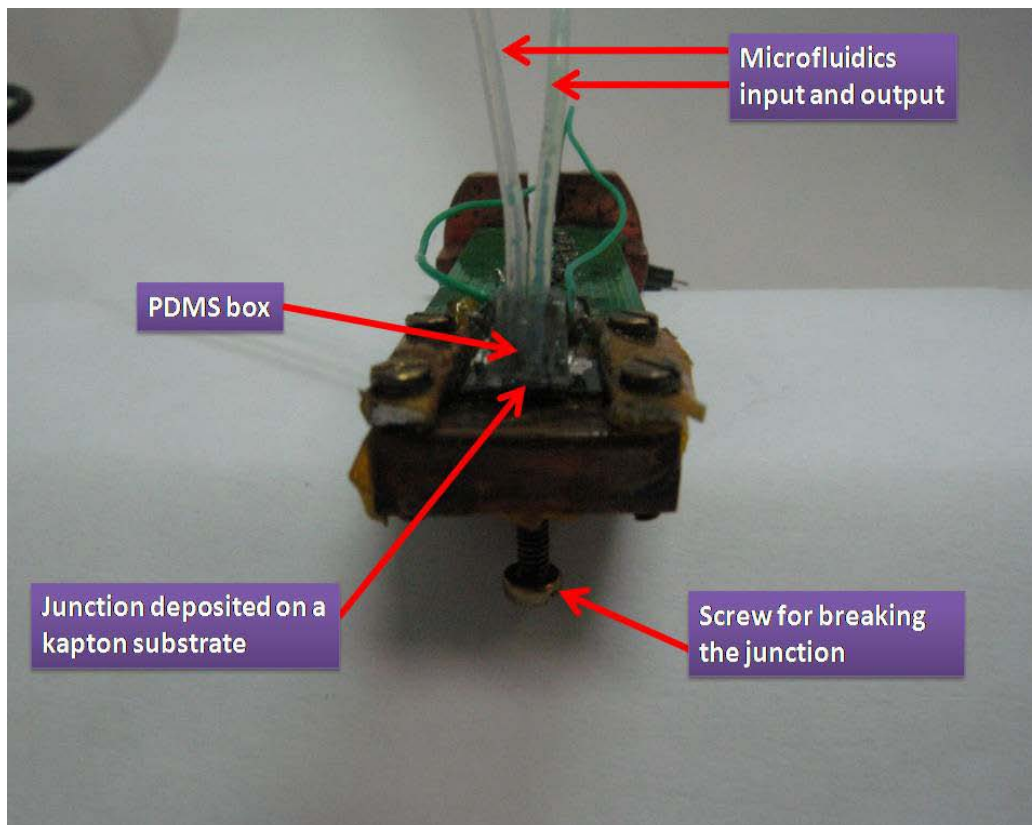
Fig.5.29 Experimental setup for combining MBJ with ECJ

It is challenging to obtain samples for studying a mechanical break junction under the influence of the electrolyte. The yields for a reliable sample fully mounted wired and correctly exposed to the electrolyte bath is around 20 %. Taking in account that the spectacular effects for MR are observed for one third of the samples, almost a 7 % chance to obtain a reliable sample is obtain.

In a first set of experiments Au is deposited between permalloy electrodes. We start by mechanically breaking an initial very fine line of Py diminishing its conductance down of few tens of G_0. MR and AMR measurements (fig.5.30) are then performed. The results obtained - 1 % AMR and 2-3 % MR - are what is expected for bulk permalloy. We should mention that no electrolyte is present at this moment of the experiment.
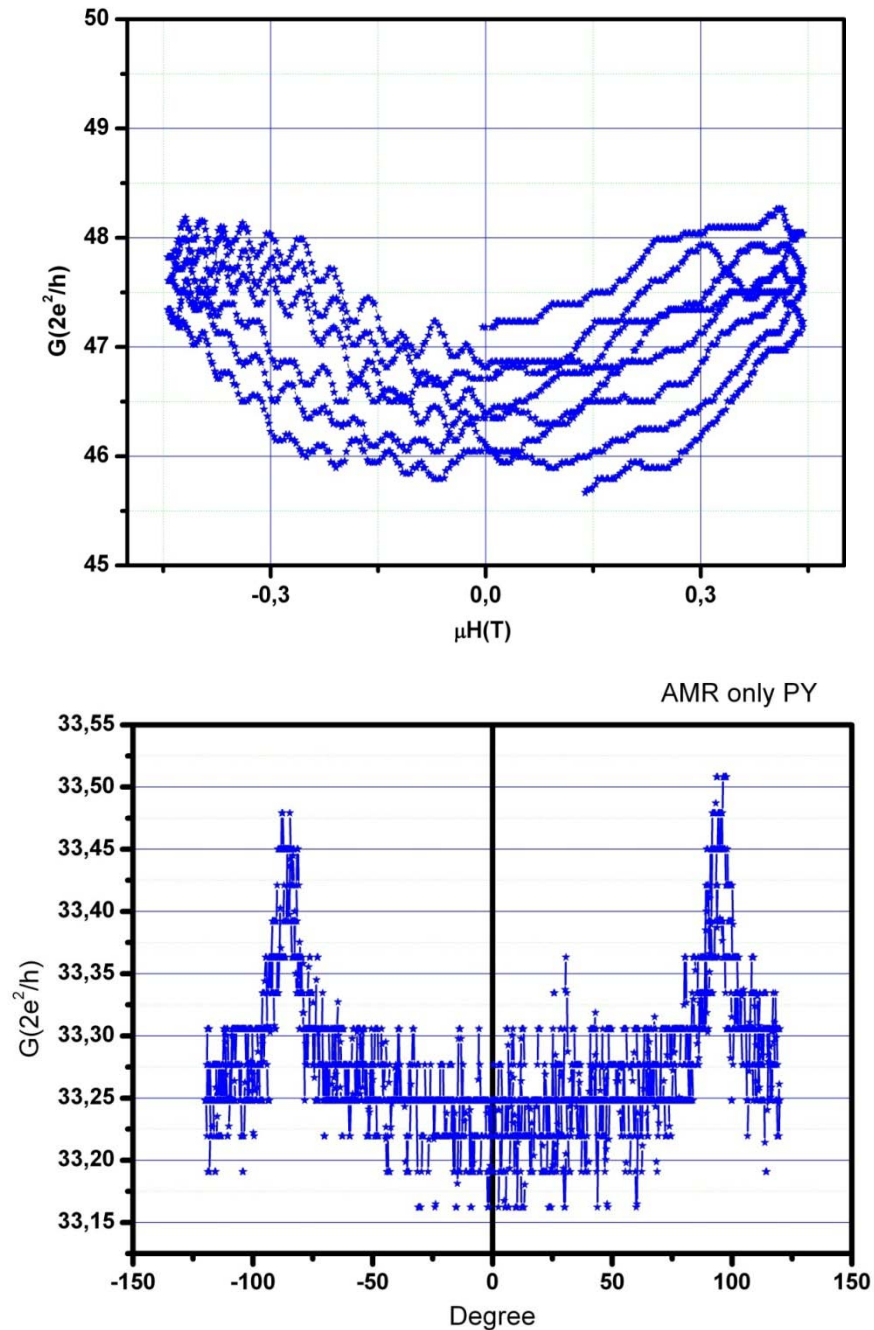
Fig. 5.30 MR and AMR curves for a permalloy contact done by MBJ.
The peaks of conductance at 90 degree angles relate to the difficulties in saturating the sample

The second step consists in breaking the Py junction until the Lock-In indicates a completely open gap. At this moment we start flowing Au solution in the system and plate at slow rate. The magnetic field is permanently swept or rotated. Conductance curves versus magnetic field angle or amplitude corresponding to the conductance magnitude of fig 5.30 are presented in fig 5.31
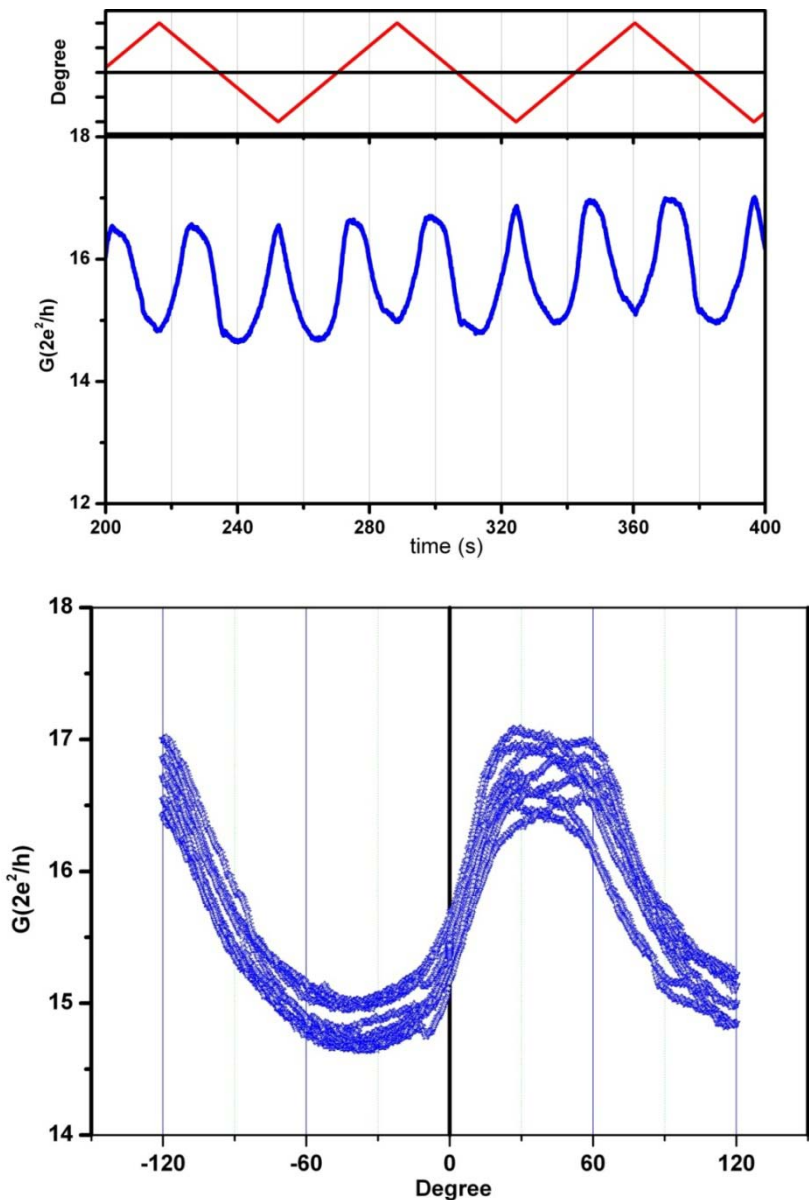
Fig.5.31 MR effects in a Au nanocontact between two permalloy electrodes, in the presence of electrolyte. Top: time evolution of conductance. Bottom: Conductance versus angle graph.

where the angular dependency of conductance is shown . The amplitude the effect is around 20% but what is remarkable is that the AMR is not maximally at 0 or 90 degrees. This can be related to a misalignment of the samples, due to very possible displacement of the junction when is broken mechanically. All measurements were performed rotating a 0.4T magnetic field at a very small rotation frequency. (~0.01Hz)

For the MR measurements the magnetic field was swept between – and + 0.4 T for several different angles between magnetic field and the current (from +120
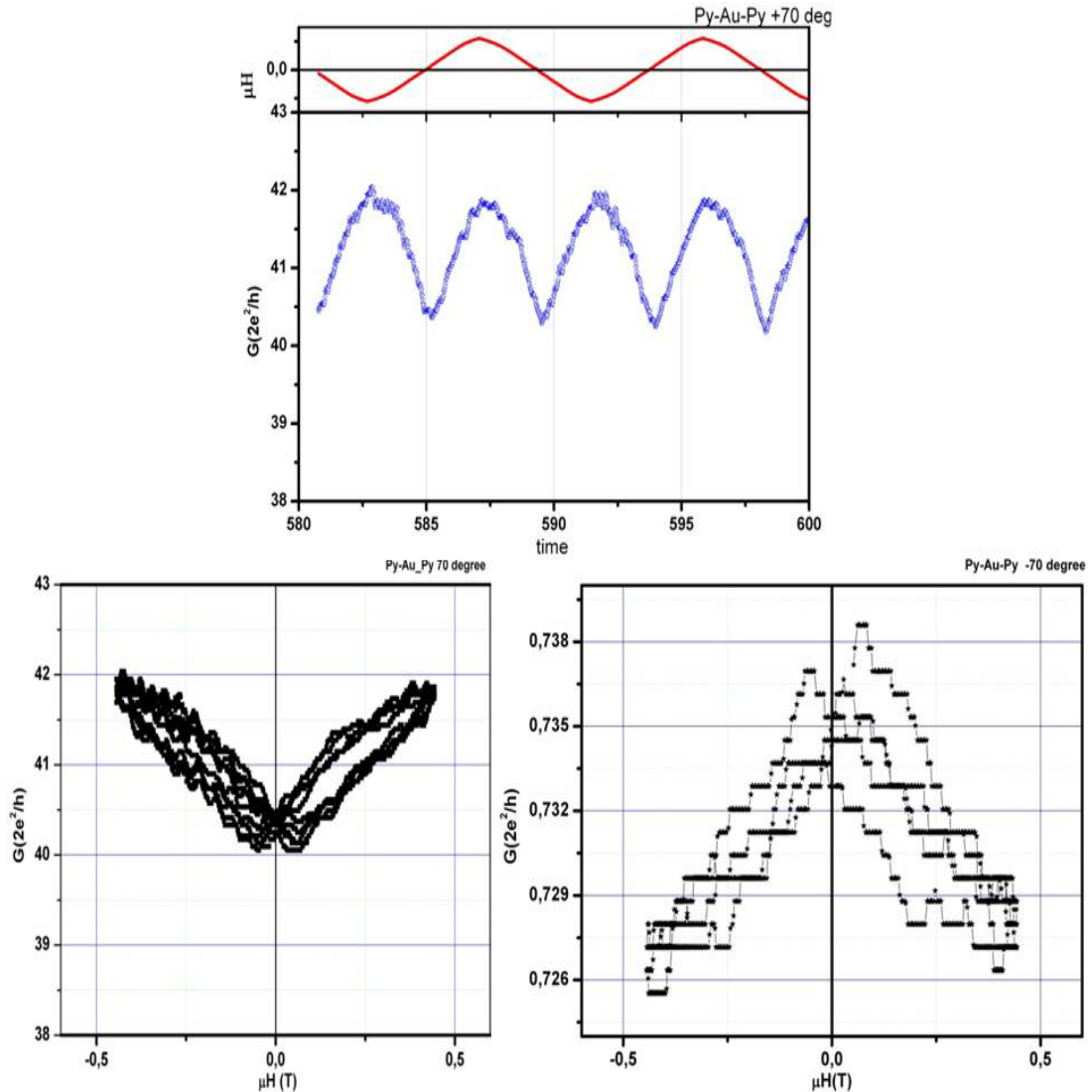
Fig.5.32 MR effects for an Au nanocontact between two py electrodes, in the presence of electrolyte. Electrochemistry combined with MBJ was used for fabricating the contact. Top: time evolution of conductance. Bottom: MR curves for two different angles between the magnetic field and the direction of the current: +70 degree (left) and -70 degree (right)

to -120 degree). In the bottom part of fig.5.32 are MR curves for two opposite orientations of the magnet are shown. Unfortunately we couldn't maintain the contact of same level of conductance, therefore the scale is different but what is important, is the behavior that can be observed. Opposite signs of MR is obtained for orthogonal orientations of the magnet. MR can therefore be interpreted as an AMR type behavior. The observed MR ratio is around 5 %, bigger than that one observed for bulk permalloy.

5.5 Discussion of the results and possible future work

The topic of magnetoresistance properties in magnetic nanocontacts is very controversial. Two reasons can be invoked: the samples are extremely challenging to fabricate, and investigations of magnetic materials under external applied magnetic field can easily result from mechanical strains or displacements caused by trivial interactions of a magnetized small entity with an external field.

Occurrence of quantized conductance, integer multiples of e2/h, in magnetic materials is also very controversial in the literature, even though simple theoretical considerations make such simple occurrence quite unlikely. Here, the chemical sensitivity of transition metal surfaces makes unambiguous experimental conclusions and comparison between experiments delicate. This is why a lot of care and time has been taken in designing an experiment where surface oxidation can be prevented, and a follow-up of the magnetoresistance properties during sample growth and dissolution can be performed.

A few clear conclusions can be drawn from the large body of experiments we performed. Plateaus of conductance, with conductance values of the order of a few multiples of e^2/h, can be obtained for several deposited materials. This is a positive indication that our setup is suitable for achieving a quasi-ballistic regime of conduction in metallic nanocontacts, lasting long enough for sweeping the external applied magnetic field and to perform measurements on electrical properties.

All observed MR data can be interpreted in terms of anisotropic change of resistance under magnetic field. When a large MR is observed, similar amplitude of changes can be observed when varying the angle between field and current. We conclude therefore that no preeminent indications of spin valve effects are found in our data.

For the magnetoresistive effects amplitudes, the results can be divided in three main categories. One third of the sample didn't show any MR effects and we attributed this to initial electrodes fabrication process. Second third from all samples presented MR ratios in the range of 10 to 70 %, as predicted by models and as reported by others. The most intriguing results relate to magnetoresistance changes beyond 100 %, reaching even thousands percents, observed for the last third of our samples. A set of experiments performed on mechanical break junctions confirmed that more spectacular effects can be observed when the contacts are exposed to an electrochemical process.

Taking advantage of the new microfluidic approach developed during this thesis we showed unambiguously proven that these spectacular MR ratio are related to the paramagnetic ions present in electrolyte solution. Exchanging the solution containing Ni ions with the boric acid buffer solution made the huge MR
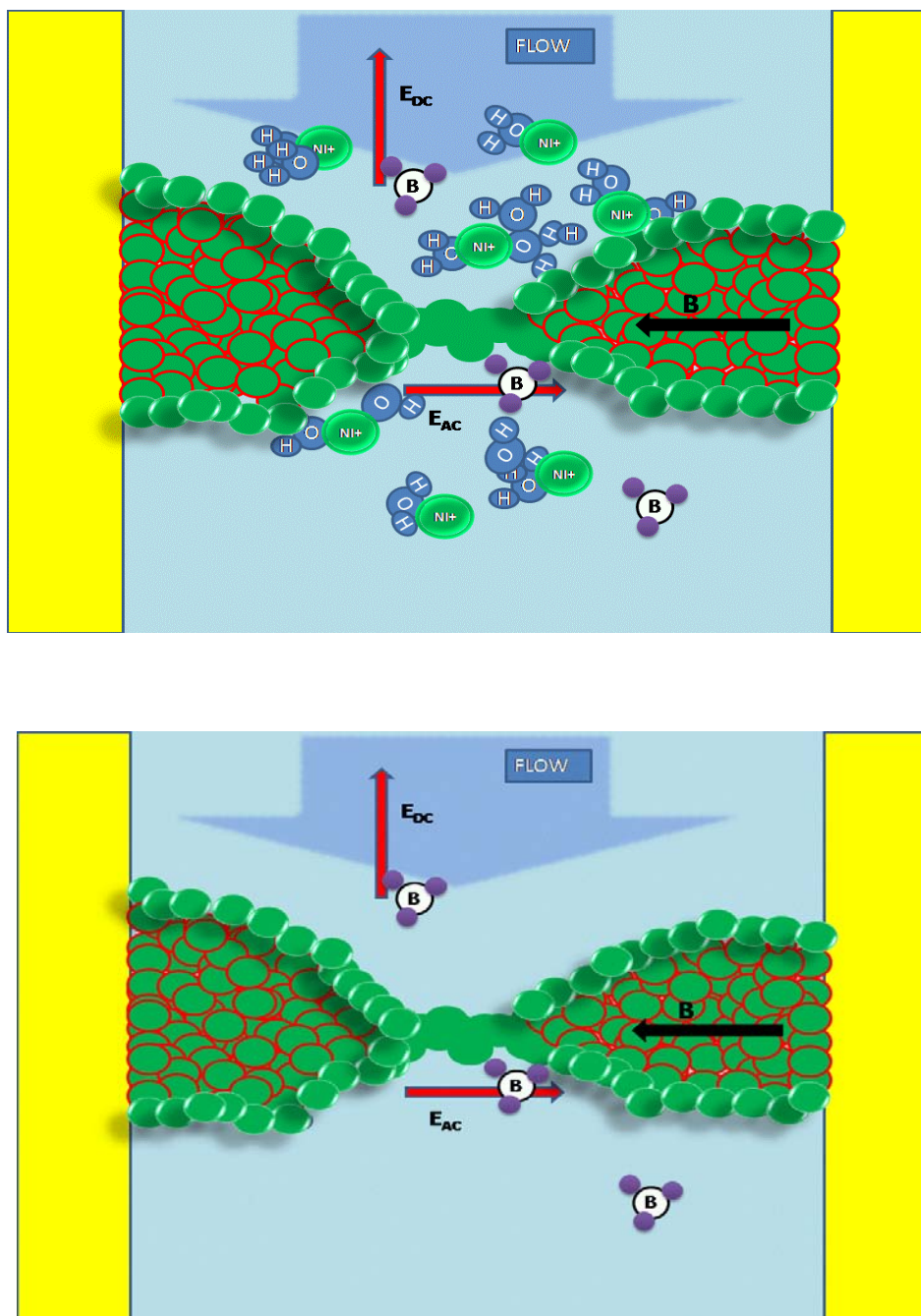
Fig.5.33 The Ni nanocontact in the presence (up) and in the absence (bottom) of nickel ions in electrochemical bath.

effects disappear. The most intriguing experiments showed stabilization of nanocontacts of conductance stabilizing a 120 G_0 exhibiting very large AMR (result shown in fig.5.24) even though ballistic regime of conduction is not expected to dominate at such large conductance values (incidentally this claim is still discussed in the literature [26]). An AMR switch effect is disappearing when no Ni ions are present in solution. For the case where ions are in the solution the MR is switching between 0 and 120 G_0 following the orientation of magnetic field. Therefore the main question is how the Ni ions from the solution can control the resistance of the nickel nanocontact which they surround? The two situations are plastically depicted in fig. 5.33 where the contact area is shown with and without nickel ions in the solution

Having shown data where bulk-like AMR is observed when the Ni ions are not present, we have pointed out experimentally unambiguously the source of the spectacular effects. By being able to measure small AMR, we also show that mechanical artifacts cannot be invoked to explain the huge MR values. This brings new light to a problem that created intense debates in the community in the past ten years. However, at the time of writing this thesis, do not have a reasonable and simple theoretical explanation for this discovery. In the following, we will focus on eliminating other possible experimental artifacts or trivial explanations.
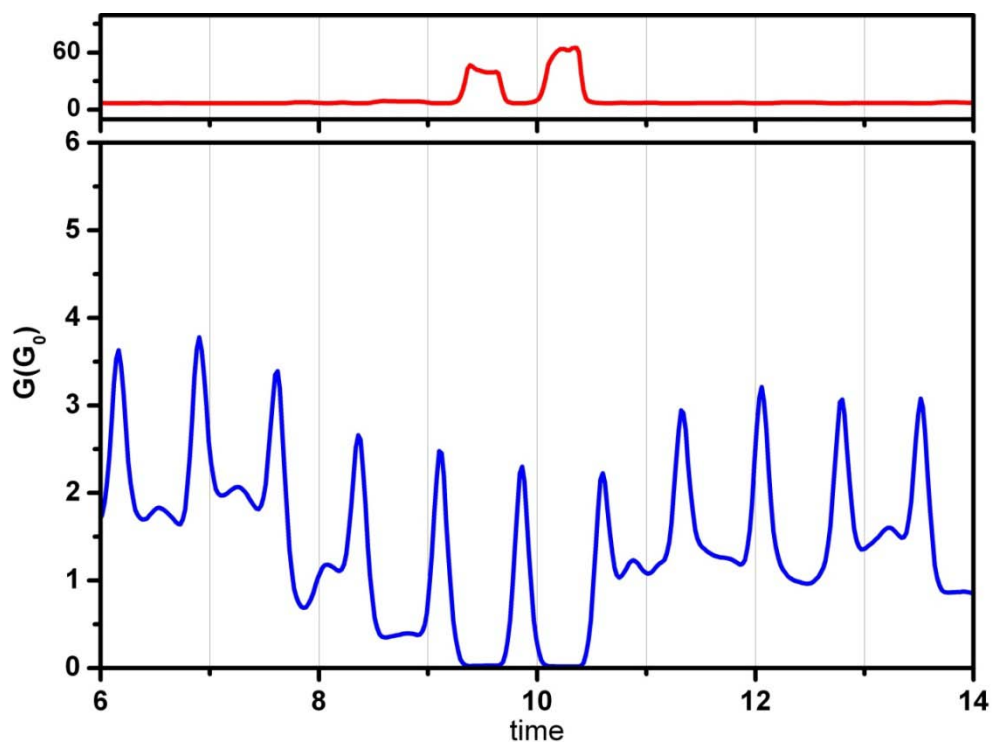
Fig.5.34 The phase is changing significantly when the contact is opening or closing. It is remaining constant while the contact is closed proving a resistive behavior of the circuit.

The possibility of capacitive effects of the electrochemical bath, related to ions displacements, (see discussion in appendix 3) can be eliminated by checking the phase of the lock-in measurements. The phase information acquired during experiments has clearly shown that the phase remains zero when the conductance is switching between two finite values, indicating a pure resistive behavior of the sample. Hence the system is preserving his capacitive or resistive behavior during switching as shown in fig.5.34.

One other hypothesis that can be discarded is related to inductive effects. One can speculate that significant induced voltage can occur when a change of orientation of a magnetic part of the circuit is occurring, being particularly amplified by the magnetic susceptibility of the ferromagnetic contact. One motivation for lock-in measurements was to avoid this type of occurrence, but we can still imagine that a large voltage can result as a perturbation at all low frequencies. We can criticize this hypothesis by mentioning that large MR were observed for Platinum nanocontacts and ions that are not presumed to have a significant inductive response. For double checking, we amplified the potential difference across the junction, when no AC excitation was imposed, and did not observe any important changes under applied magnetic field (fig.5.35).
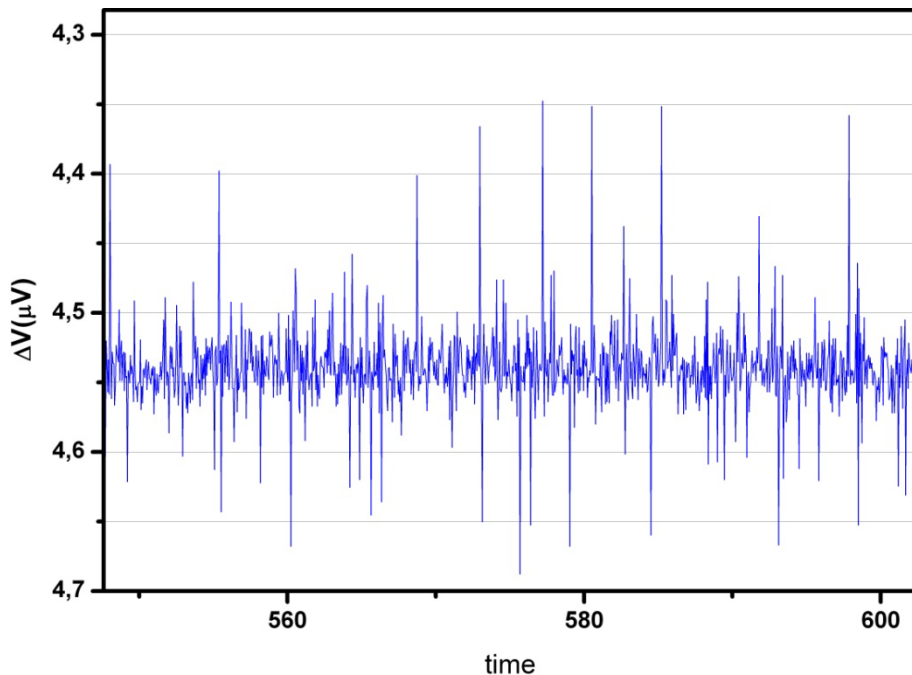
Fig.5.35 The voltage difference across the junction. The magnetic field was continuously swept or rotated but no major changes observed.

Nevertheless many experiments are still needed for better understanding of this phenomenon. The first plans aim at the improvement of our experimental setup and consist in an insertion of a second lock-in across the second R_0 resistor. In this way we gain more precision in our data by diminishing the influence of electrochemical bath on calculation of the conductance of the nanogap (fig. 5.36, and appendix IV).
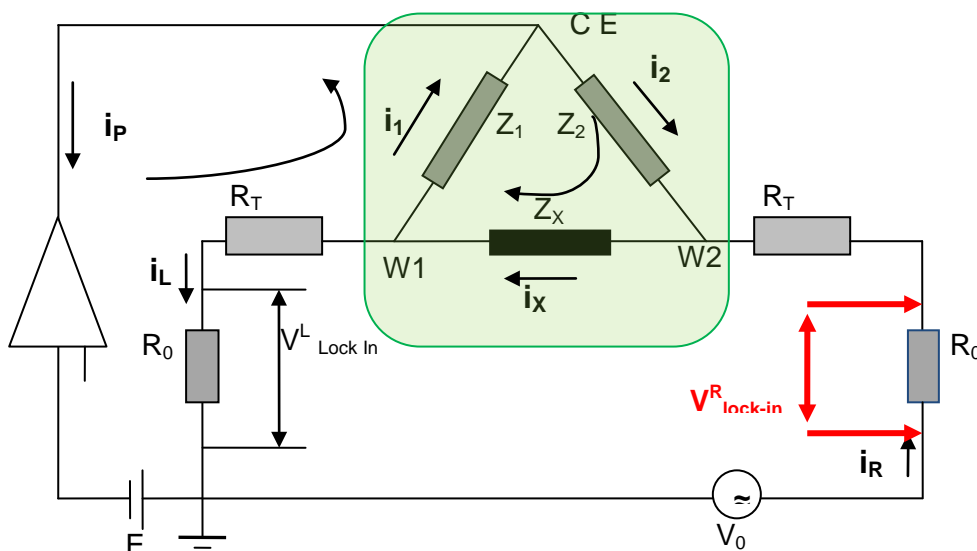
Fig.5.36 The electrical setup with a second lock-in inserted across the nanocontact

Even though many experiments and attempts were performed, it is only relatively late during this Ph.D. that we became convinced of the importance of ions in solutions. Therefore more statistics on the experiments is desirable, for example by combining DC and AC bias between the two sides of the contacts. We also lacked time to repeat experiments on Co, showing intriguing inverse AMR sign behavior (fig. 5.26).

More experiments on the influence of electrolyte are also needed. There are plans to study the dependency on concentration of ions. If the MR is indeed related to ions from solution, it should be sensitive to their concentrations as we initially observed in fig. 5.25.

Therefore we are thinking that experiments where an exchange of solution with different ions concentrations can be very useful. Following same direction we

plan to perform experiments where will exchange between electrochemical baths containing two different species of paramagnetic ions. It will be interesting to see what happens if the ions from solution are different from those ones that are forming the nanocontact.

A way to double check if this phenomenon of MR depending on the electrolyte is related to ions displacement (capacitive behavior) or to charge transfer (resistive behavior) between ions and the atoms forming the nanocontact can be performed by modifying the mobility of ions. Cooling down the electrolyte can possibly result in modifications of MR effects.

These are challenging experiments, especially when taking in account the yields of obtaining a nanocontact with a spectacular MR effect. Even for this kind of sample there it is a high chance to destroy the fragile nanocontact when exchanging the electrolytes. The pressure exerted by the flow can easily destroy a few atom contacts. More difficulties are related to electrodeposition process. In our micro-electrochemical cell always the three electrodes should remain in an electrical contact. Any spike can have irreversible effects, totally destruction of the sample can easily occurring.

Therefore, there is still plenty of work to do….

Bibliography

[1] S. Sahoo, C. -S. Yang, B. Doudin, *Physics Letters A,* **352,** (2006), 331-334.

[2] C. Zhang, *Ph.D. thesis*, University of Nebraska at Lincoln, USA, 2007

[3] C. -S. Yang, *Ph.D. thesis*, University of Nebraska at Lincoln, USA, 2004

[4] F.-Q. Xie, L. Nittler, Ch. Obermair, Th. Schimmel, *Phys. Rev. Lett.,* **93,** (2004), 128303.

[5] J. S. Newman, *Electrochemical Systems*, Prentice Hall, (1991), Englewood Cliffs

[6] M. S. Chandrasekar, M. Pushpavanam, *Electrochimica Acta,* **53,** (2008), 3313-3322.

[7] H. Kockar, M. Alper, H. Topcu, *The European Physical Journal B,* **42: 4***,* (2004), 497-501

[8] W. - H. Lee, S. -C. Tang, K. -C. Chung, *Surface and Coatings Technology,* **120-121** (1999), 607-611

[9] T. Watanabe, "*FINE PLATING: Microstructure Control and Analysis Methods for Plated Films*" 2003, published by Technical Information Association,

[10] J. M. Krans, C. J. Muller, I. K. Yanson, Th. C. M. Govaert, R. Hesper , J. M. van Ruitenbeek, *Phys Rev B,* 1993, **48**, 14721

[11] V. Rodrigues , J. Bettini , A. R. Rocha, L. G. C. Rego, D. Ugarte, *Phys. Rev. B,* **65,** (2002), 153402

[12] Y. J. Lee, M. Brandbyge, M. J. Puska, J. Taylor , K. Stokbro , R. M. Nieminen, *Phys. Rev. B,* **69, (**2004), 125409*.*

[13] M. Viret, S. Berger, M. Gabureac, F. Ott, D. Olligs, I. Petej, J. F. Gregg, C. Fermon, G. Francinet, G. Le. Goff, *Phys. Rev. B*, **66**, (2002), 220401

[14] K. I. Bolotin, F. Kuemmeth, N. Pasupathy Abhay, D. C. Ralph, *Nano Letters,* **6**, (2005),123-127*.*

[15] *Z. K.* Keane, L. H. Yu, D. Natelson, *Appl. Phys. Lett.*, **88,** (2006), 062514-3

[16] C. -S. Yang, C. Zhang, J. Redepenning, B. Doudin, *Appl. Phys. Lett.*, **84,** (2004), 2865-2867

[17] M. Gabureac, M. Viret, F. Ott, C. Fermon, *Phys. Rev. B* , **69,** (2004), 10040

[18] E. Scheer, N. Agrait, J.C. Cuevas, A. Levy Yeyati, B. Ludoph, A. Martin-Rodero, G. Rubio Bollinger, J.M. van Ruitenbeek, C. Urbina, *Nature* , **394**, (1998),154–157

[19] N. Agrait, A. L. Yeyati, J. M. van Ruitenbeek, *Physics Reports*, **377,** (2003), 279

[20] B. Doudin and M. Viret, *J. Phys.: Condens. Matter,* **20**, (2008), 083201

[21]. S. H. Chung, M. Munoz, N. Garcia, W. F. Egelhoff, R. D. Gomez, *Phys Rev Lett,* **89,** (2002), 287203*.*

[22] H .D. Chopra, Z. S. Hua, *Phys. Rev. B*, **66**, (2002), 020403

[23] N. Garcia, M. Munoz, Y.-W. Zhao, *Phys. Rev. Lett.,* **82, (**1999), 2923*.*

[24] W. F. Eghelhoff, L. H. Gan, Y. Ettedgui, C. J. Kadmon, P. J. Powell, A. J.Chen, R. D. Shapir, McMichael, J. J. Mallett, T. P. Moffat, M. D. Stiles, E. B. Svedberg, *J. Appl. Phys.*, **95**, (2004),7554-7559

[25] A. Delin, E. Tosatti, *Phys Rev B,* **68**, (2003), 144434.

[26] R. G. Gatiyatov, V. N. Lisin, A. A. Bukharaev, *Appl Phys Lett,* **96**, (2010), 093108-3.

Chapter 6

Conclusions and outlook

The work presented in this thesis aimed at two main directions. First, a reliable experimental setup was built, dedicated to fabricating metallic nanojunctions via electrochemistry and studying their transport properties. Secondly, systematic magnetoresistive measurements were performed, revealing and emphasizing the role of chemical environment.

For the first task we succeeded in building an electrochemical setup where atomic contacts exhibiting conductance values of a few quanta can be maintained for few tens of seconds. We used a lab on chip strategy what allowed better control of the electrochemical conditions during the experiments. More specifically, we developed a system allowing fast changing of electrolytes and limiting the mechanical impact on the sample. This new development for fabricating electroplated nanojunctions allowed us to unravel the crucial importance of the electrolyte on magnetoresistive properties.

The lifetime of atomic size contacts where a ballistic-type regime of conduction persisted was quite short. Hence the sweeping or rotating of the field and the acquisition data had to be done fast. Our system was able to apply a field of amplitude of 1.4 T, with frequencies for rotation or sweeping reaching 1 Hz.

We fabricated nanocontacts of nickel, cobalt, platinum, silver and gold by electrochemistry, starting from a pre-patterned pair of gold electrodes with an initial gap around 50nm. Besides the fabrication of nanocontacts, fabrication of gaps suitable for molecular junctions studies was performed. By stopping the deposition at a right time or by slightly reopening the contact after formation we obtained gaps limited to a few nanometers.

The initial experiments were focused in the study of quantized conductance and comparisons with previously reported results. They confirmed the fact that contact made of a few atoms can be achieved in a controlled manner our system Conductance plateaus, with lifetime till hundred of seconds were obtained for most of the metal studied.

Due to fragility of the atomic contacts, in situ measurements of transport properties were performed. The conductance of the contact was monitored using a low frequency technique. A small AC excitation was applied in the circuit and the voltage drop across a resistor connected in series to the contact was measured. The phase of the current in the circuit was also observed and recorded giving valuable information about the capacitive or resistive behavior of the circuit. Switches between two very low conductive states (1-2 G_0) were obtained for silver, under adequate electrochemical control.

Systematic investigations on the magnetoresistive effects, mostly on nickel nanocontacts, were performed. The results can be separated in three main categories. For almost one third of sample no effects were reported. The fact that these samples come from the same batch of preparation suggested the idea that the missing effects can be related to the sample pre-preparation process. For a second third of samples, MR or AMR effects with maximum values of 50-70 % were observed. These results are in agreement with most results previously reported and with the models elaborated until now.

The most interesting results, reported for the last third of samples, relate to values for MR and AMR ratios higher than 100%. We obtained ratios reaching 3000 %, and infinite ratios when the conductance was switching between 0 and a finite value of conductance. Similar kind of results, very promising for possible technological application, were reported before, but categorized as mechanical artifacts. Due to our new possibility to change the electrolyte from the vicinity of the nanocontact, we think another possible explanation can be proposed.

For samples exhibiting very high ratio of magnetoresistive effects we observed that their disappearance when the initial electrochemical solution, containing nickel ions, was replaced by one without nickel. We checked and repeated this for both MR and AMR studies. The most convincing experiment were obtained while studying AMR for a nickel junction having an initial conductance of $60G_0$. With magnetic field rotating continuously and the plating voltage maintained constant we observed that the oscillations in the conductance, unambiguously related to the field orientation, disappeared when the nickel ions are not present in solution, and were limited to bulk AMR ratios. As check experiment, we reintroduced nickel ions and the oscillations started again. This experiment, were the conductance remain at a finite value while sweeping the field and no ions were in solution, allowed us to discard a mechanical explanation for the large MR observed. Other series of experiments showed that the MR effects are continuously increasing or decreasing while the concentration of nickel ions is gradually increasing or decreasing. Hence a possible correlation between the concentration of magnetic ions for electrochemical bath and the MR can be also established. The lack of agreement between reported MR values on electrodeposited junctions can then be explained as differences between the concentrations used in different experiments.

We can therefore claim that transport properties across a metallic contact are seriously affected by the chemical environment; therefore the term of "magnetoresistive

effects in metallic contacts in the presence of electrolyte" should be used when one talks by junctions fabricated electrochemically. Besides these spectacular results there is no model yet to explain how the ions from the chemical bath, driven by applied magnetic field, can interact with contact conductance altering it. More interestingly, one can exhibit experimental cases where the transport across the contact is fully blocked for certain values of the angle between magnetic and the electric current.

The experiments performed on cobalt and platinum contacts confimed this idea of the influence of electrolyte on transport properties. For the cobalt contact with conductance values around 200 quanta of conductance (hence quite far from a ballistic regime) negative values of the MR ratio around 30 percents were obtained in the presence of electrolyte, values way beyond expected bulk AMR properties. For platinum, a 5d metal, with an expected magnetic behavior at low dimensions, the observed MR ratio in the presence of electrolyte was about 2000%, again very far for any reported values.

A special section of this thesis was dedicated to nanojunction obtained by combining electrochemistry with mechanical break technique. The gap, initially formed by mechanically breaking a constriction in a patterned line, was used as initial working electrodes in the electrochemical process of forming nanocontacts. Unfortunately, due to space restrictions, the magnetic field applied was smaller, having maximum values of 0.4 T. Again the results were very interesting. When electroplating gold between two mechanically broken permalloy electrodes we observed a MR ratio of 10-15 %, one order of magnitude larger than the MR of the same structure obtained by using only MBJ technique, and one order of magnitude large than expected bulk properties.

The results obtained on the work for this thesis have proven unambiguously the crucial influence of the electrolyte on magnetoresistive properties of metallic contacts. These results can put to an end the controversy which lasts in last five years, related to possible explanations of huge values of MR ratio in ferromagnetic nanocontacts obtained via electrochemistry. These values, initial attributed to mechanical artifacts can be in fact due to the influence of chemical environment. New experiments should be performed for fully understanding this new phenomenon. The influence of different species of ions should be investigated and even methods to reduce this influence should be investigated. In the same time, strategies for taking advantage of this effect can be pursued, for possible technological applications. One of the most urgent needs in this case consists in understanding and modeling the electronic transport though charged ions flowing in solution and revealing how they can be spin-dependent. What

was initially a research topic related to ballistic transport in metallic systems appears more and more a molecular electronics problem.

Appendixes

Appendix 1. Calibration curves for magnetic poles

Appendix 2. Velocity of electrolyte flowing through microfluidic channels

Appendix 3. Ions displacements studies

Appendix 4. Calculation of nanocontact conductance in a electrical circuit with two lock-ins.

Appendix 5. Curriculum vitae

Appendix 6. Publications, conferences, posters

Calibration curves for magnetic poles.

Four pair of magnetic poles, with different size of gap, were used in this thesis, depending on the sample used.

	Separation (cm)
Small poles	6
Medium poles	4
Big poles	2.5
New poles	1.5

Calibration curves for magnetic poles
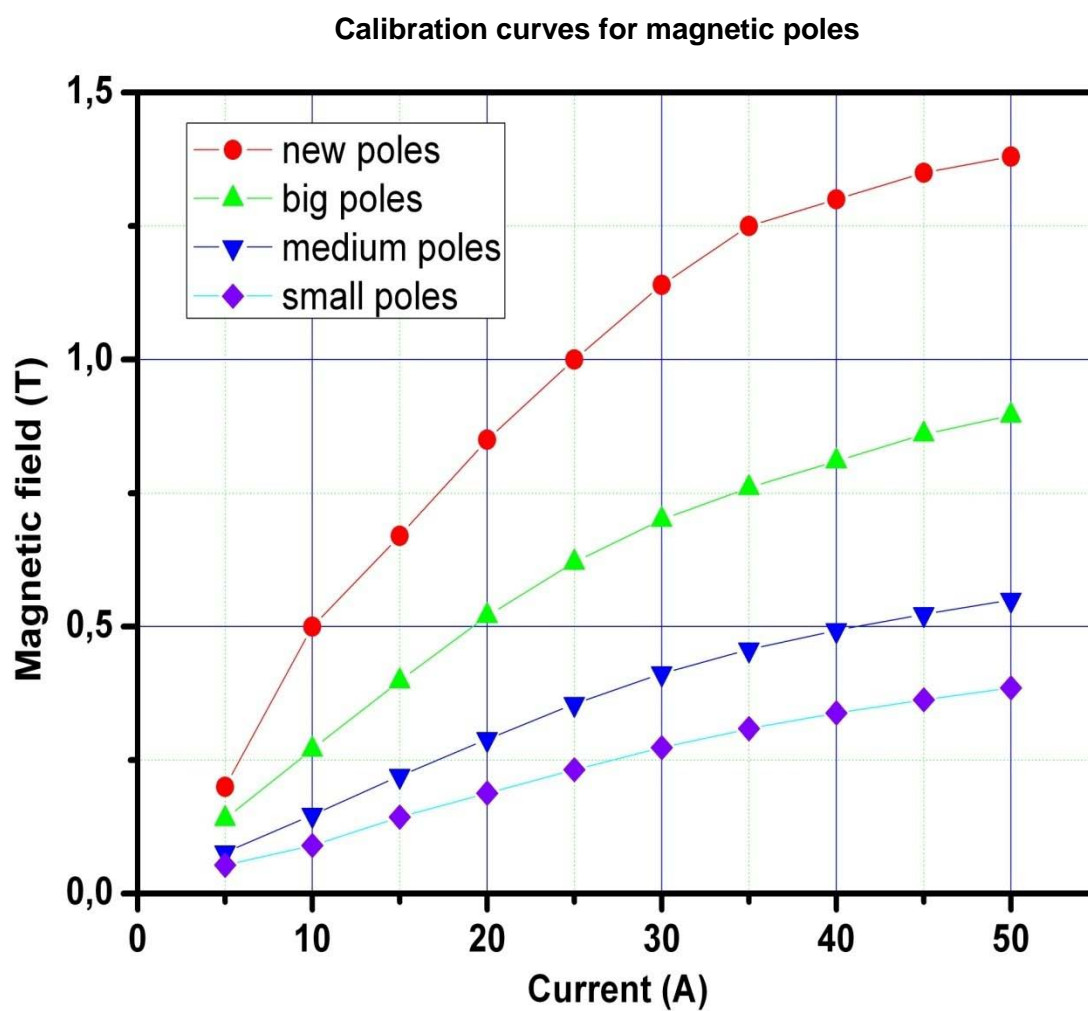
Velocity of electrolyte flowing through microfluidic channels

The debit of electrolyte' flowing is imposed automatically by the syringe pump system.

The equation for the debit is

$$Q = Sv$$

where:

Q is the debit imposed by the pumping system

S is the cross-section of microfluidics channel

v is the velocity of the electrolyte flowing through channel of cross-section S

Our microfluidic channels are having a width of 150 microns and a height of 50 microns. Hence, the cross section is

$$S = 100X10^{-6}X50X10^{-6} = 5X10^{-9}m^2$$

In SI units a debit of 0.1ml/hour is

$$Q = \frac{10^{-7}}{3600} \frac{m^3}{s}$$

Therefore, for this debit, the velocity of electrolyte through microfluidic channel is:

$$v = \frac{\frac{10^{-7}}{3600}\frac{m^3}{s}}{5X10^{-9}m^2} \approx 4 \, mm/s$$

This is a not negligible value for a very fragile, low conductance contact, formed by only a few atoms. As explained we performed experiments with a static electrolyte, above calculations referring only for times when the exchange of electrolyte is made.

Ions displacements studies
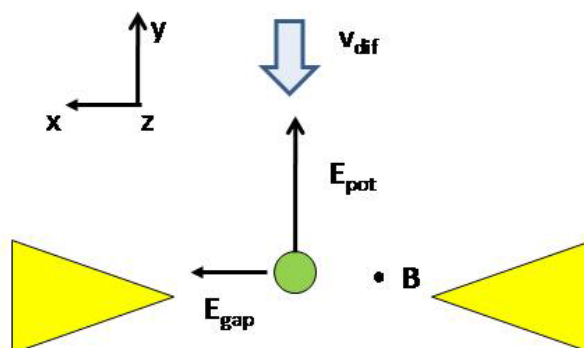
For an ion from electrolyte, found in the gap vicinity the equation of motion is:

$$m\vec{a} = q(\vec{v}X\vec{B}) + q\vec{E}gap + q\vec{E}pot + A\eta\vec{v}$$

where

- **m** – the ion mass
- **q** – the ion charge
- $\vec{a}$ – the ion acceleration
- $\vec{v}$ - the ion velocity
- $q(\vec{v}X\vec{B})$ - Lorentz force exerted due to ion moving in the magnetic field
- $q\vec{E}gap$ – electric force exerted due to AC excitation (4mV) applied between the two working electrodes
- $q\vec{E}pot$ - electric force exerted due to applied DC plating potential between counter and working electrodes
- $A\eta\vec{v}$ – the Stokes forces due to viscosity for a small spherical particle. A is a proportionality factor depending linearly on the particle's radius and η is the viscosity coefficient

We assumed here that is no pumping of the electrolyte by the syringe system. Hence, the movement of the ions is due only the forces above.

If we write explicitly the vector cross-product from Lorentz force formula, the equation of motion becomes:

$$m\frac{\overrightarrow{dv}}{dt} = q\begin{pmatrix} \hat{x} & \hat{y} & \hat{z} \\ v_x & v_y & v_z \\ B_x & B_y & B_z \end{pmatrix} + q\vec{E}gap + q\vec{E}pot + A\acute{\eta}\vec{v}$$

Let's write the vectors on their components, taking in account the axis system:

- $\vec{E}gap = (0, E_{gap}\hat{y}, 0) = (0, E_{gap}\sin\omega_{AC}t\,\hat{y}, 0)$ referring to the frequency of applied AC excitation (around 200 Hz)

- $\vec{E}pot = (E_{pot}\hat{x}, 0,0)$ Type equation here.

- $\vec{B} = (0, B\cos\omega t\hat{y}, 0)$ here we can discuss is not cosine law , is more like c X t law ; will see this that this is not important for y axis
  $A\eta\vec{v} = A\eta(v_x\hat{x} + v_y\hat{y} + v_z\hat{z})$ viscosity

Replacing all in the main equation:

$$\frac{m}{q}\frac{d\vec{v}}{dt} = \begin{pmatrix} \hat{x} & \hat{y} & \hat{z} \\ v_x & v_y & v_z \\ 0 & B\cos\omega t & 0 \end{pmatrix} + E_{gap}\sin\omega_{AC}t\,\hat{y} + E_{pot}\hat{x} + A\eta(v_x\hat{x} + v_y\hat{y} + v_z\hat{z})$$

Projecting on axis:

$$\frac{m}{q}\frac{dv_x}{dt} = -B\cos\omega t\,v_z + E_{pot} + A\eta v_x$$

$$\frac{m}{q}\frac{dv_y}{dt} = E_{gap}\sin\omega_{AC}t + A\eta v_y$$

$$\frac{m}{q}\frac{dv_z}{dt} = B\cos\omega t\,v_x + A\eta v_z$$

These are the equations of motion for the three axes

We are interested for the motion on y axis – between the two working electrodes:

$$\frac{m}{q}\frac{dv_y}{dt} - A\eta v_y = E_{gap}\sin\omega_{AC}t$$

Rearranging the terms

$$\frac{dv_y}{dt} - \frac{q}{m}A\eta v_y = \frac{q}{m}E_{gap}\sin\omega_{AC}t$$

This is linear differential equation of order 1. Typically form of this kind of equation is:

$$\frac{dy}{dx} + Py = Q$$

If $P = P(x)$ and $Q = Q(x)$ are functions of x only, for finding the solution we have to solve next equation:

$$ye^{\int Pdx} = \int Qe^{\int Pdx}dx + K$$

Following, we will neglect the integration constant K as we are not interested in exact values but in the behavior of the solution.

In our case

$$P(t) = -\frac{qA\eta}{m}$$

$$Q(t) = \frac{q}{m}E_{gap}\sin\omega_{AC}t$$

$$\int Pdt = -\int\frac{qA\eta}{m}dt = \frac{qA\eta}{m}t$$

Replacing

$$v_y e^{-\frac{qA\eta t}{m}} = \int \frac{q}{m} E_{gap} \sin \omega_{AC} t \, e^{-\frac{qA\eta t}{m}} dt = \frac{q}{m} E_{gap} \int \sin \omega_{AC} t \, e^{-\frac{qA\eta t}{m}} dt$$

From the table of integrals

$$\int e^{ax} \sin bx \, dx = \frac{e^{ax}(a \sin bx - b \cos bx)}{a^2 + b^2}$$

Using this formula we can calculate the velocity on y axis

$$v_y e^{-\frac{qA\eta t}{m}} = -\frac{q}{m} E_{gap} e^{-\frac{qA\eta t}{m}} \frac{A\eta\left(\frac{q}{m}\right)\sin \omega t + \omega \cos \omega t}{A^2\eta^2\left(\frac{q}{m}\right)^2 + \omega^2}$$

Rearranging the terms

$$v_y = -\frac{\left(\frac{q}{m}\right)E_{gap}}{A^2\eta^2\left(\frac{q}{m}\right)^2 + \omega^2}\left[A\eta\left(\frac{q}{m}\right)\sin \omega t + \omega \cos \omega t\right]$$

Integrating with respect to time we can obtain the equation of motion for the ions on the y axis

$$y = \frac{\left(\frac{q}{m}\right)E_{gap}}{A^2\eta^2\left(\frac{q}{m}\right)^2 + \omega^2}\left[\frac{1}{\omega}A\eta\left(\frac{q}{m}\right)\cos \omega t - \sin \omega t\right]$$

For a Nickel ion, assumed spherical with a radius of 10^{-10}m, in an aqueous solution (in S.I. units):

- **q/m** (*specific charge*) $\approx 6 \times 10^6$ C/Kg
- **A** = 6πR = 6π 10^{-10} m
- **η**=0.001 Kg/ms (1 centipoises at 20^0 C)
- **ω** =2π 200 Hz

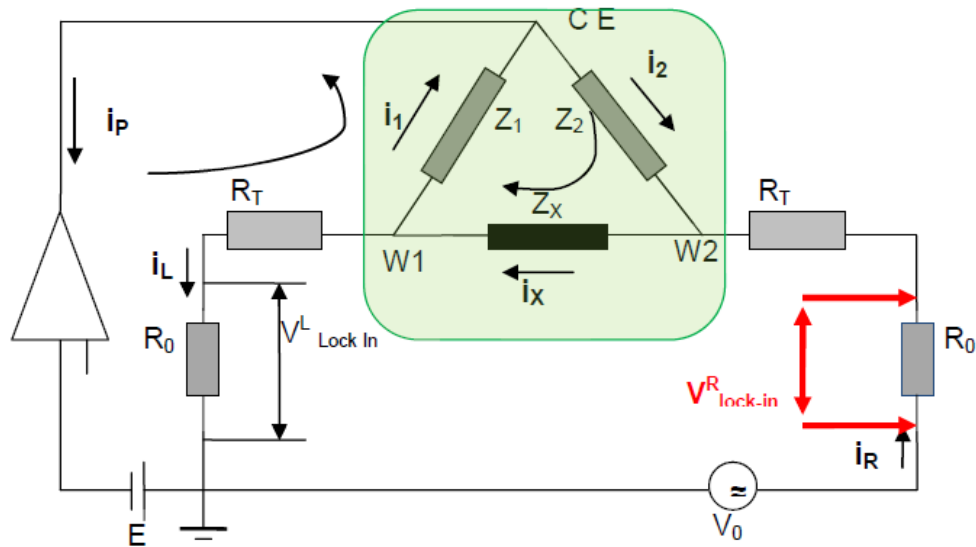The next term is giving the ratio between the in phase and out of phase components:

$$\frac{1}{\omega} A\eta \left(\frac{q}{m}\right) = \frac{6\pi 10^{-10} 10^{-3}}{2\pi 200} 6X10^6 \approx 10^{-8}$$

Hence the in phase component of the velocity of ions are negligible comparing with out of phase component.

Calculation of nanocontact conductance in a electrical circuit with two lock-ins.

The Kirchhoff equations for this electrical circuit are the same as those from the "Equivalent electrical circuit" subsection of chapter 4

$$i_1 = i_P + i_2 \tag{1}$$

$$i_X = i_L + i_1 \tag{2}$$

$$i_X = i_2 + i_R \tag{3}$$

$$i_R = i_L + i_P \tag{4}$$

$$i_1 Z_1 - i_L R = 0 \tag{5}$$

$$i_2 Z_2 + i_1 Z_1 + i_X Z_X = 0 \tag{6}$$

$$V_0 = i_R R + i_X Z_X + i_L R \tag{7}$$

We add here the two voltages read by lock-ins:

$$V^L = i_L R_0$$

$$V^R = i_R R_0$$

Assuming $Z_1=Z_2=Z$ we obtain for the nanocontact conductance (all credits for these calculations go to Bernard):

$$Z_X = \frac{(V_0 - V^L - V^R)(V_0 + V^L - V^R)}{\dfrac{V_0 V^L}{R}}$$

without doing any approximation on the value of Z, the impedance of the bath between counter and working electrodes

Petru LUNCA POPA

Institute of Material's Physics and Chemistry
Strasbourg (IPCMS)
23 rue de Loess, BP43
67034 Strasbourg, **FRANCE**
Phone: + 33(0)388107079 – office
                 + 33 (0)388107212 – lab
                 +33 (0)611690874 - mobile
E-mail: petru.luncapopa@ipcms.u-strasbg.fr
WEB: IPCMS - Group of Prof. Bernard Doudin

Birthday: 29.02.1972
Nationality: Romanian

Education

- Ph.D. Degree in Spintronics, *University of Strasbourg*, **FRANCE** *sept 2010*
  Thesis: "*In situ studies of spin electronics properties of magnetic nanocontacts fabricated using a Lab-on-chip approach*"
  Group of Prof. B. Doudin

- M.Sc. in Condensed Matter, *University of Nebraska at Lincoln*, **USA** *aug 2006*
  " Semiconducting heterojunctions of boron carbide"
  Group of Prof. J.I. Brand and Prof P. Dowben

- M.Sc. Thin Films Physics, *"Al.I.Cuza" University of Iasi*, **ROMANIA** *sept 1997*
  "Dielectric losses in polypropylene treated with copper"
  Advisor : Prof. Dr. N.Sulitanu

- B. Sc in Solid State Physics, *"Al.I.Cuza" University of Iasi*, R**OMANIA** *aug 1995*
  "Devices with dielectrics"
  Advisor : Prof. Dr. N.Sulitanu

Present position

- Research Engineer   *from sept 2006*
  Institute of Material's Physics and Chemistry Strasbourg (IPCMS)
  Strasbourg, **FRANCE**
  Group of Prof. Bernard Doudin

Past positions

- Graduate Research Assistant,   *jan 2004-aug 2006*
Department of Physics, *University of Nebraska at Lincoln,* **USA**
Group of Prof. J.I. Brand and Prof P. Dowben

- Associate Researcher,   *1997 - 2004*
Department of Physics*, "Al.I.Cuza", University of Iasi*, **ROMANIA**

- Associate Researcher   *2000-2003*
Cleanroom Laboratory, *S.C.FEPA SA Barlad*, **ROMANIA**
(Automatic devices factory) 2000-2003

- Physics Professor   *p.t.   1995-2003*
"Al.I.Cuza" National College, Barlad, **ROMANIA**

Teaching experience

Graduate Teaching Assistant
Department of Physics, University of Nebraska at Lincoln, **USA**
Classical Mechanics, Electricity, Optics, Analytical Mechanics, 50hours/semester

Physics Professor
"Al.I.Cuza" National College, Barlad, **ROMANIA**
Courses of General Physics – All Fields – upper average level, 700 hours/year

Research Topics

- *Nanostructures*
  - Nanojunctions, Nanogaps
  - Transport phenomena
  - Morphologies of nanostructures
  - Ballistic regime
  - Spin Electronics – molecular spintronics

- *Semiconductor's Physics*
  - Thin Films deposition
  - Electrical, optical and magnetic proprieties of Thin Films

- *Dielectrics*
- *Electrochemistry*
- *Nanofabrication*
- *Microfluidics – PDMS cells, SU8 masters, lab on chip design*
- *Particle Detection*

Experimental skills

- Thin films deposition methods
Plasma Sputtering, Thermal Evaporation, Electrochemical deposition, Plasma Enhanced Chemical Vapor Deposition

- Electrical, optical and magnetic measurements for Thin Films

resistivity measurements, IV characteristics, Hall measurements, photovoltaic measurements, capacitance measurements, photoemission, inverse photoemission, UV-VIS-NIR spectroscopy, magnetic measurements

- Dielectrics

Dielectric losses mechanisms, Q-meter measurements

- Nanostructures

Electrodeposition, Mechanical break junctions, Two angles deposition, Atomic Force Microscopy

- Transport measurements techniques in nanostructures

- Electrochemistry

Over and under potential deposition, Pulse plating, MEB (Multi-Electrochemical-Baths)

- Optical and E-Beam Lithography

- Detections Techniques

Neutrons and charged particles detection, alphas

Experimental setup developments

- Imagining, designing and completely building a experimental setup for electrodepositing

nanojunctions and for studying transport properties across them
*Institute of Material's Physics and Chemistry Strasbourg (IPCMS), Strasbourg, **FRANCE***

- Modifying and optimizing a PECVD system

*Department of Physics, University of Nebraska at Lincoln, **USA***

- Designing and building a Plasma magnetron sputtering system

*S.C.FEPA SA Barlad, **ROMANIA***

Languages

- Romanian – native
- English, French, – very good
- Italian, Spanish – fair

PC

- Windows OS +MS Office
- Linux Ubuntu OS
- C++ - average level
- LAB Windows
- Origin Lab, ROOT

Published papers

- High Frequency Pulse Electrodeposition for Highly Controlled
  Nanodevice Fabrication
  *N.T. Kemp, J-F. Dayen, H. Majjad, **P. Lunca Popa**, V. Faramarzi, J-B.
  Beaufrand, G. Dalmas, B. Doudin*
  Nanotechnology, 2010, *in prep*

- Electrochemistry like source of spectacular Magnetoresistance results
  ***P. Lunca Popa,** N.T. Kemp, H. Majjad, , V. Faramarzi, J-B. Beaufrand,
  G. Dalmas, J-F. Dayen and B. Doudin*
  Nanoletters, 2010, *in prep*

- On-chip electrochemistry using microfluidic cell: a versatile tool for
  fabricating nanojunctions for spintronics and molecular electronics
  studies
  *P. Lunca Popa, G. Dalmas, V. Faramarzi, J.- B. Beaufrand, J.-F.
  Dayen, H. Majjad, N. Kemp and B. Doudin*
  Lab on Chip, 2010, submitted

- Lab-On-Chip Fabrication Of Atomic Scale Magnetic Junctions
  *N.T. Kemp, H. Majjad, **P. Lunca Popa**, G. Dalmas and B. Doudin*
  ECS Transactions, 2009, **16 (45)**, 3-10 10.1149/1.3140005
  © The Electrochemical Socity

- The Band Offsets of Isomeric Boron carbide Overlayers,
  *A.N.Caruso**, P. Lunca-Popa**, Y.B.Losovyj, A.S. Gunn, J.I.Brand
  Mater. Res. Soc. Symp. Proc.*, 2005, Vol. 836, L5.40, Materials
  Research Society.

- Mercury and C2B10 Icosahedra Interaction,
  C. C. Ilie, **P. Lunca-Popa,** J. Zhang**, B.** Doudin, P. A. Dowben
  Mater. Res. Soc. Symp. Proc., 2005, Vol. **848, FF6.5.1**, Materials
  Research Society.

- Evidence for Multiple Polytypes of Semiconducting BoronCarbide (C_2B_{10})
  from Electronic Structure
  ***Petru Lunca-Popa**, J. I. Brand, S. Balaz, L. G. Rosa, N. M. Boag, M.
  Bai, B R Robertson and P A Dowben*
  J. Phys. D: Appl. Phys., 2005, **38**, 1–5.

- The Coadsorption and Interaction of Molecular Icosahedra with Mercury
  *C. C. Ilie, S. Balaz, L. G. Rosa, J. Zhang, **P. Lunca-Popa**, C. Bianchetti,
  R. Tittsworth, J. I. Brand, B. Doudin, and P. A. Dowben*
  Appl. Phys., 2005, **A 00,** 1–6

- Fabrication of Semiconducting Boron-Carbide Solid State Device to optimize Neutron Detection
A .N .Caruso, **P.Lunca-Popa**, *M. S. Hallbeck, W. K. Pitts, J. I. Brand*
S.P.I.E Use, 2004, **V**, 1 5441-8.

Conferences/Presentations/Posters

- ***Colloquium Louis Neel, 2010,*** March 1-4 Albe, **FRANCE**
Poster: *Electrochemistry like source of spectacular Magnetoresistance results*

- ***EUROMAT 2009***, September 6-9 2009, Glasgow, **United Kingdom**
Talk: *Spintronics at nanometer scale*

- ***IPCMS's scientific days***, May 4-6 2009, IPCMS, Strasbourg, **FRANCE**,
Talk: *Magnetic nanocontacts fabricated by electrochemical contact*

- ***French – Korean Nanophysics Workshop***, September 2008, Strasbourg , **FRANCE**
Posters: *Spintronics below one nanometer*
Molecules Electrical and optical detection

- ***214th ECS Meeting***, October 12-17, 2008, Honolulu, HI, **USA**
Talk: *Magnetic Nanocontacts Fabricated by Electrochemical Techniques. Application To Spin Electronics At The Atomic Scale*

- ***International workshop Nanoscopic Transport: Quantum noise, Josephson junctions, and molecular electronics,*** Nov.1-3, 2007, Freiburg im Breisgau, **Germany**

- **The 53rd Midwest Solid State Conference**, 2006, University of Missouri, Kansas City, **USA**
Talk: *The Interaction of Molecular Icosahedra with Mercury*

- ***Forward Pixel Detector Workshop***, June 5, 2005 Fermi National Laboratory, Batavia, IL, **USA**
Talk : *Silicon Particles Detector at LHC – CERN*

- ***Fermi lab Users' Meeting*** June 8-9 2005,Fermi National Laboratory, Batavia, IL, **USA**
Talk: *Silicon Particles Detector at LHC – CERN*

- ***Gordon Research Conference**, Chemistry of Electronic Materials*, 2005, New London, CT, **USA**

Talk: *The Interaction of Molecular Icosahedra with Mercury*

- ***NSF and MRSEC Second Review and Symposium**, June 2004, University of Nebraska at Lincoln, Lincoln, NE, **USA**

Talk: *Mercury coadsorption with Molecular Icosahedra of Semiconductor Boron Carbide*

- ***39th Midwest Regional Meeting**, American Chemical Society*, October 20-22, 2004, Manhattan, KA, **USA**.

Talk: *Electronic structure for polytypes of semi-conducting boron carbide*

- ***Material Research Society Fall Meeting** *, Nov 29 – Dec 3, 2004, Boston, MA, **USA**

Poster: *Direct Power Conversion from Neutrons, Photons and Alpha Particles*

- ***6th National Conference of Plasma Physics**, June 6-8, 1997, IASI, **Romania**

Organization Committee